**REPORT**
SAND2007-0358
Unlimited Release
Printed February 2007

# Operational Characteristics and Analysis of the Immersed-$B_z$ Diode on RITS-3

Dean C. Rovang, Nichelle Bruner, Graham M. Cooper, Mark D. Johnston, John E. Maenchen, John McLean, Bryan V. Oliver, Salvador Portillo, Elizabeth Puetz, David V. Rose, and Dale R. Welch

Prepared by
Sandia National Laboratories
Albuquerque, New Mexico 87185 and Livermore, California 94550

Sandia is a multiprogram laboratory operated by Sandia Corporation, a Lockheed Martin Company, for the United States Department of Energy's National Nuclear Security Administration under Contract DE-AC04-94AL85000.



Issued by Sandia National Laboratories, operated for the United States Department of Energy by Sandia Corporation.



Available to DOE and DOE contractors from
U.S. Department of Energy
Office of Scientific and Technical Information
P.O. Box 62
Oak Ridge, TN 37831

Telephone: (865) 576-8401
Facsimile: (865) 576-5728
E-Mail: reports@adonis.osti.gov
Online ordering: http://www.osti.gov/bridge

Available to the public from
U.S. Department of Commerce
National Technical Information Service
5285 Port Royal Rd.
Springfield, VA 22161

Telephone: (800) 553-6847
Facsimile: (703) 605-6900
E-Mail: orders@ntis.fedworld.gov
Online order: http://www.ntis.gov/help/ordermethods.asp?loc=7-4-0#online

SAND2007-0358
Unlimited Release
Printed February 2007

# Operational Characteristics and Analysis of the Immersed-$B_z$ Diode on RITS-3

D. C. Rovang[1] , N. Bruner[2], M. D. Johnston, J. E. Maenchen, B. V. Oliver,
S. Portillo, E. Puetz, D. V. Rose[2], and D. R. Welch[2]
*Sandia National Laboratories*
*P.O. Box 5800*
*Albuquerque, New Mexico 87185*

G. M. Cooper, J. McLean
*AWE, Aldermaston, Reading, United Kingdom*

## Abstract

The immersed-$B_z$ diode is being developed as a high-brightness, flash x-ray radiography source. This diode is a foil-less electron-beam diode with a long, thin, needle-like cathode inserted into the bore of a solenoid. The solenoidal magnetic field guides the electron beam emitted from the cathode to the anode while maintaining a small beam radius. The electron beam strikes a thin, high-atomic-number anode and produces bremsstrahlung. We report on an extensive series of experiments where an immersed-$B_z$ diode was fielded on the RITS-3 pulsed power accelerator, a 3-cell inductive voltage generator that produced peak voltages between 4 and 5 MV, ~140 kA of total current, and power pulse widths of ~50 ns. The diode is a high impedance device that, for these parameters, nominally conducts ~30 kA of electron beam current. Diode operating characteristics are presented and two broadly characterized operating regimes are identified: a nominal operating regime where the total diode current is characterized as classically bipolar and an anomalous impedance collapse regime where the total diode current is in excess of the bipolar limit and up to the full accelerator current. The operating regimes are approximately separated by cathode diameters greater than ~3 mm for the nominal regime and less than ~ 3 mm for the anomalous impedance collapse regime. This report represents a compilation of data taken on RITS-3. Results from key parameter variations are presented in the main body of the report and include cathode diameter, anode-cathode gap, and anode material. Results from supporting parameter variations are presented in the appendices and include magnetic field strength, prepulse, pressure and accelerator variations. Comparisons with analytic and computational models are discussed.

[1]Email: dcrovan@sandia.gov
[2]Permanent address: Voss Scientific, Albuquerque, New Mexico.

## Acknowledgements

The authors are grateful for the outstanding engineering and design work provided by Dave Van De Valde of EG&G and Matt Sceiford of Sandia. We are also grateful for the excellent technical and operational assistance provided by Darryl Gregerson, formerly of Ktech, Steve Cordova, Isidro Molina and Kelly Hahn of Sandia, David L. Johnson of L-3 Pulse Sciences, John O'Malley of AWE and Darryl Droemer of NSTec. We also thank the RITS-3 crew for their support in fielding these experiments, Ray Gignac and Frank Wilkins of NSTec, Derek Ziska and Ray Chavez of Ktech and Fawn Griffin of Sandia. The authors also would like to acknowledge many helpful discussions with Mike Mazarakis and Mike Cuneo of Sandia, Edl Schamiloglu of the University of New Mexico and Yitzhak Maron of the Weizmann Institute of Science.

The authors wish to acknowledge the contributions of the staff of the National High Magnetic Field Laboratory, especially Chuck Swenson, for the design and fabrication of the high field pulsed magnets and useful discussions concerning the solid hydrogen anode engineering and development. The authors also would like to express their gratitude to Dave Hanson of Sandia and Bob Johnston and Kevin Youngman of Ktech Corp. for their assistance with the cryogenic engineering and development.

This work is performed in technical collaboration with the pulsed power groups at AWE, the Naval Research Laboratory (NRL) and L-3 Pulse Sciences and we thank them for their support, encouragement and valuable discussions.

Sandia is a multiprogram laboratory operated by Sandia Corporation, a Lockheed-Martin company, for the United States Department of Energy's National Nuclear Security Administration, under contract DE-AC04-94AL85000.

# Contents


I. Introduction……7
II. Baseline operating points……10
A. Nominal and anomalous operation at 4 MV ……10
B. Nominal operation at 5 MV……13
III. Cathode diameter variations……15
IV. AK gap variation……19
V. Anode material variations……21
VI. Discussion……25
VII. Future Work ……28
References……30

Appendices ……35
Appendix A: $B_z$ variation ……35
Appendix B: Prepulse variation……38
Appendix C: Pressure variation……42
Appendix D: Accelerator/diode variation……43
Appendix E: Large cathode exceptions……45
Appendix F: Anode material exception – Polyethylene ……46
Appendix G: Comparison of experimental results to numerical and analytical models……48
Appendix H: Cryogenic coating apparatus and process description……54
Appendix I: Frozen hydrogen and related cryogenic anode results……61
Appendix J: Spectroscopy results – plasma velocity implications……64
Appendix K: Experimental Shot Summary ……69
References for Appendices ……70


# Figures


1. Schematic of immersed-$B_z$ diode ……7
2. Schematic of immersed-$B_z$ diode attached to RITS-3 accelerator ……9
3. Currents and dose rate for nominal diode operation at 4 MV……11
4. Currents and dose rate for anomalous diode operation at 4 MV ……12
5. Currents and dose rate for nominal diode operation at 5 MV……14
6. Time-dependent electrical, dose and spot size production characteristics for nominal diode operation at 5 MV ……14
7. Effect of cathode diameter on currents and impedance at 5 MV ……16
8. Effect of cathode diameter on dose rate and spot size at 5 MV ……17
9. Effect of cathode diameter on time-integrated dose and spot size at 5 MV ……17
10. Effect of cathode diameter on ESF and LSF profiles at 5 MV ……18
11. Effect of AK gap on current and impedance at 4 MV ……19
12. Effect of AK gap on dose rate and time-integrated dose and spot size at 4 MV ……20
13. Effective AK gap closure speed at 4 MV ……21
14. Effect of anode material/treatment variations on currents and impedance at 5 MV……23
15. Effect of anode material/treatment variations on dose rate and spot size at 5 MV ……23
16. Effect of anode material/treatment variations on cathode activation at 5 MV ……24

A1. Spot size vs. cathode diameter for 6, 12, and 18 T at 4 MV .....36
A2. Effect of magnetic field strength on current and impedance for 1-mm cathode at 4 MV ....37
A3. Effect of magnetic field strength on dose rate and time-integrated dose and spot for 1-mm cathode at 4MV .....37
B1. Characterization of low and high prepulse on RITS-3 .....38
B2. Effect of prepulse on diode current and impedance for 2-mm cathode at 4 MV.....39
B3. Effect of prepulse on dose rate and LSF for 2-mm cathode at 4 MV .....40
B4. Comparison of currents and dose rate for 2-mm cathode with high prepulse to 9.52 mm cathode with low prepulse at 4 MV .....41
B5. Spot profile comparison for 2-mm cathode with high prepulse to 9.52 mm cathode with low prepulse at 4 MV.....41
C1. Effect of pressure on current impedance for 3.18-mm cathode at 4 MV.....43
C2. Effect of pressure on dose rate and time-integrated dose and spot for 3.18-mm cathode at 4 MV .....43
D1. Spot size and dose as a function of cathode diameter for different accelerators/diodes.....45
E1. Diode current and dose rate for 7.14-mm cathode with late-time impedance collapse.....45
F1. Diode current and dose rate for RT anode (polyethylene) with anomalous diode behavior .....47
G1. Comparison of experimental, numerical and analytical diode currents; 4.76 mm, 5 MV…48
G2. Comparison of experimental and numerical diode currents; 2 mm, 5 MV.....49
G3. Comparison of experimental and empirical dose rates .....51
G4. Comparison of experimental, numerical and analytical spot sizes as a function of cathode diameter .....52
G5. Comparison of experimental and numerical spot profiles .....53
H1. Drawings of anodes used for frozen Xe and RT Ta experiments at 5 MV.....54
H2. Drawings of anodes used for frozen $H_2$ and $D_2$ experiments at 5 MV .....55
H3. Frozen D2 coating test temperature/pressure history and picture.....56
H4. Frozen H2 coating test temperature/pressure history and picture.....57
H5. Pressure vs. flow rate characterization for frozen $D_2$ and Xe .....57
H6. Representative cooling and coating timelines for frozen $D_2$ and Xe.....60
I1. Anomalous and quasi-normal frozen hydrogen diode currents .....62
I2. Effect of cryogenic anode material/treatment at 4T and 5 MV .....62
I3. Effect of cryogenic anode material/treatment at 4T and 5 MV.....63
I4. Effect of magnetic field strength on diode current and dose rate for cryogenic anodes.....64
J1. Description and schematics of spectroscopy diagnostics .....65
J2. Relative timing of light observed looking near cathode tip.....66
J3. Effect of anode material and filter variations on spectroscopic diagnostics looking near cathode tip.....68

## Tables

D1. Experimental configurations and results for accelerator/diode variation .....44
K1. Experimental shot summary.....69

# I. Introduction

High-power, intense electron beam diodes are routinely used as high-brightness flash x-ray sources.[1, 2] Continued development of these sources is being pursued, with emphasis on increasing the x-ray source intensity through higher end-point voltage and/or higher electron beam current, and reducing the diameter of the electron beam focal spot/x-ray source diameter. One such source is the immersed-$B_z$ diode,[3, 4, 5] which is a foil-less electron-beam diode with a long, thin, needle-like cathode inserted into the bore of a solenoid. The magnetic field of the solenoid guides the electron beam emitted from the cathode to the anode while maintaining a small beam radius roughly that of the cathode tip. The electron beam strikes a thin, high-atomic-number anode and produces bremsstrahlung.

A schematic of the immersed-$B_z$ diode is shown in Fig. 1. The magnetic field is produced by a pulsed high-current solenoid that entirely surrounds the anode-cathode (AK) vacuum gap. The cathode is a long, thin needle, typically made of tungsten and the anode is typically composed of an electron-range-thin high-atomic-number material (e.g. tantalum) that acts as a bremsstrahlung converter, backed by an electron-range-thick low-atomic-number material (e.g. carbon) that stops the electron beam. The cathode needle is attached to the center conductor of a coaxial transmission line driven by an inductive voltage adder or other pulse forming line. A shaped conical section connects the center conductor of the Magnetically Insulated Transmission Line (MITL) to the cathode needle; the shape is carefully engineered such that the applied magnetic field lines are nearly tangential to the conically-shaped conductor surface. This is done to prevent electron flow, from the large radius conical section and upstream of the diode region, from entering the AK gap region inside the magnet bore.

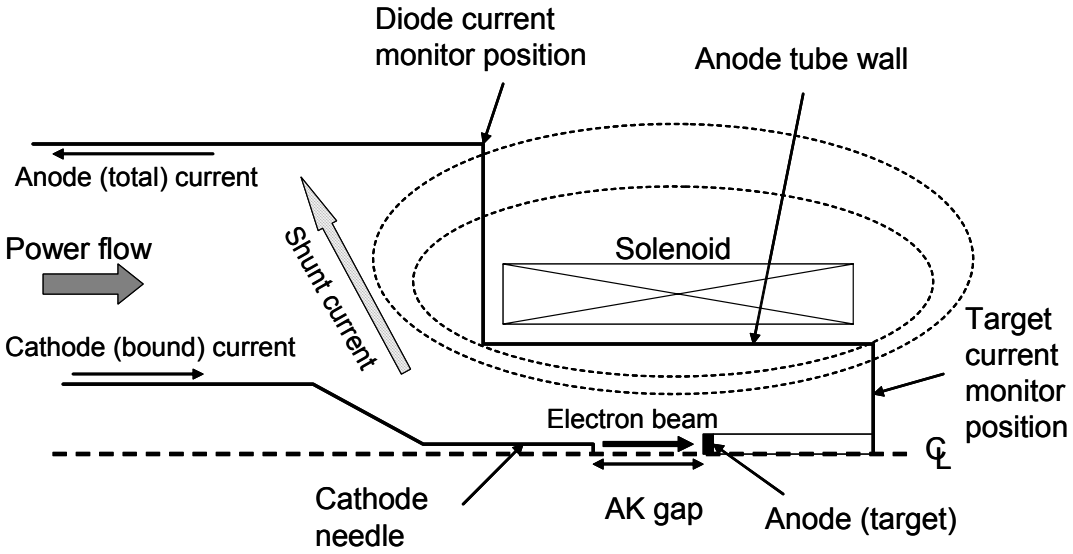


**Figure 1.** Schematic of immersed-$B_z$ diode, showing the cathode, anode/target, and solenoid.

The temporal impedance evolution of the immersed-$B_z$ diode should be characterized by a monopolar then bipolar current flow phase. In the limit of a uniform-current density beam propagating in a conducting pipe (the bore of the anode tube), the maximum current flow is described by the space-charge limit. The bipolar current phase begins as the electron beam bombards the anode and forms a plasma from which ions can be accelerated across the gap towards the cathode. The bipolar space-charge-limited current flow in cylindrical geometry is then[6]

$$I_b\ (\mathrm{kA}) \simeq 17\ \frac{\left(\gamma^{2/3}-1\right)^{3/2}}{1+2\ln\left(r_A/r_K\right)}\left(1-f\right)^{-1}, \qquad (1)$$

where $f$ is the fractional ion to electron beam charge ratio, $r_A$ is the radius of the anode tube, $r_K$ is the cathode needle radius, and $\gamma$ is the electron relativistic mass factor. The monopolar limiting current is obtained by setting $f = 0$ in Eq. (1). Previous computational modeling has shown that $f$ is typically of order 0.155, independent of ion mass.[6]

Once in the bipolar operating phase, the counter propagating electron and ion beams are ion-hose unstable.[6, 7, 8] For AK gap settings larger than the effective betatron wavelength, the instability grows rapidly and saturates. This increases the electron beam radius on target by an amount[6]

$$\varepsilon\ (\mathrm{mm}) \simeq \sqrt{2\gamma\frac{I_b(\mathrm{kA})}{17}}\ \frac{1.7}{B_z(\mathrm{T})}\quad , \qquad (2)$$

where $B_z$ is the magnetic field strength in Tesla. Enhanced growth and saturation of the ion hose instability has been observed in numerical simulations when cool, dense neutral atoms are ionized in the AK gap.[7, 9] At saturation of the instability, this effect can increase the electron beam radius by factors of 2 to 3, independent of the magnetic field strength.

Because the impedance of the immersed-$B_z$ diode is typically higher than that of the accelerator, much of the current supplied by the accelerator is shunted or diverted to the wall upstream of the diode, by the fringe magnetic fields as suggested by the shunt current path shown in Fig. 1. This feature actually allows diode current monitors (B-dot monitors) to be placed outside the confined diode region where there is typically more room to accommodate current monitor installations.

Experiments with two different diode configurations were conducted on the RITS-3 accelerator,[10, 11] a room temperature (RT) configuration and a cryogenic diode configuration. The RT diode was essentially the same diode used for experiments on SABRE,[3, 12] HERMES III,[13] and TriMeV.[5] In the RT diode configuration it was possible to locate additional current monitors, referred to as target current monitors, in the end wall of the diode region as shown in Fig. 1. However, because of design requirements and space constraints, it was not practical to install current monitors at that position in the cryogenic diode.

During the course of this study, the center conductor of the RITS-3 accelerator was replaced with a smaller diameter (higher impedance) design in order to achieve higher end-point voltages.[14] Therefore, we present sample data sets from both operating regimes: the original center

conductor (referred to as low-impedance operating mode) routinely achieved operating voltages of about 4 MV. The high-impedance operating mode used a smaller diameter center conductor to achieve operating voltages of about 5 MV. For all data sets presented in this report, we note the operating voltage to indicate which of these two accelerator modes (4 MV or 5 MV) is used. Figure 2 shows a drawing of the cryogenic diode attached to the RITS-3 accelerator with the small-diameter high-impedance center conductor (5 MV mode).

Figure 2 also shows the location of the current monitors at positions F and G. The diode voltage presented here is calculated from the anode and cathode currents measured at position F using the pressure balance formulation of Mendel.[15] The currents measured at position F were used because of concerns about the proximity of position G monitors to the diode and possible disruption of the power flow equilibrium by the applied magnetic field.

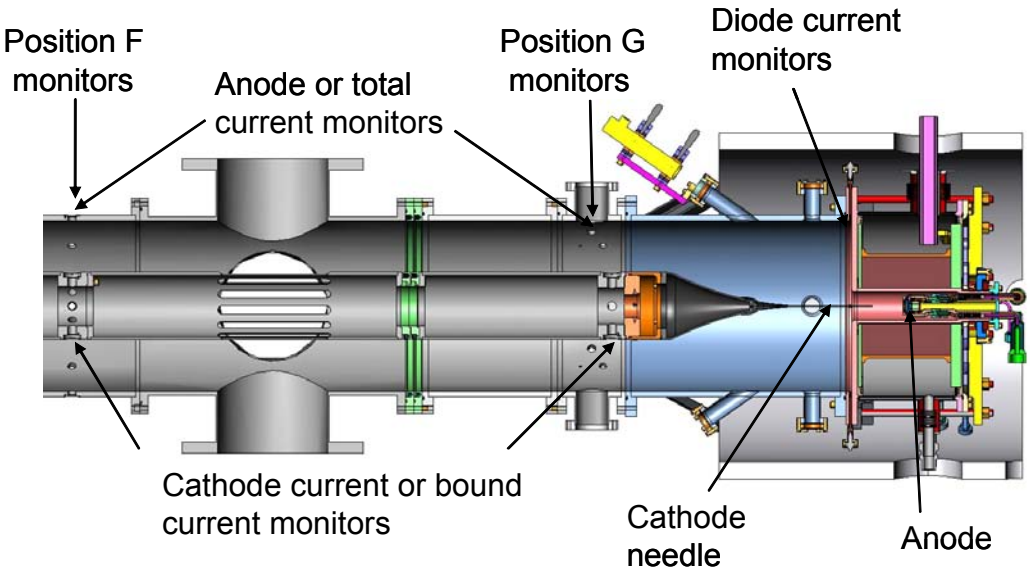


**Figure 2.** Schematic of the RITS-3 accelerator and transmission line and diode region showing positions F & G diode current monitors. The configuration shown is the 5 MV configuration with the high-impedance MITL and cryogenic diode.

This report is organized as follows. In Sec. II, baseline operating points of the immersed-$B_z$ diode are presented using electrical and radiographic measurements. The radiographic measurements are used to infer spatial and temporal information about the electron beam as it strikes a bremsstrahlung converter (a range-thin, high-atomic-number planar target). Representative data are given that highlight two broadly defined operating regimes; a nominal operating regime characterized as giving an impedance history that is approximately bipolar (≈V/I, where V is the diode voltage and I is the diode current) and a so-called "anomalous" impedance collapse regime where the total diode current "runs away", drawing total currents in excess of the bipolar limit, up to the full accelerator current. In Secs. III through V, the impact of parameter variations on the immersed-$B_z$ diode operating characteristics is presented. These variations offer some insight into the physics governing the impedance evolution of the immersed-$B_z$ diode and motivate a discussion presented in Sec. VI that includes a summary of

possible mechanisms that may contribute to the anomalous impedance collapse. Motivated by these observations, Sec. VII gives a list of possible future experiments that might help to identify the mechanisms leading to the impedance collapse. Following Sec. VII, a series of eleven appendices presents additional experimental data as well as some results from basic computational modeling of the immersed-$B_z$ diode.

## II. Baseline operating points

We introduce two diode "operating points" that, in general, characterize the observed operation of the immersed-$B_z$ diode. The first operating point describes the nominal behavior of relatively large diameter cathodes, namely, with diameters larger than or equal to 4.76 mm. The second operating point, describes the anomalous behavior of smaller cathode diameters typically less than 3.18 mm. Nominal diode operation with larger cathodes is characterized by relatively stable diode impedances. Anomalous diode operation with smaller cathodes is characterized by a fairly rapid rise in diode currents to levels well beyond those predicted in Eq. (1). This important effect with cathode diameter is discussed in more detail in Sec. III with supporting information also found in Appendices D, E, and G. Because the diode behavior and accelerator response are closely coupled, it is instructive to consider the operation of the combined system before focusing just on the physics of the diode. In Sec. IIA, we describe the operation of the combined system for normal and anomalous diode behavior at 4 MV for the RT diode configuration. In Sec. IIB, we discuss the operation of the combined system for nominal diode behavior at 5 MV for the cryogenic diode configuration.

### IIA. Nominal and anomalous operation at 4 MV

In Figs. 3 and 4 we compare and contrast the electrical and radiation production characteristics of an immersed-$B_z$ diode with a 4.76-mm cathode exhibiting nominal behavior (Fig. 3) to those of a 1-mm cathode exhibiting anomalous behavior (Fig. 4). Figure 3a shows that diode current and target current are equal and fairly stable rising quickly to around 13 kA and then gradually increasing with time to a peak of 23 kA. It is interesting to consider that in this mode the high diode impedance is shunting all of the current in the power flow sheath, and is also shunting a portion of the cathode current that was still "bound" to the inner MITL conductor at position F (total shunted current is the difference between the anode or total current and the diode current, ~ 120 kA). It should be noted that the accelerator currents have been shifted to the time frame of the diode. The diode voltage shown in Fig. 3b is calculated using the anode and cathode currents at position F using Mendel's pressure balance formulation.[15, 16] This technique estimates the diode voltage reasonably well, especially when the impedance of the diode is higher than the characteristic impedance of the MITL, i.e. diode current < "bound" cathode current. The calculated voltages used here do not try to accommodate the very early part of the power pulse during the vacuum precursor when the anode current equals the cathode current. Although it is fairly straight forward to calculate the voltage for this part of the pulse using the vacuum impedance of the MITL (see Appendix B) the difficulty comes when trying to combine the two phases (before and after electron emission) into a single voltage waveform. For simplicity and consistency we have chosen to use just the Mendel formulation for calculating the voltage throughout unless stated otherwise.

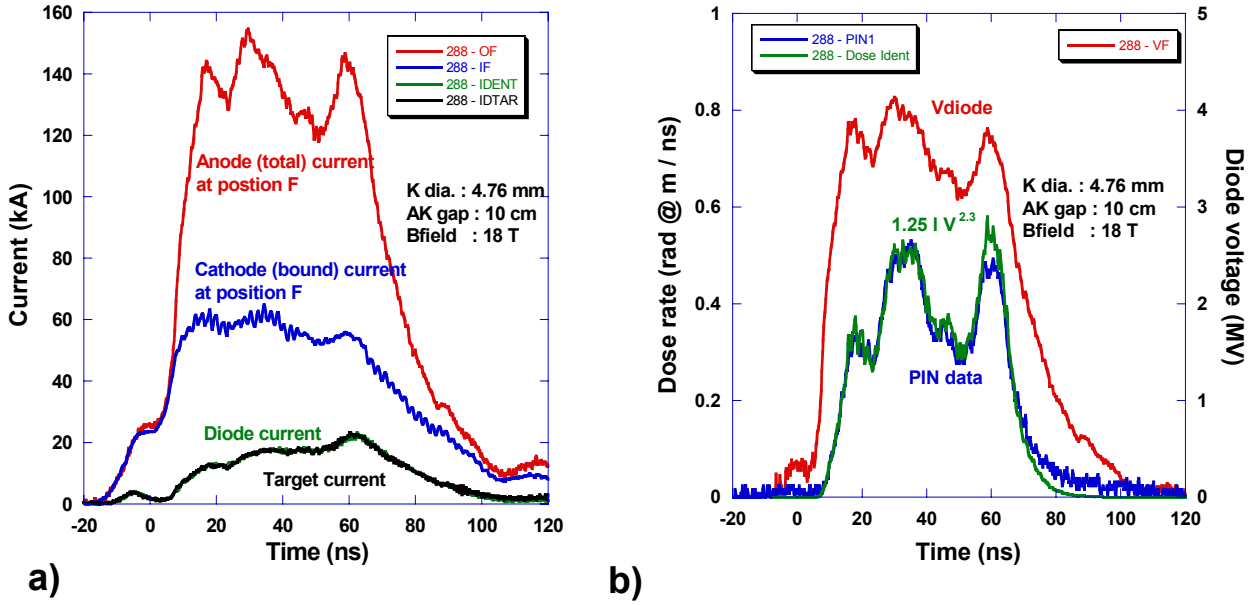


**Figure 3.** Measured and calculated electrical traces from a nominal well-behaved shot at 4 MV. Measured currents are shown in a) and the calculated voltage, calculated dose rate and measured dose rate (PIN data) are shown in b).

Besides fairly stable diode currents and impedances, the other characteristic of large cathodes is good dose production. One metric of good dose production is the agreement between the calculated dose rate expected from scaling with current and voltage based on a radiographer's equation[17] and the measured dose rate (PIN data) as shown in Fig. 3b. It should be noted that although the constant used to obtain the fit shown in Fig. 3b is lower than that determined in [17] (1.25 $IV^{2.3}$ versus 2 $IV^{2.3}$), it does appear to follow the scaling with $IV^{2.3}$ for most of the pulse, indicating that the dose production lasted as long as the applied voltage pulse. The difference in the scaling constant is not understood at this time.

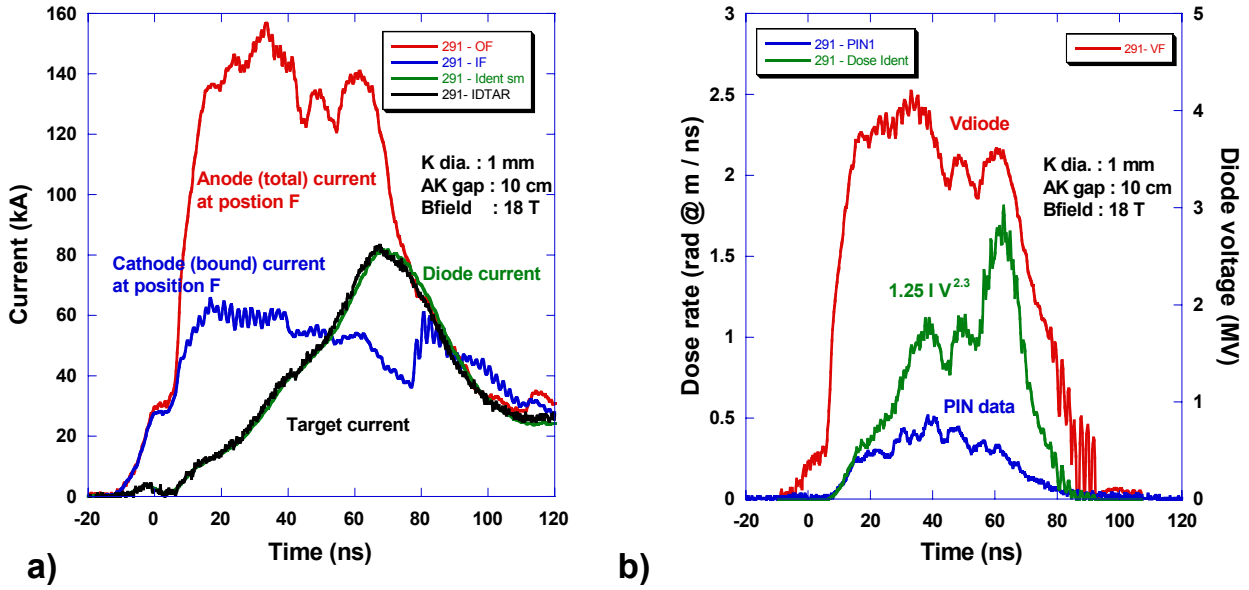


**Figure 4.** Measured and calculated electrical traces from a shot at 4 MV with dramatic impedance collapse. Measured currents are shown in a) and the calculated voltage, calculated dose rate and measured dose rate (PIN data) are shown in b).

Measured dose rates at 4 MV presented here were obtained with a positive-intrinsic-negative or PIN diode. Interaction of the incident x-ray photons with the PIN diode creates charge in the PIN device through ionization (creation of electron-hole pairs). The amplitude of the PIN signal is directly proportional to the amount of radiation and resulting free charge created in the device. The PIN diode (PIN1) was placed approximately 7.5 degrees off-axis at a distance of ~ 80 cm from the source or high-atomic number target. For every shot the dose rate was calibrated to on-axis thermoluminescent dosimeter (TLD) measurements placed approximately 75 cm from the source (i.e., the integral of the dose rate measurement is set equal to the TLD measurement.) At one point in the experiments, PIN diode measurements were placed on-axis and no appreciable difference was seen between the on-axis (PIN4) and off-axis measurements when normalized to the TLD measurement.

Figure 4a shows the current traces for the anomalous or poor diode operation observed with small cathodes, in this case a 1-mm diameter cathode. The very early part of the pulse, for $t < 20$ ns, is similar in shape and magnitude to the larger cathode results, but then the current rises steadily to a peak value slightly above 80 kA. At this current level, which is higher than the bound cathode current, current is being drawn into the diode from electrons flowing in the MITL power flow gap. The measured diode current and target current are nearly identical indicating that no current is being lost to the anode tube wall. This is an important result suggesting that the impedance loss mechanism is confined to the AK gap region and is not a result of some parasitic load or loss to the anode tube wall.

This increase in current, well above what is expected from classic bipolar operation [Eq. (1)], is not accompanied by an associated increase in dose production as shown in Fig. 4b, where the measured dose rate is substantially below the calculated dose scaling that gave such good agreement for the 4.76-mm cathode. It is also interesting to note that the measured and

calculated dose rate separate very early in time (t = 16 ns) suggesting that the transition to this anomalous mode of operation occurs at this time. This transition occurs at roughly the time the diode current has reached its monopolar value of 12 kA for 4 MV. Although some of this difference may be attributable to the lower voltage late in the pulse when the diode current exceeds that of a matched load (load current = bound cathode current), this is not the case for the first two-thirds of the pulse where the diode current is still less than the upstream cathode current. This large discrepancy between the expected calculated dose and the measured dose must be due to either space charge created in the gap or heating of the electron beam (high transverse velocity). Electrons born in the gap due to some anomalous charge creation mechanism would have only one-half the accelerating potential of electrons being accelerating across the entire gap and therefore yield 5x smaller dose based on the expected power law scaling with voltage (energy), $\alpha V^{2.3}$. Although we can expect an increase in ion current during this phase, the fraction of ion current will be roughly constant and small compared with the electrons. This possibility of charge created in the gap is consistent with the steady rise in diode current throughout the pulse because without charge creation in the gap the current should ultimately reach a steady state current as predicted by theory and simulations (Appendix G).

### IIB. Nominal operation at 5 MV

Characteristic electrical and radiation results for nominal operation are shown in Figs. 5 and 6 for a 4.76-mm cathode operating at 5 MV. Figure 5a shows that the diode current rises quite rapidly to 20 kA and then rises slowly and steadily to a plateau slightly above 40 kA. Although significantly higher than 23 kA obtained at 4 MV shown in Fig. 3a, the diode current is still lower than the bound cathode current, indicating that the diode is shunting all of the power flow current as well as some of the bound cathode current. As mentioned previously the cryogenic diode configuration did not have target monitors and although nothing absolute can be said about the current loss in the diode, it is assumed based on the results presented in Sec. IIA, all the diode current is reaching the target. In Fig. 5b the measure dose rate is compared to the calculated dose rate quantity, $0.9*IV^{2.3}$. The measured dose rate agrees quite well with the calculated dose rate for the first half of the pulse with some slight discrepancy during the second half until the end of pulse when they overlay again as the dose production falls off as the voltage falls off. Here a multiplier of 0.9 was used to give the best fit with the first half of the pulse. This is even lower than the factor of 1.25 used for the fit shown for 4 MV operations shown in Fig. 3b. This difference may have been a result of additional attenuation due to thicker stainless steel hardware used for the beam stop, debris shields and vacuum walls used on the cryogenic diode configuration vs. the RT diode configuration, (0.45” vs 0.26”).

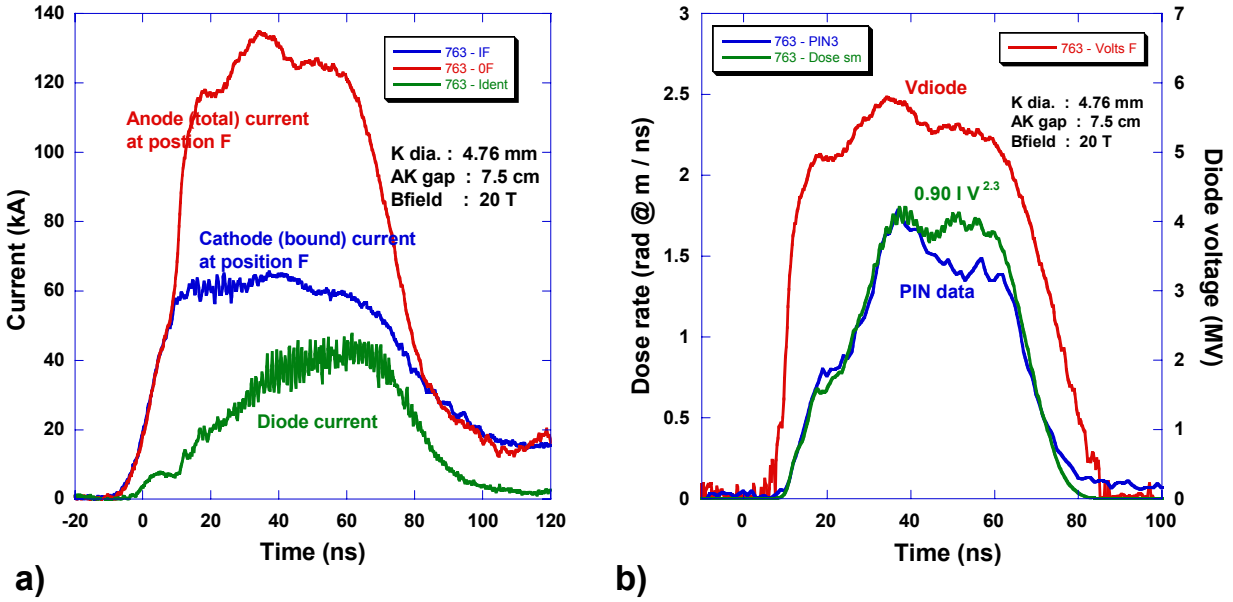


**Figure 5.** Measured and calculated electrical traces from a nominal well-behaved shot at 5 MV. Measured currents are shown in a) and the calculated voltage, calculated dose rate and measured dose rate (PIN data) are shown in b).

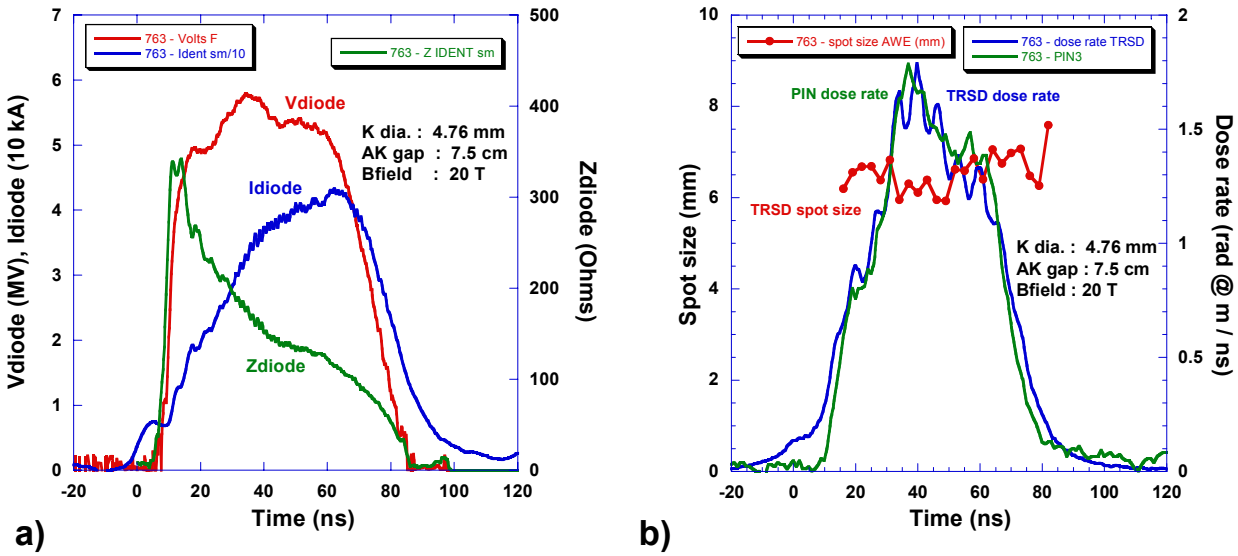


**Figure 6.** Measured and calculated electrical traces from a nominal well-behaved shot at 5 MV. Calculated voltage, calculated impedance and measured current are shown in a) and measured dose rates and measured time-resolved spot size are shown in b).

Although diode currents will primarily be used to compare the electrical behavior of different configurations and effects presented below, it is expedient to consider the diode impedance because it basically normalizes out variations in diode current due to diode voltage variations.

Figure 6a shows the calculated diode impedance for this nominally well-behaved diode at 5 MV. The diode impedance starts out just above 300 Ohms briefly during the rise of the voltage pulse but then decreases steadily before it levels out around 135 Ohms for about 15 ns and then falls off again at the end of the voltage pulse.

One of the diagnostics that was not available during the operation of RITS-3 at 4 MV but was available during the experiments conducted at 5 MV was the Time Resolved Spot Diagnostic (TRSD).[18, 19] Figure 6b shows that the dose rate measured with the on-axis TRSD compares very well with dose rate measured by the PIN diode which was 7.5 degrees off-axis. There are some slight differences but overall the duration and shape are the same. Figure 6b also shows that the spot size for this nominally well-behaved diode remained fairly constant throughout the pulse varying between 6 and 7.5 mm. The spot size definition used throughout this work unless otherwise stated is the AWE definition obtained using the 0-100% extrapolation of the edge spread function (ESF).[2] The ESF is obtained by analyzing the distribution of the penumbral shadow cast by a two-axis tungsten rolled edge (radius = 0.5 m). As shall be discussed below the time-integrated spot size measured with the TRSD was in good agreement with the time-integrated spot size from the film diagnostic, 6.3 mm and 6.1 mm respectively.

## III. Cathode diameter variations

The potential of the immersed-$B_z$ diode as a radiographic source is the expected scaling of spot size with cathode diameter and that small cathodes should produce correspondingly small spot sizes (see Appendix G). Unfortunately, as noted above, the behavior of small cathodes is generally characterized by low impedance and relatively poor dose production. In addition, the resulting spot size is much larger than expected. Although voltage prepulse can cause deleterious effects in pulsed power devices, prepulse is not believed to be responsible for the anomalous diode behavior for small cathodes reported here. The reasoning for this is two-fold. Prepulse was controlled and limited in these experiments to < +/- 5 kV. Further, experiments were purposely conducted without prepulse suppression (yielding prepulse levels of 100 – 200 kV for 200 ns) and the diode behavior was fundamentally different from those presented here with low prepulse (see Appendix B for additional details regarding shots with high prepulse levels). Results presented here were obtained with the cryogenic diode at 5 MV. Even though the cryogenic diode was used, the results presented in this section were obtained with a standard room temperature Ta converter optimized for dose production at 5 MV (i.e. thickness = 0.025" or 1/3 of an electron range at 5 MV). Electrical and radiation results are presented for 1, 2, and 4.76-mm cathodes operating at 20 T with a 7.5-cm AK gap.

Figures 7a and 7b show dramatic differences in diode current and impedance between the 4.76 mm cathode and the smaller cathodes. It is interesting to note that the early time behaviors up to t = 20 ns are surprisingly very similar but then the currents for the 1 and 2-mm cathodes rise rapidly to peak currents in excess of 120 kA and the associated impedances decrease steadily and rapidly compared to the impedance of the larger cathode. This anomalous electrical behavior is accompanied by low dose production as shown in Fig. 8a where the dose rate waveform for the smaller cathodes have lower amplitudes and duration than for the 4.76-mm cathode case.

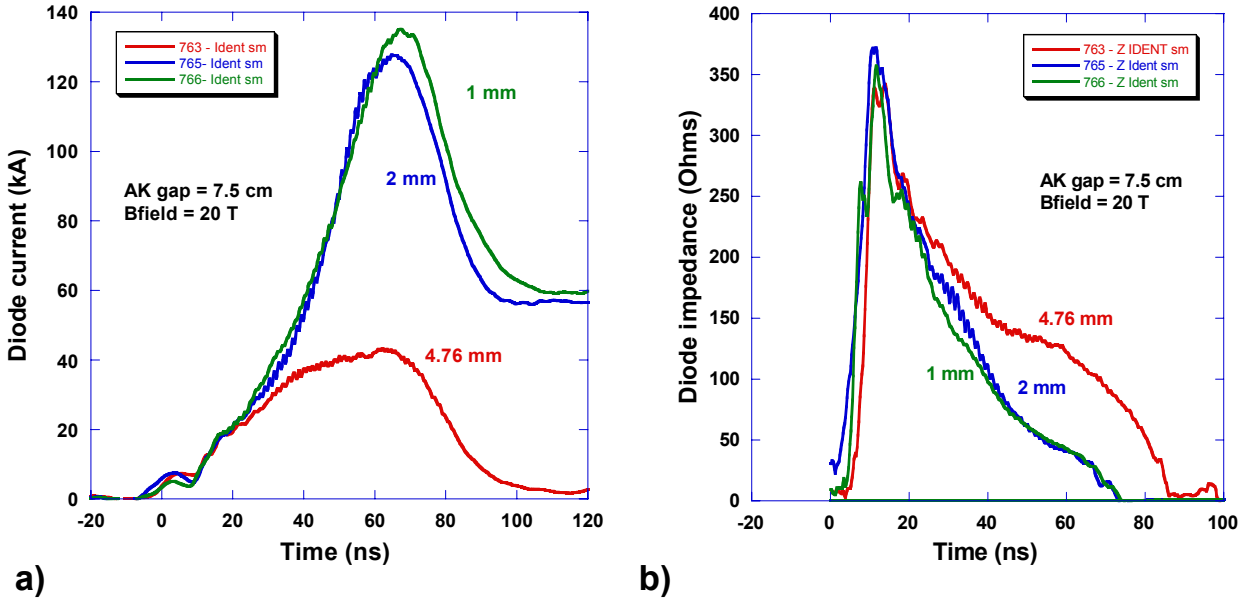


**Figure 7.** Effect of cathode diameter on diode performance for 1, 2, and 4.76-mm diameter cathodes at 5 MV, a) measured diode current and b) calculated impedance.

The time resolved spot size measurements for the three cathode sizes are shown in Fig. 8b. The spot size for all cases starts out at roughly the same value. The spot size for the 4.76-mm cathode remains fairly constant while the spot size increases steadily for the smaller cathodes. What is somewhat surprising about these data is that unlike the TriMeV results,[5 20] there is no indication that the spot sizes for the small cathodes were ever small. The TriMeV results (at 3 MV) showed that there was a brief time, ~ 5 ns, when the spot size was very small, 1.5 – 2.5 mm (for cathode diameters between 0.5 and 2 mm), before growing quickly to 3.5 and 4 mm. The spot sizes shown for 1 and 2-mm cathodes never approach either of these values. Either the diode on RITS-3 is behaving dramatically different and there is no period when the spot is small – or the TRSD diagnostic used on RITS-3 was unable to capture this early time behavior when the spot was relatively small. Previous results on Hermes III[13] had suggested that the spot size grew rapidly as the diode transitioned from nominal operation to anomalous operation with accompanying impedance collapse. Although it is still generally believed that the same mechanism that causes the impedance loss in small cathodes is also responsible for the loss in dose production and large spot, there is no direct correlation observed in Figs. 7 and 8 that would necessarily support the previous observations from TriMeV and Hermes III.

The corresponding time integrated dose and spot size from Figs. 8a and 8b are shown in Figs. 9a and 9b as a function of cathode diameter. The results shown in Fig. 8a emphasize loss in dose as the cathode diameter is reduced below 4.76 mm. Similar results have been observed by other experimenters and are discussed in Appendix D.

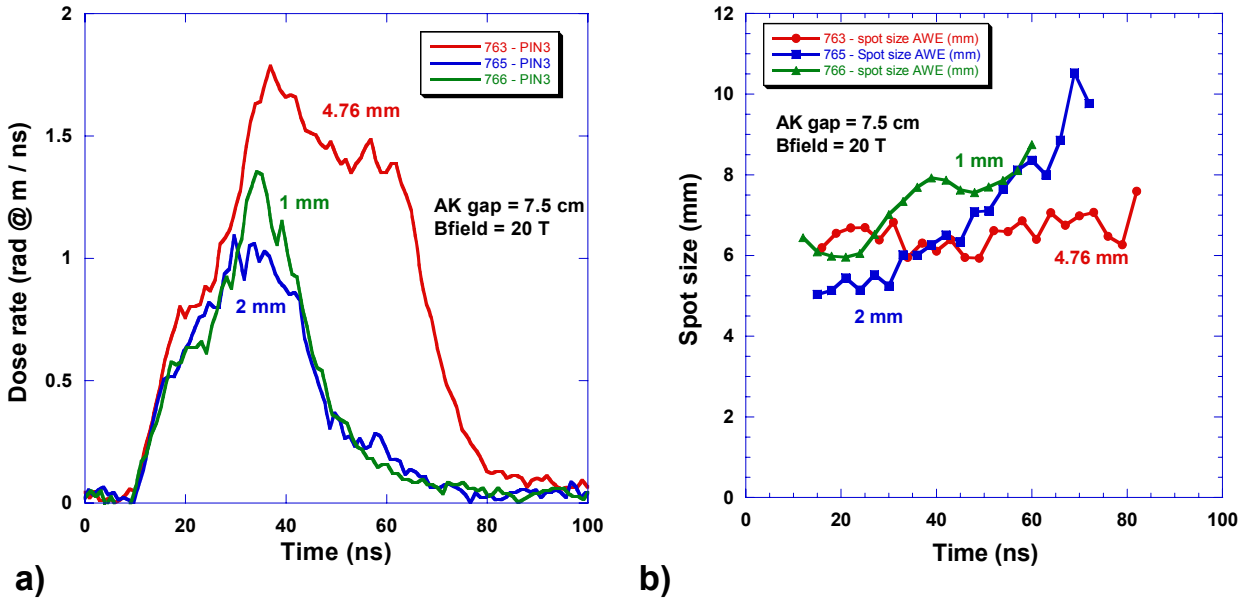


**Figure 8.** Effect of cathode diameter on diode performance at 5 MV for 1, 2, and 4.76-mm diameter cathodes, a) measured dose rate and b) time-resolved spot size.

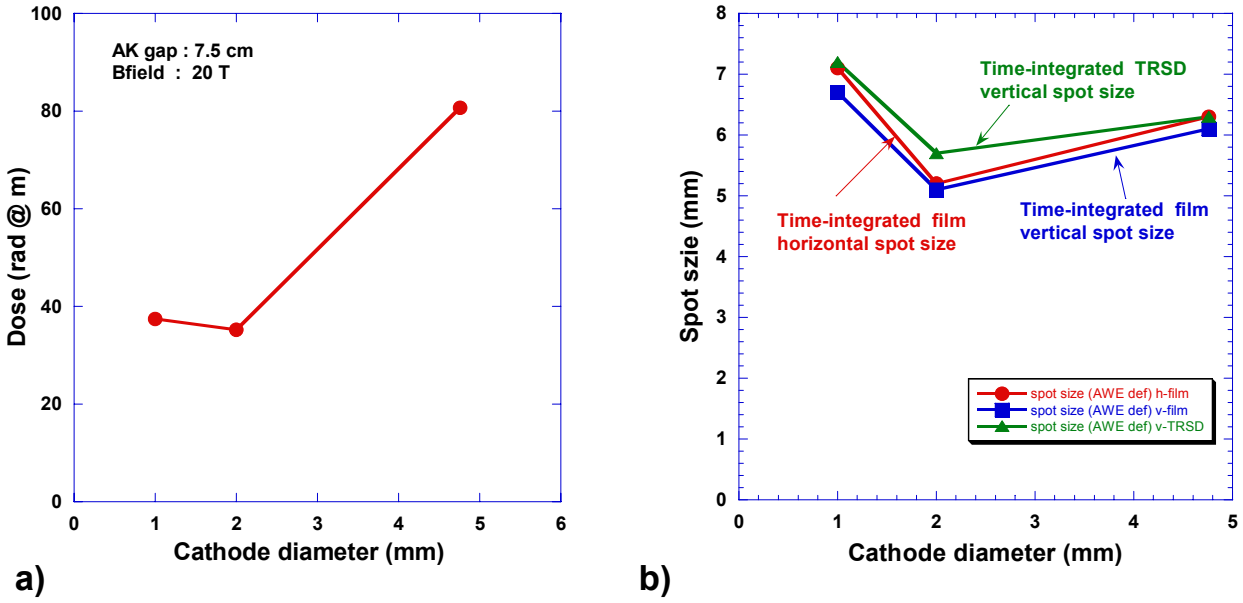


**Figure 9.** Time-integrated radiographic measurements as a function of cathode diameter at 5 MV, a) measured total dose and b) horizontal and vertical spot size for film compared to vertical spot from TRSD.

The time-integrated TRSD results (green triangles and line) are shown in Fig. 9b. The time-integrated film spot size for the horizontal (red circles and line) and vertical (blue squares and line) directions are also shown in 9b. All these diagnostics show similar trends and suggest that over this range of cathode diameters the spot size was fairly independent of cathode diameter.

The similarity in time-integrated film spot sizes for the horizontal and vertical directions indicate the spot was fairly symmetric. During these experiments the TRSD only provided vertical spot size information. The agreement between the vertical time-integrated film results and TRSD time-integrated results shown in Fig. 9b support the validity of the time-resolved results shown in Fig. 8b.

Because of its importance, time-integrated spot size results are often the only metric presented when discussing radiographic performance. However, when trying to gain further insight it is sometimes instructive to consider the associated edge spread function (ESF) and its derivative the line spread function (LSF).[21] Horizontal ESF and LSF for the different cathode diameters are shown respectively in Figs. 10a and b. Note that the peak intensity for each profile has been normalized to unity. There are only slight differences in either the ESF or LSF profiles. The LSF for the 2-mm cathode does reflect a slightly smaller spot with a smaller, brighter core. This however is not true of the 1 mm LSF that looks very similar to the 4.76-mm LSF.

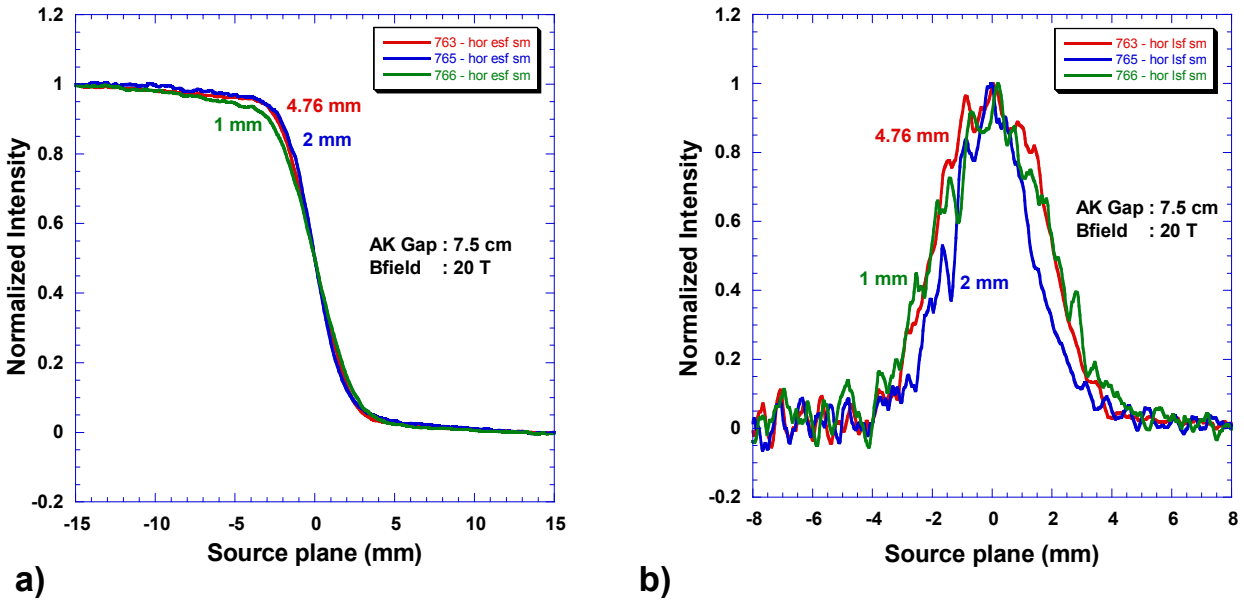


**Figure 10.** Time-integrated radiographic measurements as a function of cathode diameter at 5 MV, a) horizontal ESF from film and b) horizontal LSF from film.

It is noteworthy that sometimes it is possible to see substantial difference in the LSFs for similar size spots (see Appendix B where the LSF from a large cathode with low prepulse is compared to small cathode with high prepulse). These differences can sometimes give insight to the underlying diode physics. Unfortunately, comparing the LSFs shown in Fig. 10b did not reveal much additional information. Both the spot size and spot profile are close to expected values and shapes for large needles > 4.76 mm based on numerical and analytical models as presented in Appendix G. Based on those models one would expect smaller spots and narrower LSFs for the 1 and 2-mm diameter cathodes. The mystery remains as to why the small cathodes result in such large spot sizes with broad LSFs.

## IV. AK gap variation

Earlier experiments on Hermes III[13] had suggested that it was possible to control the impedance of the immersed-$B_z$ diode by making the AK gap larger. The data for these experiments was never formally documented and because this effect is believed to be important, an AK gap survey was conducted on RITS-3 at 4 MV. The AK gap was varied from 2 to 30 cm using a 1-mm cathode. Changes in AK gap were primarily achieved by keeping the anode position constant near the peak field of 18 T and changing cathode tip position by simply shortening the length of the cathode. This was basically true for all the gaps except the 30-cm gap in which the anode was moved back by 12.5 cm from its nominal position, which reduced the field at the anode to 12.3 T. Although this may obfuscate the results slightly, the data is included here for the sake of completeness. (Note that anode for the 20-cm gap was actually moved back from its nominal position by 2.5 cm but the field was only reduced to 17.7 T.)

Figures 11a and 11b show that there is a large effect on the diode current and impedance with AK gap. Small gaps are characterized by very high currents and very rapid loss of impedance. As the gap is increased the diode current rises more slowly and the impedance falls less rapidly, but even for the largest gaps the rise in current and fall in impedance is continuous.

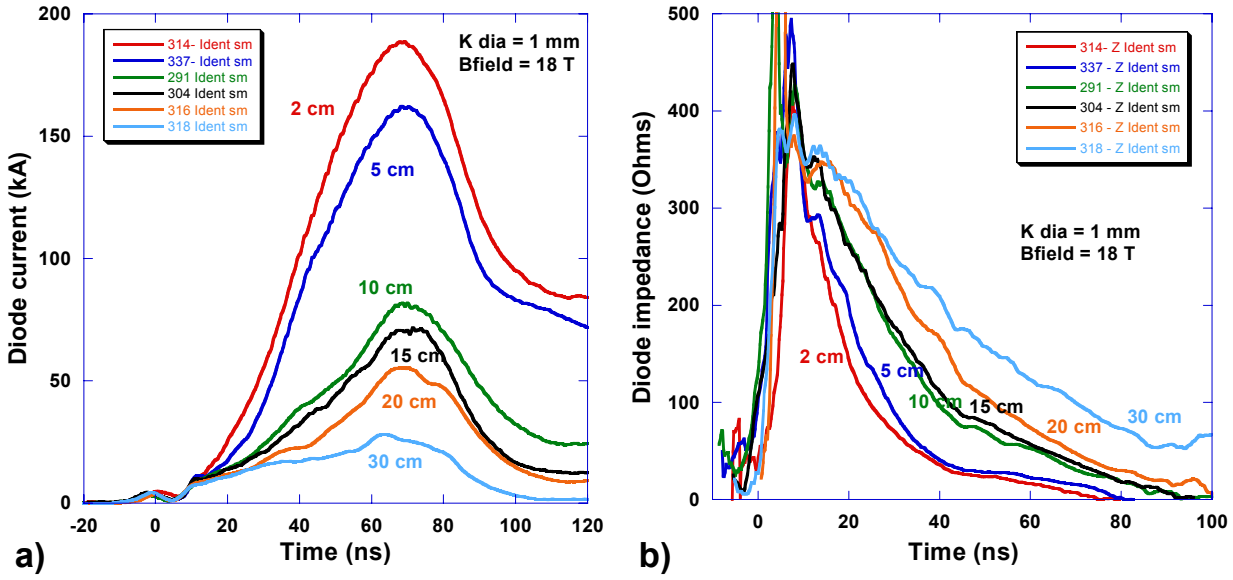


**Figure 11.** a) Diode current and b) diode impedance as a function of time for AK gap settings between 2 cm and 30 cm at 4 MV.

There is also a large effect on the dose rate production with AK gap size as shown in Fig. 12a. Very small gaps (2 and 5 cm) give very short and small amplitude radiation pulses. There is a large change in the radiation pulse between 5 and 10-cm gaps and then a more gradual increase in magnitude and duration for gaps beyond 10 cm. Note the dose rate data for shot 318, the 30-cm gap, was not available. As with the cathode diameter, the AK gaps with the worst electrical behavior – high currents and low impedance – tend to yield the lowest dose production. Figure

12b shows the effect on total integrated dose and reflects the time-resolved dose rate data observed in Fig. 12a. There is a rapid improvement in dose production at first as the AK gap increases and then the improvement tapers off at large gaps. Although the total dose measurement for the 30-cm gap is shown in Fig. 12b, the dose rate waveform for the 30-cm gap is not included in Fig. 12a because no time-resolved results were obtained due to data acquisition problems. Figure 12b also shows that the spot size increases as the AK gap increases for this small 1-mm cathode.

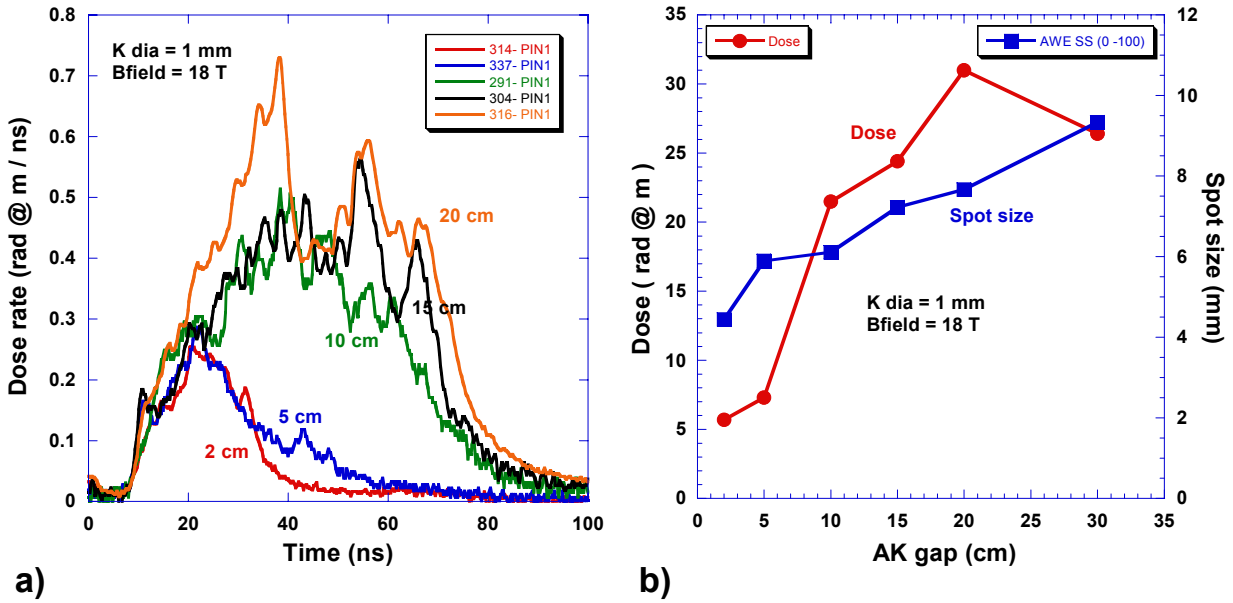


**Figure 12.** a) Dose rate as a function of time and b) time-integrated dose and spot size measurements at 4 MV for gap settings between 2 and 30 cm.

At one time in the development of the immersed-$B_z$ diode it was thought that if one could control the impedance of the diode that that would lead to improved spot sizes. That was not the case here where we were able to improve the impedance behavior and dose production of the diode with larger gaps, but these improvements were unfortunately accompanied by ever increasing spot sizes. Small needles with large gaps act similarly to large needles with smaller gaps; they have fairly good impedance behavior and dose production but result in fairly large spot sizes.

As mentioned above, experiments on Hermes III also saw an effect on the impedance behavior with AK gap. The time that it took the impedance to fall below some nominal value was defined as the impedance lifetime. This "impedance lifetime" was observed to vary directly with the AK gap in Fig. 13. The slope of this plot gives an indication of the relative speed (~ 1 cm/ns) at which the impedance of the diode was affected. This speed suggests that something other than classic gap closure produced by thermal electrode plasmas with typical expansion velocities of 1-2 cm/μs are responsible for the impedance loss observed for the immersed-$B_z$ diode. This observation lead to the conjecture that ion stripping of non-protonic ions emitted from the anode might be responsible for the impedance behavior of small cathodes. Figure 13 shows a plot of time at which the impedance equals 200 Ohms as function of AK gap. These data were taken

directly from Fig. 11b. The effective speed is the inverse of the slope of this curve and is calculated to be 1.2 cm/ns. Ideally there should not be any effect on impedance with AK gap for a cylindrical diode operating in a classic bipolar mode for AK gaps that are few times larger than the bore radius. Thus the rate at which the impedance is affected seems to be relevant to better trying to understand and model the anomalous behavior observed. Further implications of the effect of AK gap on diode behavior are discussed below in the discussion section.

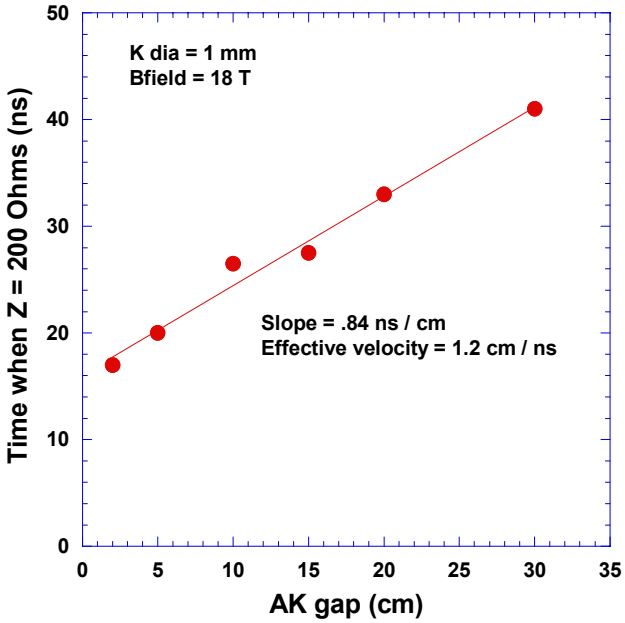


**Figure 13.** Effective gap closure speed estimated from the impedance histories shown in Figure 11b.

## V. Anode material variations

The rapid impedance collapse that is consistently observed for the smaller diameter cathodes (≤ 3.18 mm) leads one to consider the dynamics and composition of electrode plasma formation. The influence of anode plasma constituents and their acceleration into the AK gap was examined by varying the anode materials. The question of surface contaminates clouds the interpretation of the results for all of the RT anodes used in this study. Improved control over the anode plasma constituents was attempted by applying *in situ* coatings to anode target substrates under cryogenic conditions. A cryogenic coating system was engineered that would enable a variety of noble or otherwise inert gases to be coated directly onto the anode substrate. The system was developed to operate under vacuum, such that the accelerator could be fired as soon as the coating process could be completed. An overview of the coating system is presented in [22]. A detailed description of the engineering, testing, characterization, and experimental application of this system is presented in Appendix H.

As mentioned above the basic premise for developing cryogenic anodes was an attempt to modify the behavior of the diode by controlling and limiting the anode plasma ion species. It was conjectured that the impedance behavior observed for untreated, room temperature anodes might be due to charge creation in the AK gap. Two prevailing theories for charge creation by anode plasmas evolving from an untreated anode with various hydrocarbon contaminants are 1) avalanche ionization due to stripping of non-protonic ions because of ion-ion collisions, e.g. carbon and 2) recombination and subsequent reionization of protons.[23] Originally, it was hoped that the cryogenically treated anode could be designed to challenge the first theory by eliminating the non-protonic contaminants by coating the anode with pure frozen hydrogen ($H_2$) or deuterium ($D_2$). Similar techniques had been applied successfully to ion diodes in creating high purity ion beams.[24, 25,] Although we were successful in demonstrating the capability to coat out thick uniform layers ( > 100 microns) of $H_2$ and $D_2$ , the beam experiments on RITS-3 behaved anomalously and shorted out very quickly at modest magnetic fields > 4 T. It is speculated that some mechanism related to the pulsed magnetic field liberated gas into the diode region during the rise of the magnetic field (time to peak ~ 15 ms) and caused the diode to short when the main accelerator pulse arrived at the diode. These results are discussed in more detail in Appendix I. Additionally, some interesting results including preliminary spectroscopic measurements were obtained at 4 T for frozen $D_2$ and other cryogenic anodes including Ne and are discussed in Appendices I and J.

A separate set of experiments were designed to test the role that hydrogen contaminants (protons) play in the behavior of the diode by basically trying to eliminate them using pure frozen coatings of Xe and comparing their behavior to untreated room temperature anodes. In this section, experimental results for six different anode material and cryogenic treatments are presented, two at room temperature (RT) - one Ta and one stainless steel (SS), and four cryogenically treated anode experiments – one where the anode was cooled but not purposely coated (LHe-cooled SS) and three Xe-coated experiments where the pumpout delay time was varied to try and reduce or affect the amount of recontamination of the front surface by limiting the amount of time that the frozen Xe surface was exposed to the other vacuum constituents and contaminants. The pumpout delay time ($t_d$) is defined as the amount of time prior to the shot when the flow of Xe gas was turned off. Results are presented for pumpout delay times of 0, 45, and 90 seconds. For the 0-second delay experiment, the Xe gas was never shut-off and continued to flow during the accelerator pulse.

Figure 14 shows the effect of these different anode materials and treatments on the diode current and diode impedance. Figure 15a shows the time dependent measured dose rate for these experiments and Fig. 15b shows the resulting time-integrated spot size. The only significant effect on the diode behavior observed was for the experiment where the Xe gas was allowed to flow through the accelerator pulse (Xe $t_d$=0). Although little difference in diode current is observed early in time in Fig. 14a, it appears that the diode current "hangs-up" late in time possibly suggesting the diode has shorted out. This effective shorting out may also explain the shorter and lower radiation pulse observed in Fig. 15a. It should be noted that the diode current remains high late in time for all these shots and may indicate that some shorting is occurring and that the Xe $t_d$=0 case, might only be an extreme example.

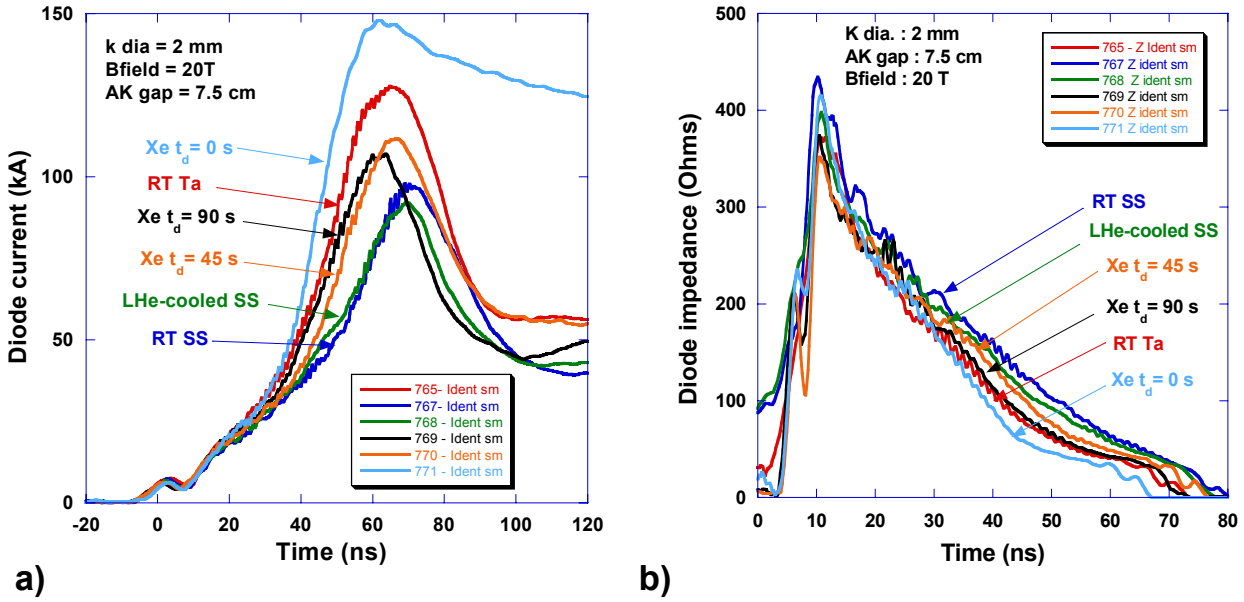


**Figure 14.** Effect of anode material and frozen Xe coating process variations at 5 MV on a) diode current and b) diode impedance.

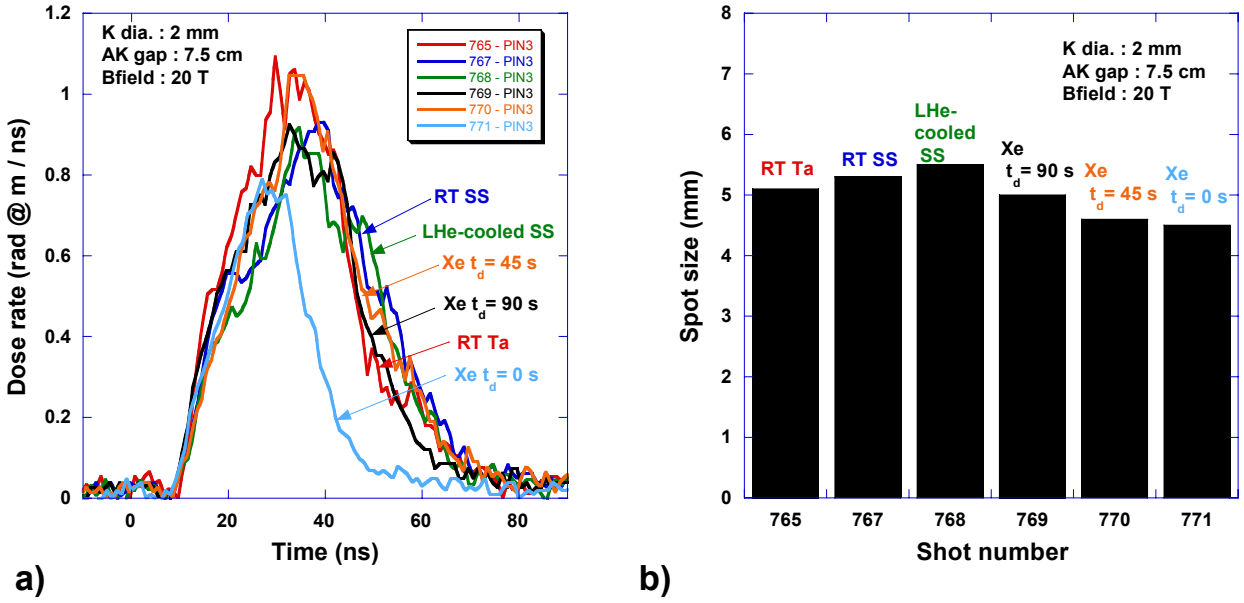


**Figure 15.** Effect of anode material variations and frozen Xe coating process variations at 5 MV on a) measured dose-rate and b) spot size.

Proton activation of the cathode needles was used to quantify the energetic proton content of the beam. The cathode activation is routinely measured after each experiment on RITS-3 as part of the radiation health physics safety protocol. In this case, it was used as a diagnostic. Titanium alloy (Ti-6Al-4V) cathode needles were chosen because of titanium's susceptibility to activation

by protons at these energies, ~ 5 MV.[26] When considering the data, it should be kept in mind that the high threshold of the reaction does not rule out protons of lower energy that would be expected if not born on the anode. Figure 16 shows that there was a significant reduction in the level of activation for all the cryogenically-treated anodes, but especially for the Xe-coated experiments. However, the slight increase in activation for the $t_d$= 0 is unexpected because one would have thought it would have the least contamination since Xe was being frozen on the anode at the estimated equivalent rate of 180 monolayers/second all the way through the accelerator pulse [Appendix H].

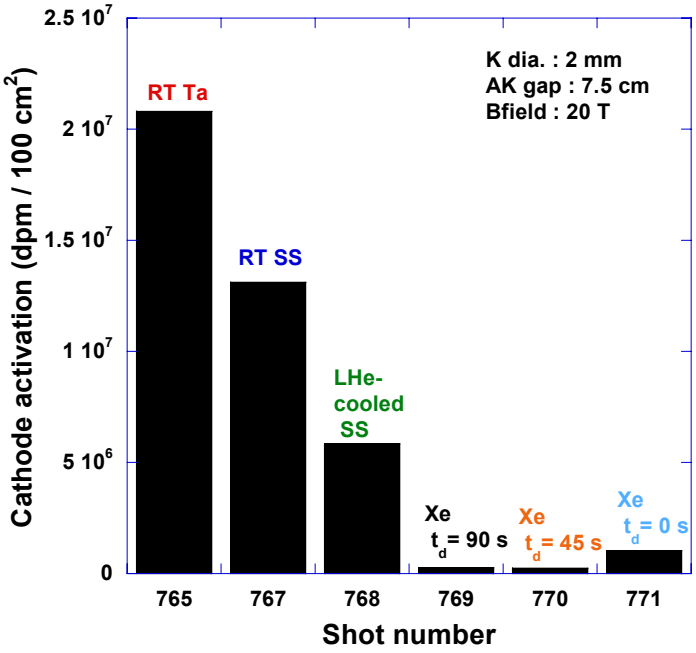


**Figure 16.** Effect of anode material and Xe coating process at 5 MV on activation of cathode needle.

A possible explanation why the activation is lower for the LHe-cooled SS than the RT SS could be that the LHe-cooled SS anode pumps non-hydrogenous species from the vacuum that do not readily stick to RT surfaces, e.g. $N_2$, $O_2$, $CO_2$. The difference between RT Ta and RT SS might be simply due to the difference in materials and the fact that Ta is known to be fairly good getter of hydrogen.

Irrespective of the absolute proton content of the beam there does not appear to be any correlation between the relative proton content of the beam and the observed impedance behavior of the diode. Figure 14b shows that the impedance histories for the Xe-coated experiments with the lowest activation ($t_d$ = 45 and 90 seconds), lie between those impedance traces for the RT Ta and RT SS which both had the highest and second highest energetic (> 5 MeV) proton content respectively.

## VI. Discussion

Intense flash x-ray radiographic specifications require, in general, smaller electron beam spot sizes, which drive the need for smaller electron beam sources.[1] The promise of immersed-$B_z$ diodes as potential radiographic sources has always lay in the assumption that the spot size would basically scale with cathode diameter and that 1-mm diameter cathodes would be able to achieve spot sizes approaching 2 mm (Appendix G). Early work[3, 12] suggested that immersed-$B_z$ diodes with small cathodes showed some promise as potential radiographic sources capable of producing small spot sizes, 1 – 2 mm diameter, with large doses, ~ 1000 rad @ m. Those results were based on a very limited set of experiments conducted on the SABRE accelerator that had a short pulse (FWHM of 20 ns).[3, 12] Results presented in this report suggest an anomalous impedance collapse mechanism is limiting the radiographic performance (spot size and dose production) of the immersed-$B_z$ diode at RIT3-3 operating parameters (4-5 MV, 70 ns FWHM voltage pulse).

We have identified two basic operating regimes that are primarily a function of the cathode diameter. Relatively large diameter cathodes ($\geq$ 4.76 mm) with sufficient gap sizes and large magnetic fields exhibit nominal diode behavior with electrical and radiographic performance consistent with results expected from analytical modeling and numerical simulations. Small cathodes ($\leq$ 2 mm) exhibit anomalous behavior with very rapid impedance collapse and loss of dose. Parameter explorations in AK gap and anode material variations so far have not resulted in a small cathode operating point with the desired diode performance, (i.e. small spot size with high dose). However, these parameter variations (and additional studies presented in the Appendices) provide some insight into the physics that govern the observed anomalous diode behavior and suggest studies for future work (which are given in Sec. VII).

It is generally assumed that the anomalous behavior of the immersed-$B_z$ diode, i.e. rapidly rising diode currents and collapsing impedance, must be due to charge creation in the gap. While other high power diodes may suffer from gap closure due to the thermal expansion of electrode plasmas either because of their planar geometry or small physical size, e.g. ion diodes[27,28] and rod pinch diodes[29,30], the immersed-$B_z$ diode is assumed to be impervious to impedance collapse due to AK gap closure from thermal plasma expansion because of its unique coaxial geometry where the governing impedance is basically independent of the size of the axial AK gap (Eq. 1).

Possible sources for charge creation in the gap discussed in the previous section are avalanche ionization of non-protonic ions due to ion-ion collisions and recombination and reionization (charge exchange) of protons born at the anode. The other possible sources are fast moving cathode or anode plasmas that are somehow able to cross their respective acceleration sheaths and get out into the gap. Because we have been unable to effect a single change that moved the diode behavior towards the ideal, it is impossible to absolutely eliminate any of these possibilities. Similarly, because of the limitations of nuclear activation, especially its energy threshold dependence for detecting protons below 4-5 MeV, it is impossible to determine whether or not lower energy protons might still be present or play a significant role in the diode physics or contribute to the observed anomalous behavior for small cathodes. For example, ionization of a neutral hydrogen atom in the gap that is subsequently accelerated to the cathode would have approximately half the total accelerating energy of a proton formed at the anode and

therefore probably would not be detectable by our nuclear activation diagnostic. However, irrespective of this limitation we believe it is still possible to seriously call into question both the charge exchange theory and avalanche ionization and point instead to a mixture of anode and cathode plasma physics as being responsible for the effect that govern the measured impedance.

The basic premise of the charge exchange theory is that protons accelerated from the anode interact with a layer of neutral gas that has been desorbed from the anode. These accelerated protons undergo charge exchange as they pass through the layer of desorbed gas and become "fast" neutrals that then flow into the AK gap. Once in the gap these fast neutrals can interact with other particles and become reionized. This extra positive charge can change the potential gradients near the cathode and enhance the electron current coming from the cathode resulting in higher beam currents and rapidly falling impedance. Based on the anode material variation results shown in Sec. IV, it appears that the behavior of the diode is independent of the high-energy proton content in the beam, (i.e. protons born at the anode and acquire the full accelerating energy). Therefore, it seems unlikely that recombination/reionization of hydrogen coming from the anode can be considered as a dominant mechanism given that the impedance basically remained unchanged even though the amount of hydrogen coming from the anode was substantially reduced.

It is similarly argued that avalanche ionization by stripping of anode ions due to ion-ion collisions must be seriously questioned. The basic premise of this argument is that ion-ion stripping is a strong function of cross section. It seems unlikely that the behavior of the diode where this was the dominant mechanism would remain unchanged from RT anodes abundant in H and C contaminants compared to frozen Xe anodes that appeared almost pure. (Although activation does not measure C content directly, it is argued that it is unlikely to have C contamination without H based on ion diode experiments.[25, 27,31])

This process of elimination leads one to consider fast moving cathode and anode plasmas as the next most likely mechanisms that might explain the observed anomalous behavior of the immersed-$B_z$ diode. It is not clear at this time whether one or the other is predominantly responsible for the observed behavior. Based on a similar line of reasoning as presented above for the avalanche ionization or charge exchange theories, it would be easy to reason that if fast moving anode plasmas were the dominant mechanism, then the anode material variation experiments should have affected the diode behavior more than they did based simply on a constituent mass argument, i.e. Xe is much more massive than H or C and therefore should expand much more slowly. This heuristic argument would tend to point away from the anode and point primarily to processes related to cathode plasmas. We would caution against jumping to such a conclusion and provide the following arguments and considerations.

The effect with AK gap suggests that some feedback mechanism is involved between the two electrodes. The basic premise for this argument is that it is difficult to envision a process whereby cathode or anode plasmas acting independently could result in impedance collapse. For example, let us suppose that plasmas with velocities of 50 cm/μs were expanding from both electrodes. In 50 ns, these plasmas would only move a combined distance of 5 cm. This could affect the impedance due to associated changes in electric fields near the electrodes and possible geometric effects if the plasmas are expanding radially but the effect should be independent of

gap for gaps that are modestly larger than this effective closure length, i.e. gaps of 10 cm or greater would maybe have falling impedances but the effect should be independent of gap. One possible coupled mechanism that has been suggested is the bombardment of the cathode plasmas by ions coming from the anode causing subsequent stripping due to ion-ion collisions. Unfortunately, this theory is not supported by the frozen Xe data where, absent high-energy protons, there may have been very little ion current getting to the cathode at all and yet the impedance collapsed and was unchanged from the RT Ta anodes where there could have been significantly more anode ions interacting with the cathode plasma early in time.

Preliminary spectroscopic results presented in Appendix J suggest that there are very fast plasmas expanding at velocities on the order of 10's of cm/μs from both the cathode and anode. Although there are no quantitative estimates of the respective densities of these plasmas at this time, there are indications based on the relative intensities of the H-α signals shown in Appendix J as well as other supporting spectroscopic data, e.g. brighter lines of continuum[32] suggesting that the anode plasmas are hotter and denser than the cathode plasmas.

The prepulse data presented in Appendix B suggests that cathode plasmas preformed due to prepulse can greatly affect the behavior the diode. On one hand this would seem to infer that cathode plasmas are a plausible mechanism for affecting the diode behavior. On the other hand, if cathode plasmas are the dominant mechanism, one must wonder why the diode behavior is so radically different between diodes with cathode plasmas that are supposedly preformed during the prepulse stage for high prepulse experiments as opposed to those supposedly formed during the main pulse for low prepulse experiments.

In Appendix E, we present results showing that sometimes even the impedance of large cathodes can fall unexplainably. This exception to the generalization that large cathodes are always well behaved with good impedance raises questions about any hypothesis that depends on things getting worse as the cathode diameter decreases (e.g. Joule heating). Further, simple scaling arguments where things gets worse as the diameter decreases are not sufficient in and of themselves to explain the effect of AK gap results presented above for a 1-mm cathode. It is argued that if processes related solely to the cathode diameter were dominant, there would be a less pronounced effect with AK gap.

In Appendix F, we present results showing that we were able to effect large changes in the diode behavior with the use of anodes made of polyethylene. Although this is the only observed exception to the generalization that anode material variations did not affect the diode behavior, it leaves the door open for conjecture that processes related to the anode plasma formation can affect the diode behavior.

The bottom line is that we believe that both cathode and anode plasmas are playing a role in determining the behavior of the immersed-$B_z$ diode. Future work needs to focus on characterizing and/or mitigating these electrode plasmas and their effects.

## VII. Future Work

Based on analytical scaling and simulations [Appendix D], it would appear as if the immersed-$B_z$ diode has the potential to achieve the radiographic objectives of obtaining a small spot with a high dose (2 mm, 1000 rad @ m). The challenge lies in trying to understand the difference between the nominal operation of the large cathodes and the anomalous diode behavior associated with the small cathode operation. If the nominal operation observed with large cathodes could be extended to small cathodes, the immersed-$B_z$ diode might still be considered a contender as a possible source for future flash X-ray research facilities.[2] Efforts in several areas will be needed to move beyond our present understanding and capability:

- Improved space and time-resolved electrode plasma formation and expansion measurements
- Continued efforts to anticipate and mitigate known problems associated with electrode contamination,[31]
- Continued efforts to improve understanding by analyzing and interpreting all results with theory and simulation support.

In the past, most of our efforts involved trying to anticipate and mitigate possible problems related to electrode contamination. These efforts were often based on our experience and that of others in related high-energy-density experiments and insights provided through analytical models and numerical simulations. Our efforts have suffered from limited resources devoted to obtaining space and time resolved electrode plasma information. It now appears evident that trying to isolate the mechanisms that limit the performance of the immersed-$B_z$ diode will require improved plasma diagnostics. Several years ago, a split-magnet diode was designed and fabricated to provide improved diagnostic access to the AK gap region.[20] Although we have observed tantalizing results with initial spectroscopic studies using the standard cryogenic diode configuration and have observed changes in anode plasma velocity characteristics with anode material variations (Appendix J), we have not observed any changes that correlate directly to the transition from nominal to anomalous diode behavior. The direct radial diagnostic access of the split-magnet configuration would allow us to better isolate the plasma formation at both the cathode and anode and expansion of their respective plasmas into the gap. The first priority would be to characterize the cathode and anode plasmas as the cathode diameter is decreased.

Without further insight that might be afforded through additional electrode plasma characterization, it is difficult to decide where to concentrate future mitigation efforts. However, several ideas have been suggested and that are worth noting and discussing are, heated cathodes, heated anodes and anode foils.

To date, there have been not been any serious efforts to try and modify the behavior of the immersed-$B_z$ diode by mitigating cathode plasmas through cleaning or conditioning of the cathode. There have been some limited sets of experiments that have involved coating the cathode with gold at AWE. Although some improvement was observed there was not the dramatic effect one would have hoped for. Because it has not been thoroughly explored and because so little change in behavior has been observed with anode material variations, cathode

material variations and cathode conditioning should be explored. Electron beam heating of the cathode using a scheme similar to that developed by Hinshelwood[33] for rod pinch diodes might warrant consideration as a method for cleaning or conditioning the cathode.

The rationale for considering heated anodes is not quite so obvious. On one hand, heating Ta anodes to eliminate hydrogen contaminants has improved the impedance and performance of other bremsstrahlung diodes.[34] On the other hand, substantial demonstrated reductions in high-energy proton content of the beam with frozen Xe experiments discussed above did not result in improved impedance or radiation performance. Therefore, one must question whether much difference or improvement with heated anodes over the results already obtained with frozen Xe should be expected. In any case, because it has not been tried for immersed-$B_z$ diodes and because there are limited anode plasma mitigation schemes to try, it must be considered in any discussion involving future work with the immersed-$B_z$ diode.

The idea for trying anode foils is based primarily on anecdotal evidence from self-magnetic pinch (SMP) diodes suggesting that SMP diodes without anode foils have relatively poor radiographic performance (large spot and low dose production) compared to SMP diodes that use anode foils.[35] These anode foils are typically made from thin foils of aluminum (12.5 microns) and positioned in front of the Ta converter with a small vacuum gap (.030") separating the foil and Ta converter. Anode foils were also used successfully in early immersed-$B_z$ diode work to generate cold, intense "cookie-cutter" electron beams.[36] Although these were large diameter beams (2 cm), because the electron beam annulus was so thin, the reported beam current densities were extremely high (400 kA/cm$^2$). Whether or not these results are relevant, the fact that they were able to obtain the desired results in an immersed-$B_z$ diode with extremely high current densities makes their results and the fact that they used anode foils worthy of consideration. Based on these arguments and the fact that this idea would be relatively easy to implement and test, makes the anode foil idea worthy of consideration.

Considerable effort has gone into modeling of immersed-$B_z$ diodes and some of the comparisons to experiment and insights gained are discussed in Appendix G. A complex experimental system such as the immersed-$B_z$ diode always benefits from insights gained from theory and numerical simulations. Recently we have revitalized efforts to carefully benchmark LSP simulations against experimental results for nominally well-behaved diodes with large cathodes as well as anomalous operation with small cathodes. These efforts are on going and will be reported later in a subsequent report or paper. The bottom line is that any experimental program with complex systems such as the immersed-$B_z$ diode must have a robust theoretical and modeling effort to help understand past results and guide future work and experiments.

## References


[1] J. Maenchen, G. Cooperstein, J. O'Malley, and I. Smith, "Advances in pulsed power-driven radiography systems," Proc. IEEE **92**(7), pp. 1021-1042, (2004).

[2] T. J. Goldsack, T. F. Bryant, P. F. Beech, S. G. Clough, G. M. Cooper, R. Davitt, R. D. Edwards, N. Kenna, J. McLean, A. G. Pearce, M. J. Phillips, K. P. Pullinger, D. J. Short, M. A. Sinclair, K. J. Thomas, J. R. Threadgold, M. C. Williamson, and K. Krushelnick, "Multimegavolt multiaxis high-resolution flash x-ray source development for a new hydrodynamics research facility at AWE Aldermaston," IEEE Trans. Plasma Sci. **30**(1), pp. 239-253, (2002).

[3] M. G. Mazarakis, J. W. Poukey, D. C. Rovang, J. E. Maenchen, S. R. Cordova, P. R. Menge, R. Pepping, L. Bennett, K. Mikkelson, D. L. Smith, J. A. Halbleib, W. A. Stygar, and D. R. Welch, "Pencil-like mm-size electron beams produced with linear inductive voltage adders (IVA)," Appl. Phys. Lett. **70**(7), pp. 832-834, (1997).

[4] G. M. Cooper, J. McLean, R. Davitt, and T. J. Goldsack, "Recent immersed Bz x-ray diode experiments", Beams 2002: 14th International Conference on High-Power Particle Beams, edited by T. A. Mehlhorn and M. A. Sweeney (Am. Inst. Phys., New York, 2002), pp. 155-158.

[5] P. R. Menge, D. L. Johnson, J. E. Maenchen, C. L. Olson, and D. C. Rovang, D. Droemer, E. Hunt, B. Oliver, D. Rose and D. Welch, "Experimental Comparison of 2-3 MV X-Ray Sources for Flash Radiography", SAND2002-0082, January 2002.

[6] D. R. Welch and T. P. Hughes, "Effect of target-emitted ions on the focal spot of and intense electron beam", Laser and Particle Beams **16**(2), p. 285-294, (1998).

[7] B. V. Oliver, R. E. Clark, T. C. Genoni, T. P. Hughes, D. V. Rose, and D. R. Welch, " Anode-target effects in Electron Beam Driven Radiography", Proc. 14th International Conference on High Power Particle Beams, BEAMS 2002, pp. 207-212.

[8] D. V. Rose, T. C. Genoni, and D. R. Welch, "Ion-hose instability growth and saturation for counterstreaming electron and ion beams in an applied magnetic field," Phys. Plasmas **11**(11), pp. 4990-4997, (2004).

[9] D. R. Welch, B. Oliver, D. V. Rose, D. Rovang, and J. E. Maenchen, "Impedance loss due to ion-ion collision in a high power magnetically immersed electron diode", Bull. Am. Phys. Soc. **48**, 95 (2003).

[10] I. D. Smith, V. L. Bailey, Jr., J. Fockler, J. S. Gustwiller, D. L. Johnson, and J. E. Maenchen and D. D. Droemer, "Design of a Radiographic Integrated Test Stand (RITS-3) Based on a Voltage Adder to Drive A Diode Immersed in a High Magnetic Field", IEEE Trans. Plasma Sci,, **28**(5), Oct. 2000, pp. 1653-1659.

[11] D. L. Johnson, I. Smith, P. Corcoran, V. Bailey, J. Douglas, V. Carboni, I. Molina, S. Portillo, K. Hahn, E. Puetz, S. Cordova, D. Droemer, T. Guy, R. Gignac, F. Wilkins, and R. Woodring, "Advances in the Pulsed Power Modeling and Experimentation on the RITS Accelerator", Proc. of the 14th IEEE International Pulsed Power Conference, (2003), pp.379-382.

[12] M. G. Mazarakis, J. W. Poukey, J. E. Maenchen, D. C. Rovang, P. R. Menge, D. L. Smith, J. A. Halbleib, S. R. Cordova, L. Bennett, K. Mikkelson, R. Pepping, W. A. Stygar, T. G. Trucano, D. R. Welch, T. J. T. Kwan, B. G. DeVolder, R. J. Kares, and C. M. Snell, "Inductive Voltage Adder Advanced Hydrodynamic Technology Demonstration," Sandia National Laboratories Report SAND97-0816, April 1997.

[13] M. G. Mazarakis – private communication.

[14] V. L. Bailey, D. L. Johnson, P. Corcoran, I. Smith, J. E. Maenchen, I. Molina, K. Hahn, D. Rovang, S. Portillo, B. V. Oliver, D. Rose, D. Welch, D. Droemer, and T. Guy, " Design of a High Impedance MITL for RITS-3", Proc. of the 14th IEEE International Pulsed Power Conference, (2003), pp. 399-402.

[15] C.W. Mendel, Jr., D. B. Seidel, and S. E. Rosenthal, "A simple theory of magnetic insulation from basic physical principles', Laser and Particle Beams, Vol. 1, pp. 311-320, 1983.

[16] B. V. Oliver, T. C. Genoni, D. L. Johnson, V. L. Bailey, P. Corcoran, I. Smith, J. E. Maenchen, I. Molina, K. Hahn, " Two and Three-Dimensional MITL Power-Flow Studies on RITS", Proc. 14th IEEE International Pulsed Power Conference, 2003, pp. 395-398.

[17] D. V. Rose, D. R. Welch, B. V. Oliver, R. E. Clark, D. L. Johnson, J. E. Maenchen, P. R. Menge, C. L. Olson, and D. C. Rovang "Coupled particle-in-cell and Monte Carlo transport modeling of intense radiographic sources," J. Appl. Phys., vol. 91, no. 5, pp. 3328-3335, Mar. 2002.

[18] S. Lutz, D. Droemer, D. Devore, D. Rovang, S. Portillo, and J. Maenchen, " Development of a Dynamic Spot Size Diagnostic for Flash Radiographic X-Ray Sources", Proc. 14th IEEE International Pulsed Power Conference, 2003, pp. 197-200.

[19] S. Portillo, S. S. Lutz, L. P. Mix, K. Hahn, D. Rovang, J. E. Maenchen, I. Molina, S. Cordova, D. Droemer, R. Chavez, and D. Ziska, " Time-Resolved Spot Size Measurements from Various Radiographic Diodes on the RITS-3 Accelerator", IEEE Trans. Plasma Sci., vol. 34, no. 5, Oct. 2006, pp. 1908-1913.

[20] D. Rovang, D. Welch, H. Ives, D. L. Johnson, M. Kincy, B. Lesch, J. Maenchen, P. Menge, I. Molina, B. Oliver, C. Olson, C. Swenson, and D. VanDeValde, "Status and plans for the next generation magnetically immersed diodes on RITS-3", Beams 2002: 14th International Conference on High-Power Particle Beams, edited by T. A. Mehlhorn and M. A. Sweeney (Am. Inst. Phys., New York, 2002), pp. 127-130.

[21] J. C. Dainty and R. Shaw, *Image Science*, London, U.K., Academic Press, 1974.

[22] D. Rovang, D. Van De Valde, D. Gregerson, E. Puetz, N. Bruner, G. Cooper, S. Cordova, D. Droemer, K. Hahn, M. D. Johnston, J. Maenchen, J. McLean, I. Molina, B. Oliver, J. O'Malley, S. Portillo, and D. Welch, "Development and Testing of Immersed-$B_z$ Diodes with Cryogenic Anodes", Proc. 15th IEEE International Pulsed Power Conference, to be published.

[23] D. S. Prono, H. Ishizuka, E. P. Lee, B. W. Stallard, and W. C. Turner, " Charge-exchange neutral-atom filling of ion diodes: Its effect on diode performance and A-K shorting", J. Appl. Phys. **82**(4), April 1981, pp. 3004-3011.

[24] K. Kasuya, K. Horioka, T. Takahashi, K. Ohbayashi, and H. Yoneda, "High Purity Pulse Proton Source With Cryogenic Anode", Proc. 5th International Pulsed Power Conference, (1985), pp. 110-113.

[25] D. L. Hanson, J. L. Porter, and R. R. Williams, "High-purity ion beam production at high current densities with liquid-helium-cooled series-field-coil extraction ion diode", J. Appl. Phys., **70** (6), (September 1991), pp. 2925-2938.

[26] F. C. Young and D. V. Rose, "Radioactivities produced in commonly used materials by proton and deuteron beams up to 10 MeV", Atomic Data and Nuclear Data Tables **64,** Article No. 0022, pp. 223-251, 1996.

[27] M. E. Cuneo, P. R. Menge, D. L. Hanson, W. E. Fowler, M. A. Bernard, G. R. Ziska, A. B. Filuk, T. D. Pointon, R. A. Vesey, D. R. Welch, J. E. Bailey, M. P. Desjarlais, T. R. Lockner, T. A. Mehlhorn, S. A. Slutz, and M. A. Stark, "Results of Vacuum Cleaning Techniques on the Performance of LiF Field-Threshold Ion Sources on Extraction Applied-B Ion Diodes at 1-10 TW", IEEE Transactions on Plasma Science, **25**(2), pp. 229-251, April 1997.

[28] A. B. Filuk, J. E. Bailey, M. E. Cuneo, P. W. Lake, T. J. Nash and D. D. Noack, and Y. Maron, "VUV absorption spectroscopy measurements of the role of fast neutral atoms in a high-power gap breakdown", Phys. Rev. E, **62**(6), pp. 8485-8492, Dec. 2000.

[29] P. R. Menge, D. L. Johnson, J. E. Maenchen, D. C. Rovang, B. V. Oliver, D. V. Rose, and D. R. Welch, " Optimization of a rod pinch diode radiography source at 2.3 MV", Rev. Sci. Inst. **74**(8), pp. 3628-3635, August 2003.

[30] F. C. Young, R. J. Commisso, R. J. Allen, D. Mosher, S. B. Swanekamp, G. Cooperstein, F. Bayol, P. Charre, A. Garrigues, C. Gonzales, F. Pompier, and R. Vezinet, " Rod-pinch diode operation at 2 to 4 MV for high resolution pulsed radiography", Phys. Of Plasmas **9**(11), pp, 4815-4814, November 2002.

[31] M. E. Cuneo, "The effect of electrode contamination, cleaning, and conditioning on high-energy, pulsed-power device performance," IEEE Trans. Dielect. Elec. Insul., vol. 6, no. 4, pp. 469-485, Aug. 1999.

[32] M. D. Johnston, K. Hahn, D. Rovang, S. Portillo, and J. Maenchen, D. Droemer, D. Welch, B. Oliver, D. Rose, E. Schamiloglu, and Y. Maron, " Plasma Spectroscopy Diagnostics in Pulsed-Power X-Ray Radiography Diode Research", Proc. 15th IEEE International Pulsed Power Conference, June 2005, to be published.

[33] D. D. Hinshelwood, G. Cooperstein, D. Mosher, P. F. Ottinger, J. W. Schumer, S. J. Stephanakis, S. B. Swanekamp, B. V. Weber and F. C. Young, "Improvement in rod-pinch diode performance with anode heating", Abstracts 29th IEEE International Conference on Plasma Science, ICOPS 2002, May 2002.

[34] B. V. Weber, R. J. Allen, B. G. Moosman, S. J. Stephanakis, F. C. Young, N. R. Pereira, J. R. Goyer, "Improved Bremsstrahlung from Diodes with Pulse-Heated Tantalum Anodes", IEEE Trans. Plasma Sci., Vol. 30, no. 5, pp. 1806-1815, Oct. 2002.

[35] J. Threadgold, private communication.

[36] R. L. Sheffield, M. D. Montgomery, J. V. Parker, K. B. Riepe, and S. Singer, "Generation of a cold, relativistic, electron beam using a magnetized foilless diode", J. Appl. Phys. **53**(8), Aug. 1982, pp. 5408-5413.

# Appendices

The following set of appendices highlight additional material including additional data sets and computational analyses that compliment the main body of the report. In some cases the data is considered preliminary, e.g. Appendix J on spectroscopic results. The results are tantalizing but have not benefited from in-depth and substantial experimental investigations.

## Appendix A: $B_Z$ variation

Historically, the interest in using higher fields with the immersed-$B_z$ diode was to achieve smaller spot sizes by controlling the size of the ion hose instability. Theoretically, the size of the offset is believed to scale with the electron cyclotron radius with which scales as 1/B.[i]

This 1/B scaling applies to diodes operating in a bipolar mode. Although improvements in spot size that appear to scale with 1/B have been sighted by other authors[ii] and though some improvement in spot size was observed in these experiments, one is cautioned when trying to apply this scaling to experiments where the diode is not behaving quasi-classically or at a minimum is well behaved with nominally high impedance.

Figure A1 shows the spot size for three different magnetic field strengths 6, 12 and 18 T as function of cathode diameter for 4 MV operations on RITS-3. The AK gap was held constant at 10 cm. There is a notable improvement in spot sizes with increasing magnetic fields for cathodes smaller than 4.76 mm. Big differences are not expected for the larger cathodes because the spot size is determined primarily by the size of the cathode. (Although there might be some contribution due to ion hose it is small relative to the cathode diameter. This is true in part because there cathodes are well behaved and therefore the ion hose contribution is expected to be consistent with theory.) Although it might be tempting to try and apply the 1/B scaling for the smaller diameters, e.g. the 1-mm cathode, as is discussed below, those experiments exhibited poor electrical behavior.

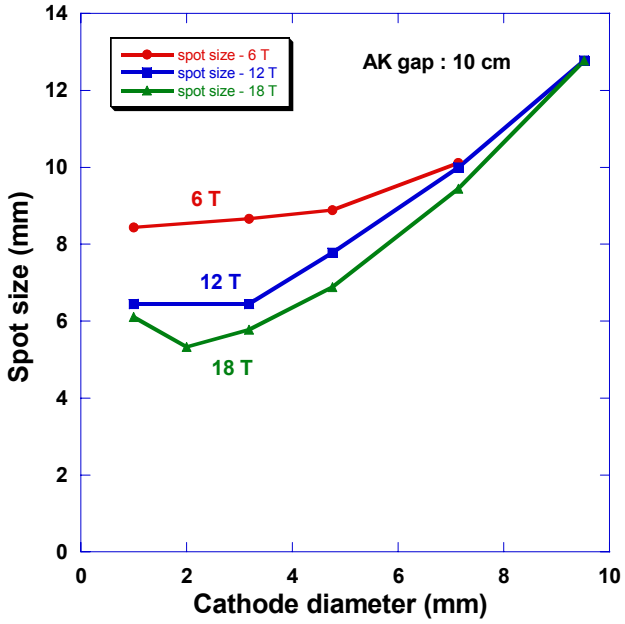


**Figure A1.** Spot size as a function of cathode diameter for 6, 12, and 18 T at 4 MV.

Detailed results for the 1-mm cathode experiments are presented in Fig A2 and A3. No consistent trends are observed with increased magnetic field except for the continued decrease in spot size with magnetic field as shown in Fig. A3b. However, a couple interesting observations can still be made. One is that the early time impedances are independent of the applied magnetic field but that there appears to be some effect on late time diode current, especially for the 6-T case. This effect on diode current might look like it is a fluke – especially given the fact the 18-T current lies below the 12-T current. However, a similar effect is noted in Appendix J for cryogenically cooled anodes where a comparison is made between 4 and 20-T operation. The other interesting observation is that there was no notable effect on dose production, on either the magnitude or the duration (Figs. A3a, A3b) even though the spot size went up as the field went down (Fig. A3b). Typically, dose production improves with spot size as observed for larger cathodes and larger AK gaps but does not appear to be the case for increased spot sizes resulting from lower magnetic fields. This is true as well for the results presented in Appendix J on the difference between 4 and 20 T.

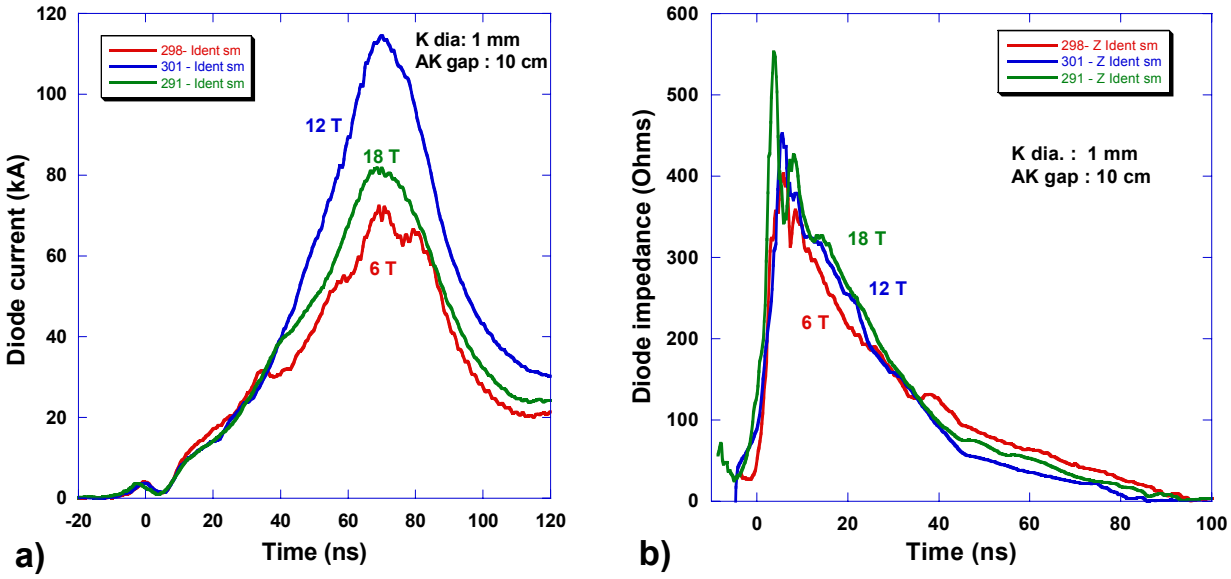


**Figure A2.** a) Diode current and b) impedance as function of time for 6, 12 and 18 T at 4 MV.

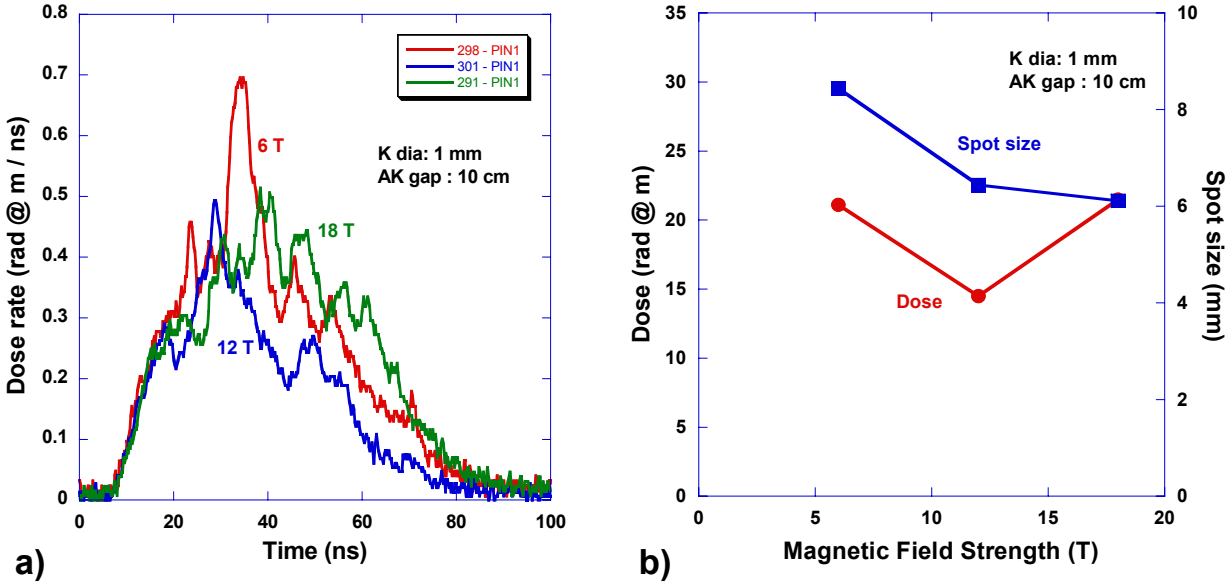


**Figure A3.** a) Dose rate as function of time and b) time-integrated dose and spot size measurements as a function of magnetic field strength at 4 MV.

The other noteworthy feature about the measure-dose rate is the anomalous spike in the dose rate for the 6 T case (Fig. A3a – red trace). This spike occurs almost exactly at the same point in time, near t = 35 ns, that the diode current and diode impedance plateau for a brief instant. The cause of this anomaly is not understood and may not be significant but was considered noteworthy and may be of significance to other students of the immersed-$B_z$ diode.

## Appendix B: Prepulse variation

The original intent and design of the prepulse experiments presented here was to provide some empirical information for defining how much prepulse might be tolerable in future accelerator systems that desire to use an immersed-$B_z$ diode as the radiation source. Although this goal was partially achieved, some unexpected insights and results were obtained as well.

RITS-3 was designed to produce very low prepulse using a combination of water and oil switches designed to suppress the prepulse.[iii] Simulating high prepulse operation simply required shorting these switches. Three separate monitors were used to measure the prepulse, capacitive voltage monitors at F and G measured the prepulse on the MITL and in addition there was a single cavity resistive monitor that measured the prepulse at one of the cavity locations. Figure B1 shows the very low level of prepulse that was achieved for normal operation on RITS-3, < +/- 5 kV. Figure B2 shows the level, duration, and timing of the prepulse relative to the arrival of the main pulse. The arrival of the main pulse is represented by the abrupt increase in the calculated voltage derived by multiplying the cathode and anode currents at F times the vacuum impedance of the MITL (black and orange traces respectively.) The voltage measured by the single monitor has been scaled by a factor three to approximate the total prepulse resulting from all three cavities. All of the monitors seem to agree quite well. Without prepulse suppression the prepulse lasts for almost 200 ns and increases from 100 kV to slightly over 200 kA when the main pulse arrives (Fig. B1b).

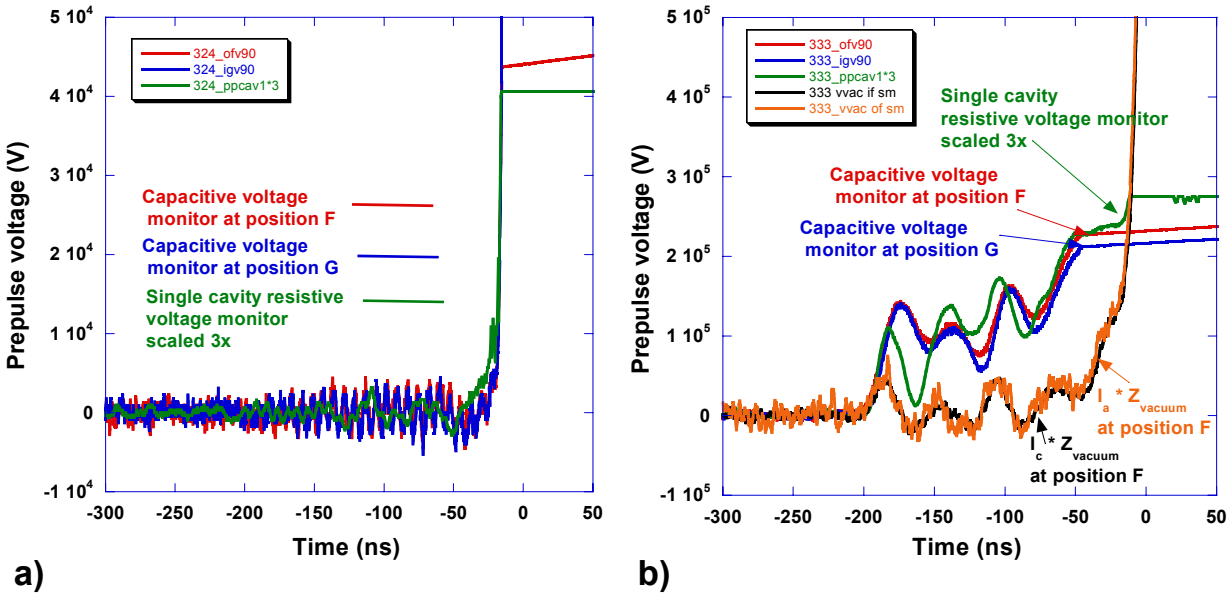


**Figure B1.** a) Characteristic RITS-3 prepulse with prepulse suppression (low prepulse) b) Characteristic RITS-3 prepulse without any prepulse suppression (high prepulse).

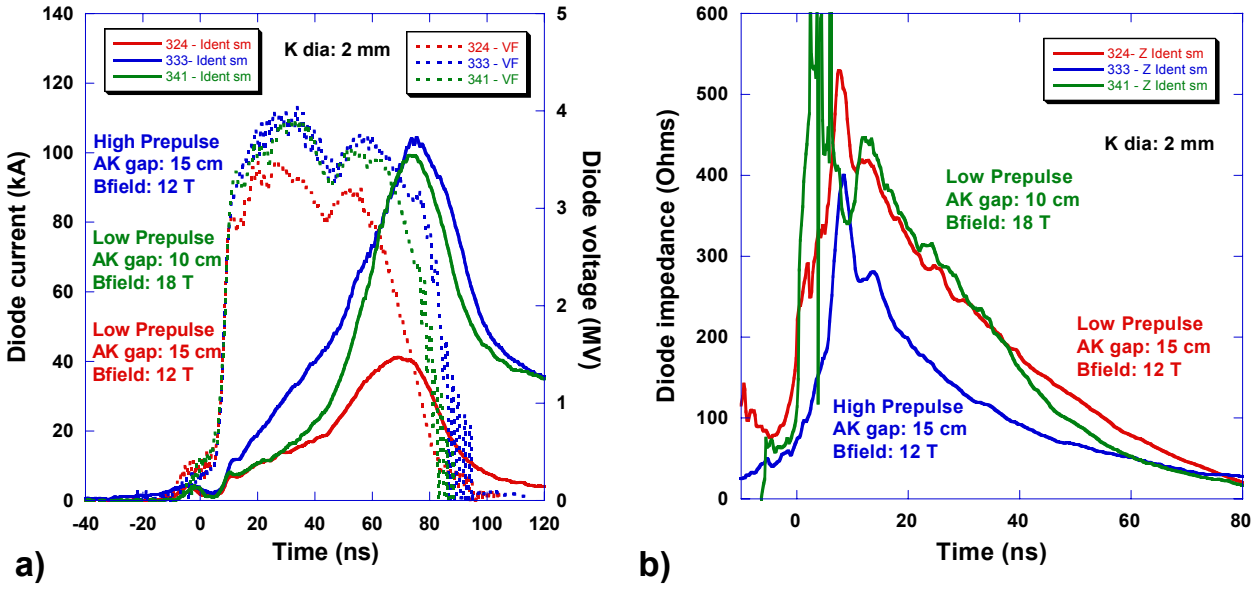


**Figure B2.** a) Diode current (solid lines) and voltage (dashed lines) and b) diode impedance for low and high prepulse experiments at 4 MV.

Ideally, it would have been desirable to compare the results from a single low prepulse experiment with a single high prepulse experiment. Unfortunately, the low prepulse experiment with exactly the same diode parameters as the high prepulse shot, 2-mm dia., 15-cm gap and 12 T, had a reduced diode voltage (Fig. B2) due to unrelated pulsed power problems. For completeness, a similar experiment with more typical diode voltage but with slight differences in B field strength and gap (18 T and 10-cm gap) is included for comparison. Figures B2a and B2b show that there is a substantial difference in early time diode current impedances between the high prepulse and low prepulse experiments. Although late in time the currents of the two low prepulse experiments are quite different.

There is also a dramatic difference observed in the measured dose rate between the low and high prepulse experiments (Fig. B3a). The low dose rate for the low prepulse experiment (red trace) is mostly attributed to the low diode voltage. What is striking is the difference in dose rate late in time for the other low prepulse experiment and the high prepulse experiment. Near 60 ns, the current and voltage for these two experiments were almost identical but had dramatically different dose production.

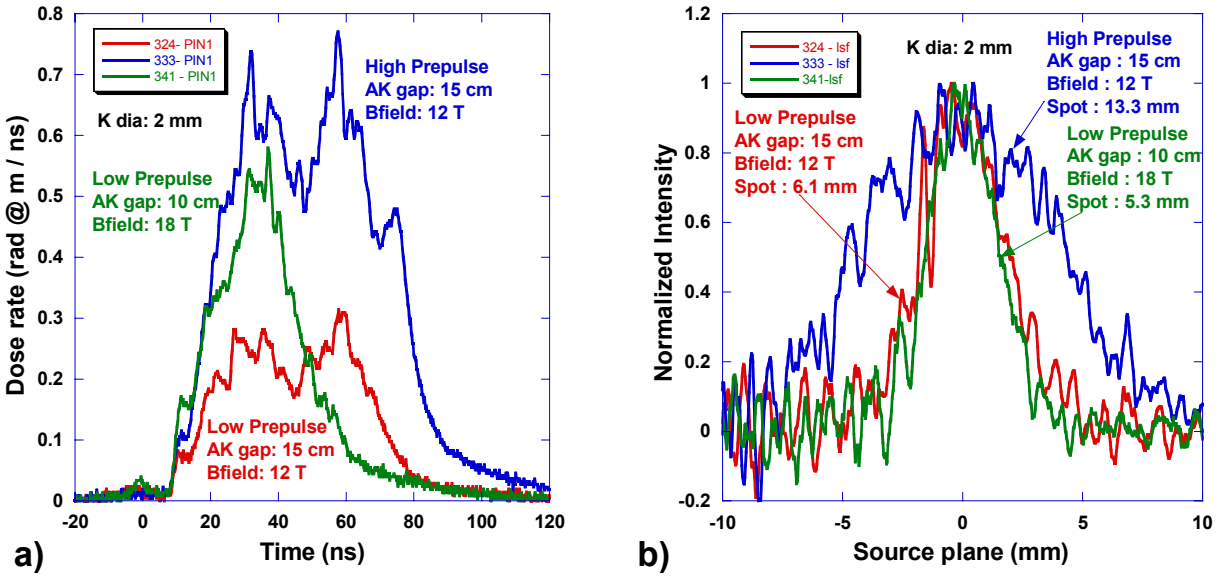


**Figure B3.** a) Dose rate and b) spot profile (LSF) for low and high prepulse experiments.

Despite the differences in behavior between the low prepulse experiments, they had very similar spot sizes and LSF profiles (Fig. B3b). However, the high prepulse experiment resulted in a very broad LSF and a corresponding spot size that was more than two times larger than the lower prepulse experiments, 13.3 mm vs 5.3 and 6.1 mm.

It is interesting and insightful to compare the results in Figs. B4 and B5 between the results from a low prepulse, large cathode - 9.52 mm - (red trace) with the high prepulse results for the 2-mm cathode (blue trace). The somewhat surprising result is how the dose production was very similar in amplitude and duration (Fig. B4b) resulting from very different diode currents (Fig. B4a). There is also a substantial difference in the shape of the resulting LSF (Fig. B5). Although the resulting spot size is almost the same for both, 12.8 vs 13.3 mm, the LSF for the large cathode with low prepulse is basically flat topped or slightly hollow with very sharp edges, where as the profile for the small cathode with high prepulse is much more rounded.

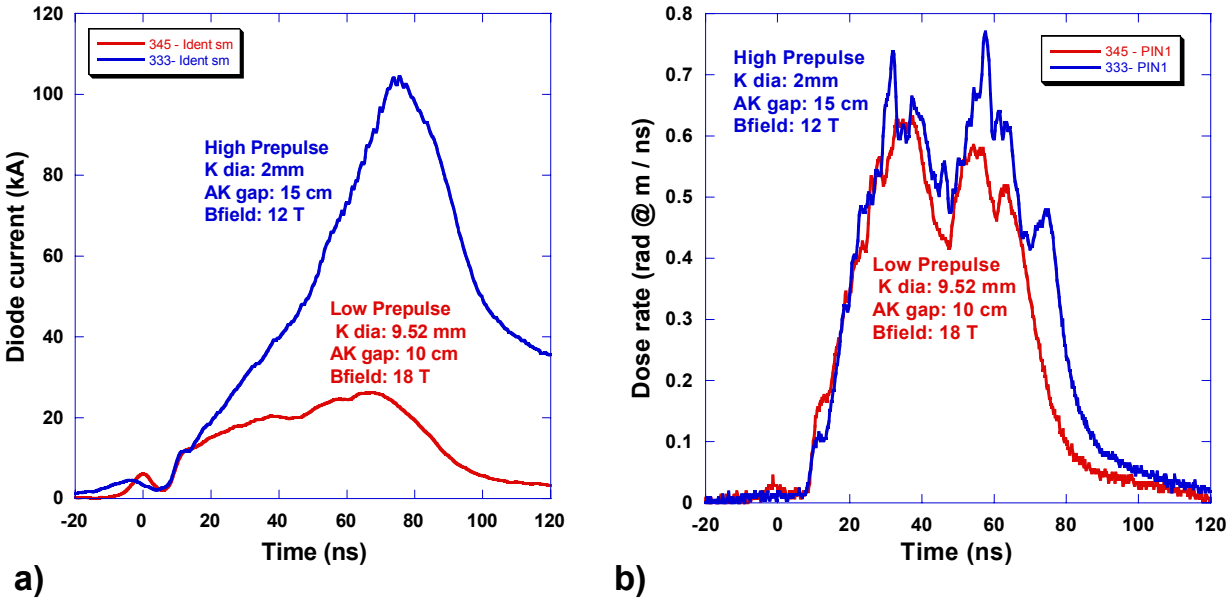


**Figure B4.** a) Diode current and b) dose rate for 2 mm cathode with high prepulse compared to 9.52 mm cathode with low prepulse at 4 MV.

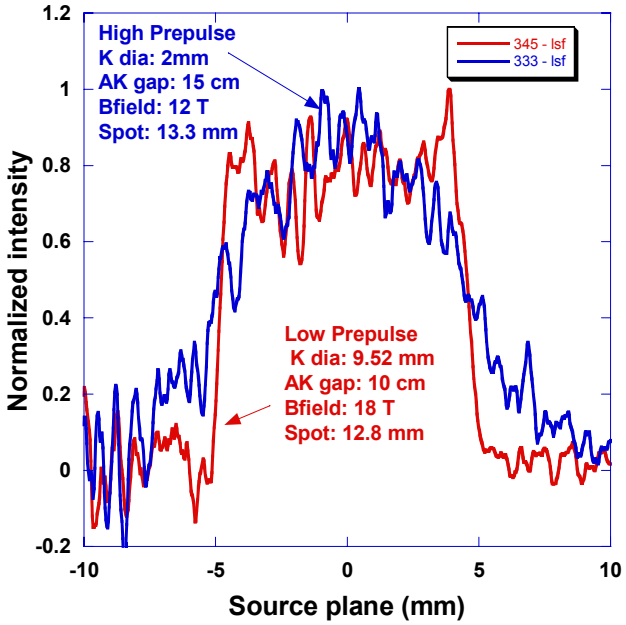


**Figure B5.** Spot profile (LSF) for 2 mm cathode with high prepulse and 9.52 mm cathode with low prepulse at 4 MV.

Although it is impossible to tell for sure what happened for the high prepulse experiment, the results suggest that there was a large preformed plume or cloud of plasma surrounding the cathode when the main pulse arrived. This would be consistent with the large spot and rounded profile. The current and dose production might be a little bit harder to explain but one possibility is that most of the current for the high prepulse case was due to electrons that were accelerated out of the cathode plasma out in the gap in front of the cathode sheath. These electrons would only have approximately half the accelerating potential of electrons originating at cathode and therefore although they would contribute to the current they would make very little difference in dose production because of the strong scaling of dose with voltage ($D \alpha V^{2.3}$).

## Appendix C: Pressure variation

The original intent of these experiments was to determine the relative importance of background accelerator vacuum pressure on immersed-$B_z$ diode behavior. This information would be relevant to future system designers and also provides a more direct comparison to other immersed-$B_z$ diode experiments conducted at AWE which typically were conducted at higher pressures (5 e-5 Torr) than the typical pressure used for immersed-$B_z$ diode experiments on RITS-3 ( < 5 e-6 Torr).

The experimental results for three different pressures, 3.6 e-6, 1.8 e-5, and 1.6 e-4 Torr, are presented in Figs. C1 and C2. The higher pressures were achieved by turning off some of the vacuum pumps and where necessary artificially raising the pressure by introducing small, controlled leaks upstream of the diode in the MITL portion of the accelerator. All these experiments were conducted at 4 MV using a 3.18-mm cathode, at 12 T with 15-cm gaps. Although some variation behavior is observed, there is not a consistent trend with pressure. For the limited pressure range and diode parameters investigated here, it does not appear that pressure plays a significant role in affecting the behavior of the diode. It should be noted that two experiments were conducted at similar pressures but only one set has been presented here for the sake of clarity. There was no consistent trend with pressure observed in either set of experiments. The differences are believed to reflect the shot-to-shot variability and are not believed to be attributable to the difference in pressure. However, it is worth noting that once again there is an anti-correlation between diode current and dose production, higher diode currents correspond with lower dose production especially in the second half of the pulse.

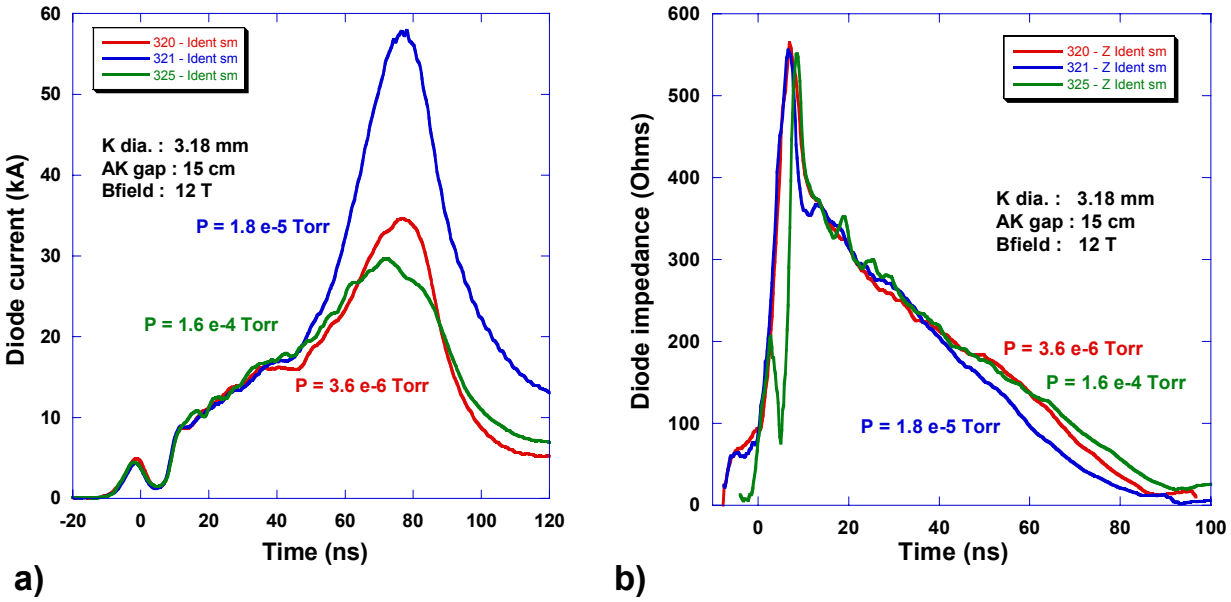


**Figure C1.** a) Diode current and b) impedance as a function of time for different accelerator pressures at 4 MV.

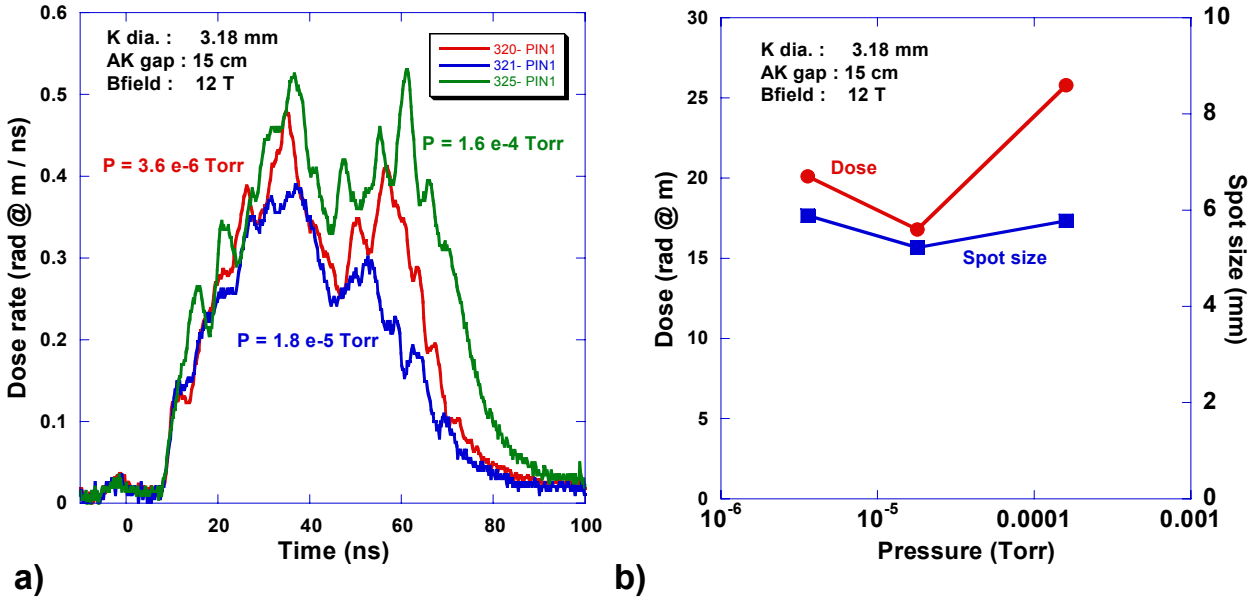


**Figure C2.** a) Dose rate as a function of time and b) time-integrated dose and spot size measurement as a function of accelerator pressure at 4 MV.

## Appendix D: Accelerator/diode variation

The potential of the immersed-$B_z$ diode as a radiographic source is that the large AK gap separation would inhibit impedance collapse and that the spot size would scale with cathode diameter. As was shown in Sect. III, the use of small cathodes is characterized by

loss of impedance and decrease in dose, without any further improvement or reduction in spot size. This inability to achieve small spot sizes with good dose production is probably the single most important result that will ultimately limit the utility of the immersed-$B_z$ diode as a radiographic source. Because of this importance, it is incumbent to show that this effect with cathode diameter was not unique to the experiments presented here and that this limitation has been observed by other researchers using different diodes on different accelerators, Superswarf[iv] and Asterix[v].

Table D1 lists the important accelerator and diode parameters along with the resulting spot and dose for representative experiments on RITS-3 at 4 and 5 MV, SuperSwarf at 5.5 MV[vi] and Asterix at 6 MV. Figs D1a and D1b compare the effect of cathode diameter spot size and dose results associated with each of the different set of accelerator experiments.

**Table D1**. Experimental configurations and results for accelerator/diode variations

| Accelerator | Shot number | Voltage (MV) | Anode or drift tube bore size (mm) | AK gap (cm) | Bfield at anode (T) | Cathode diameter (mm) | Spot size (mm) | Dose (rad @ m) |
|---|---|---|---|---|---|---|---|---|
| RITS3 | 291 | 4 | 88.9 | 10 | 18 | 1 | 6.1 | 21.5 |
| RITS3 | 341 | 4 | 88.9 | 10 | 18 | 2 | 5.3 | 17.6 |
| RITS3 | 287 | 4 | 88.9 | 10 | 18 | 3.18 | 5.8 | 20.9 |
| RITS3 | 288 | 4 | 88.9 | 10 | 18 | 4.76 | 6.9 | 23 |
| RITS3 | 339 | 4 | 88.9 | 10 | 18 | 7.14 | 9.4 | 30.9 |
| RITS3 | 345 | 4 | 88.9 | 10 | 18 | 9.52 | 12.8 | 31.6 |
| RITS3 | 766 | 5 | 65.2 | 7.5 | 20 | 1 | 6.9 | 37.4 |
| RITS3 | 765 | 5 | 65.2 | 7.5 | 20 | 2 | 5.1 | 35.2 |
| RITS3 | 763 | 5 | 65.2 | 7.5 | 20 | 4.76 | 6.2 | 80.7 |
| SuperSwarf | A894 | 5.4 | 44 | 7.7 | 19 | 0.8 | 7 | 23 |
| SuperSwarf | A1105 | 5.6 | 60 | 7.6 | 18 | 3 | 5.7 | 73 |
| SuperSwarf | A1103 | 5.7 | 60 | 8.6 | 18 | 6 | 5.3 | 113 |
| Asterix | 7785 | 6 | 60 | 8.5 | 16 | 1 | 9.3 | 72 |
| Asterix | 7784 | 6.2 | 60 | 8.5 | 16 | 3 | 7.4 | 117 |
| Asterix | 7786 | 6.4 | 60 | 8.5 | 16 | 6 | 6.2 | 220 |

As discussed above, all of the experiments show a limitation in the spot size as the cathode diameter is reduced. In some cases, the spot size actually starts to increase as the cathode diameter is reduced (Fig. D1a). It is somewhat reassuring and noteworthy that although there are some differences in spot sizes, that overall the spot sizes were similar in size for similar sized cathodes and often overlapped one another. Figure D1b shows that all the experiments experience a reduction in dose as the cathode diameter is reduced (Fig. D1b). This reduction appears to become more severe as the characteristic voltage (power) of the accelerator increases.

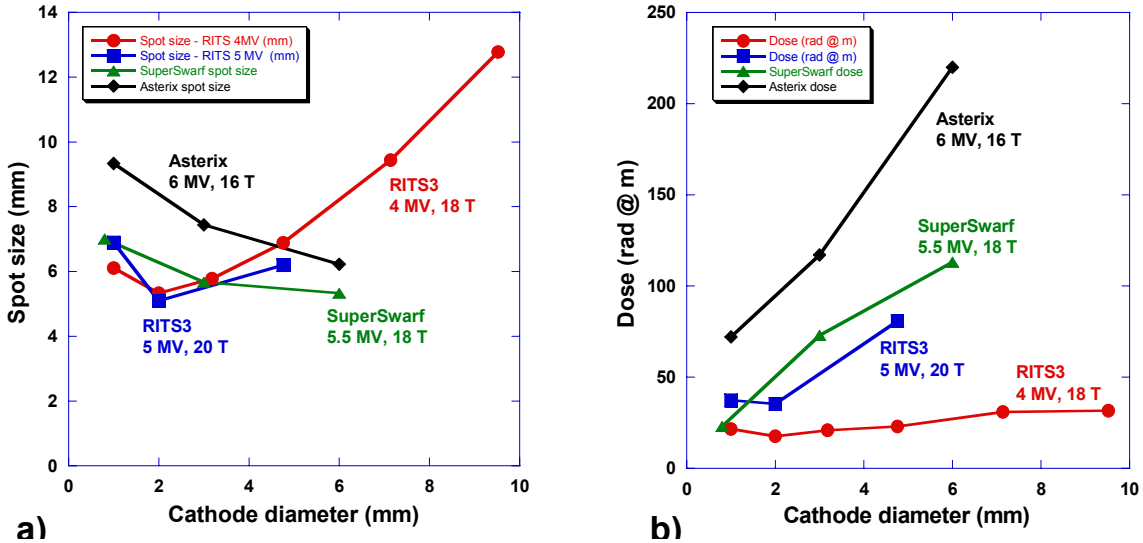


**Figure D1.** a) Spot size and b) dose as a function of cathode diameter for different accelerators/diodes.

## Appendix E: Large cathode exceptions

In general, experiments with large cathodes were fairly well behaved, exhibiting relatively good impedance with low diode currents and good dose production. However, there were noteworthy exceptions to this generalization. Figures E1a and E1b show the time dependent diode currents and measured dose rate for a variety of cathode diameters. These particular experiments were conducted on RITS-3 at 4 MV with 10-cm gaps and 18-T magnetic fields.

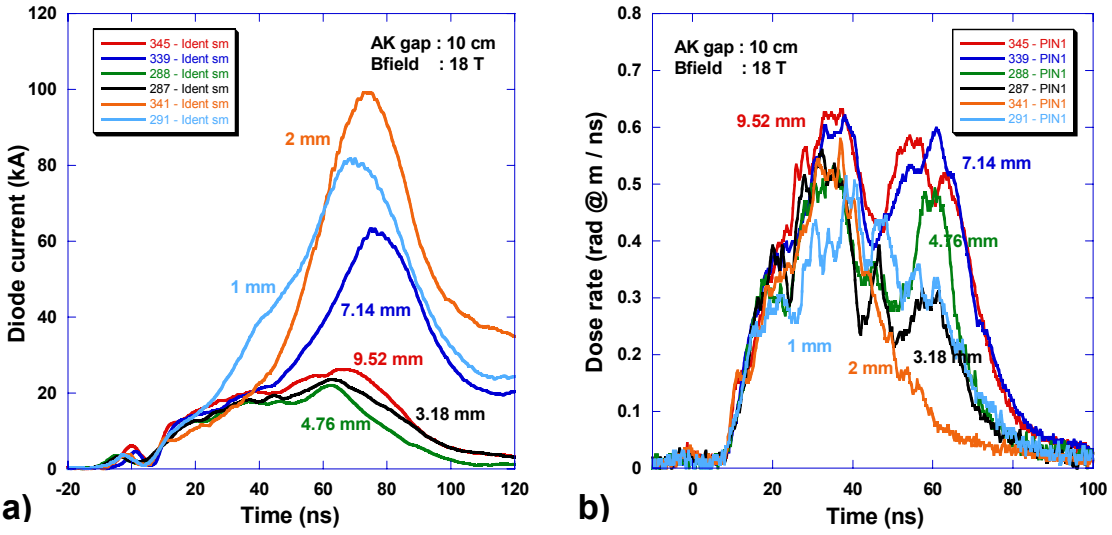


**Figure E1.** a) Diode current and b) dose rate as a function of time for different cathode diameters at 4 MV. Note the late-time impedance collapse of the 7.14-mm cathode.

The highest currents belong to the smallest cathodes, 1 and 2 mm. The rest of the diode currents for the other cathode diameters never exceed 30 kA, except for that of the 7.14-mm diameter cathode. The associated dose rate production for the 7.14-mm cathode is also somewhat exceptional (Fig. E1b). Typically, very high diode currents are accompanied by relatively poor dose production with shorter and smaller radiation pulses. That is not the case here for the 7.14-mm cathode. Although its radiation pulse does increase as a result of the increased current, it does exhibit a pronounced second peak in dose rate, similar to the 4.76 and 9.52-mm cathodes but unlike the smaller cathodes (1, 2 and 3.18 mm) which do not have exhibit a second peak.

Had this exceptional behavior – anomalously high diode currents – for large cathodes been a single occurrence, it might have been quite easy to dismiss as an experimental anomaly but it was observed on other shots similar to 339 e.g. shots 305 and 308. The configurations for shots 305 and 308 were identical to 339 except 305 had a 12-T B field and 308 had a 5-cm gap. It is noteworthy that while shot 308 exhibited a large second peak in radiation, 305 did not. What is consistent is that all of them had fairly well behaved currents during the first half of the pulse that grew very rapidly later in the pulse.

The question one might ask is, "why expend so much effort and energy on the exceptional behavior of large cathodes?" The reason is because based on much of the other data presented in this work, e.g. anode material variations presented in Sec. V, it would be easy to come to the conclusion that the cathode, and processes that get worse as the cathode gets smaller, are solely responsible for the anomalous behaviors observed in the immersed-$B_z$ diode. The purpose of presenting the data for large cathodes exhibiting poor behavior is to caution those who might be tempted to jump to such conclusions. This reasoning is further supported by anecdotal evidence on Hermes III where large cathodes exhibited better impedance behavior and dose production than small cathodes but still had currents that greatly exceeded the currents based on bipolar flow.

## Appendix F: Anode material exception - Polyethylene

As discussed in Sec. V, a careful study of the effect of anode materials showed that there was very little change in diode behavior (impedance, dose production and spot size) with anode material. There were, however, two notable exceptions, the frozen hydrogen experiments, that are described in Appendix I and experiments that involved the use of relatively thick sheets (.020") of polyethylene placed in front of the Ta converter. It is believed that the frozen hydrogen experiments suffered from some mechanical or thermal mechanism related to the pulsed magnet that liberated $H_2$ or $D_2$ into the diode region prior to the accelerator pulse that became a gaseous discharge effectively shorting out the diode. The other notable exception that is not well understood is the polyethylene experiments presented here. As has been stated previously, based on the arguments and results presented in the main body of this report it would be tempting to conclude that processes involving the cathode are primarily responsible for the limitations observed with small cathodes, i.e. the inability to achieve small spot size with good dose-production and nominally good impedances. The results presented here suggest that at least in some cases processes surrounding the anode are responsible for anomalous behaviors.

Figures F1a and F1b show the diode current and measured dose rates for two experiments with polyethylene-covered anodes and four experiments with various other room temperature materials were used, Ta, (Stainless-steel) SS, Au and C in graphite form. The detailed construction of each of the anodes is listed in Fig. F1. The Ta and Au anode experiments were followed by a .1" stainless steel beam stop. All the other foil materials were placed directly in front of a Ta converter and followed directly by a .1" thick stainless steel beam stop. All of these experiments were conducted at 4 MV with 3.18-mm cathodes, 10-cm AK gaps and 12-T B fields. The diode currents for the non-polyethylene experiments are quite similar while the currents for the polyethylene experiments rise very quickly and diverge from the other currents very early in the pulse at ~ t = 20 ns. This dramatic difference in current is not reflected in the measured dose rates, even though the dose rates for one of the polyethylene shots is slightly larger than the other dose rates. Some of the differences in dose rates can be attributed to slight differences in diode voltages between experiments. There was only time-dependent dose rate data available for the first of the polyethylene experiments because of diagnostic problems. However, the integrated dose for the second polyethylene experiments reflected a slight increase in dose as well. The average total dose for the non-polyethylene shots was 17.7 rad @ m while the dose for first and second polyethylene shots was 21.4 and 21.5 rad @ m respectively. It is interesting to note here again that, somewhat different from other effects, high diode currents are accompanied by relatively good dose production. The only other effect where this was most pronounced was in the case of high prepulse (Appendix B).

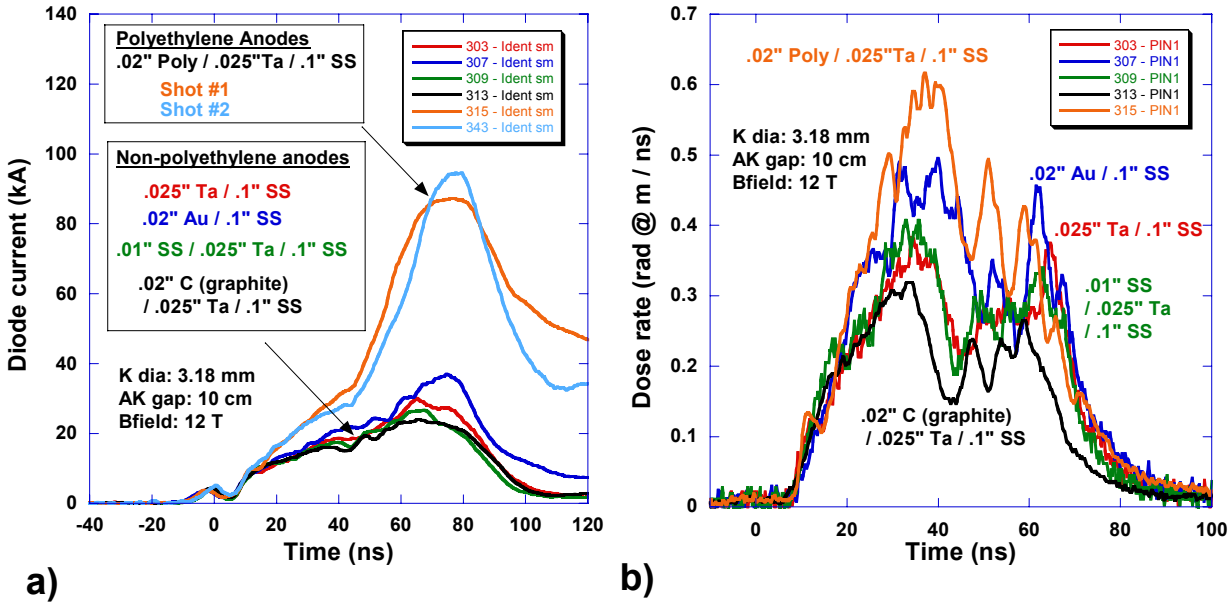


**Figure F1.** a) Diode current and b) dose rate as a function of time for different room temperature anode materials, including polyethylene, at 4 MV. Note the anomalous behavior of the polyethylene anodes.

# Appendix G: Comparison of experimental to numerical and analytical models

Much effort has gone into trying to understand and model the electrical behavior of immersed-$B_z$ diode as well as its radiographic performance, i.e. spot size and dose production both with analytic and numeric models. The theoretical and modeling efforts to better understand the immersed-$B_z$ diode are on going. The results presented are representative of those efforts and to some degree represent a snapshot of our understanding at this time. In general, there is better agreement of the models and simulations with experimental results for larger cathodes, > 4 mm in diameter. However, even for larger cathodes there are some differences that still need to be explained and better understood. Contemplating these differences can be insightful and where possible may allow us to challenge existing theories and previously conceived notions concerning the operation of the immersed-$B_z$ diode.

## Diode currents

Figures G1 and G2 show a comparison of experimental diode currents with simulation results from LSP for various anode conditions and ion species. Figure G1 shows a comparison of LSP results to experimental diode currents obtained for shot 763, a 4.76-mm cathode, discussed extensively in Secs. II and III. Figure G2 compares LSP results to experimental results for the 2-mm cathode results for the anode material/treatment variation experiments discussed in Sec. V.

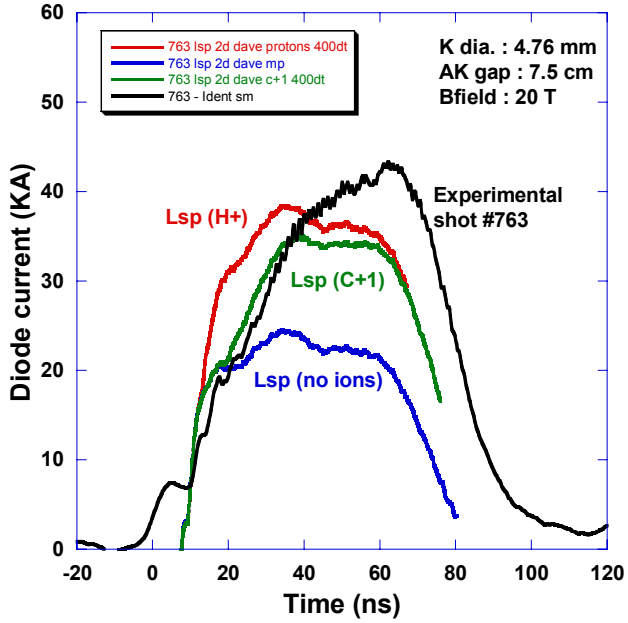


**Figure G1.** Comparison of simulated and experimental diode currents for shot 763, RT Ta anodes at 5 MV.

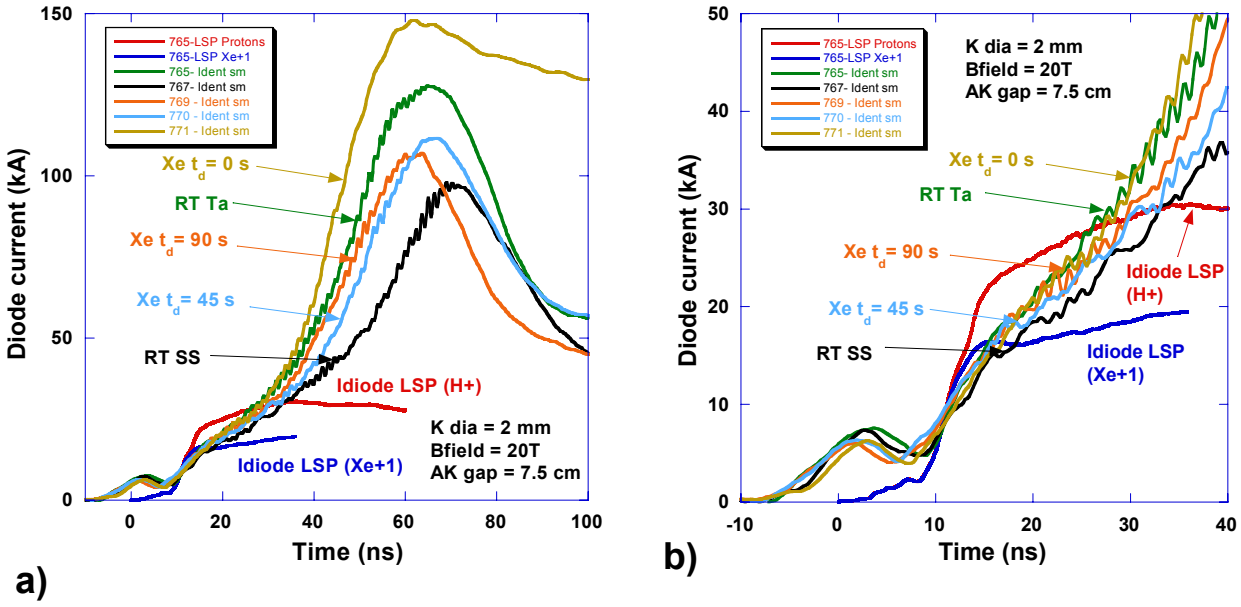


**Figure G2.** a) Full-pulse diode current and b) early-time diode current comparison with anode material/treatment variation of experimental and numerical results for 2-mm cathodes at 5 MV.

All the LSP simulations were 2D (r,z) and modeled only the diode region (i.e. only the cathode and anode region) and used the experimental diode voltages as the input voltages (voltages for Shot 763 and 765 were used respectively for Figs. G1 and G2). All the simulations where ion emission from the anode was modeled allowed for backscattering of the electrons and thermal emission of ions after a 400 degree C temperature rise.

There are several noteworthy observations to be made regarding the results in Figs. G1 and G2. The first most notable difference is the fact that the experimental results are in much better agreement with the LSP results for the 4.76-mm cathode (Fig. G1) than the 2-mm cathode (Fig. G2). This is especially true for the peak currents. In Figure G1 the peak experimental current (43 kA) barely exceeds the peak LSP current for the proton case (38.5 kA) or the singly charged C ion case (35 kA). For the 2-mm cathodes shown in Fig. G2, all of the experimental currents exceed the ideal proton bipolar current by more than 75 kA. The other notable difference is in the current rise time and shape. In Fig. G1, the experimental current rises slowly and appears to be more closely approximated by the C+ model than the H+ model. In Fig. G2b the experimental currents for the 2-mm cathode appear to closely match the rate of rise predicted by the ideal simulation for high-energy protons but then continue to rise well above the bipolar current of the simulation. The other surprising result is there was no notable change in the rate of current rise for the Xe coated experiments that suggested a substantial reduction in high-energy proton content based on activation (Sec. V). Had the diode been operating "classically", one might have expected at least some slowing in the rate of experimental current rise for the Xe coated anodes that would more closely approximate that of the Xe+ simulation. The diode current from the Xe+ simulation, shown in Fig. G2b, is similar to what would be expected for

monopolar conditions with no ions for a long time because it takes so long for the massive Xe+ ions to cross the gap and enhance the electron current being accelerated from the cathode.

Historically, based on previous work on Hermes III, it was generally assumed that the immersed-$B_z$ diode behaved quasi-normally or classically early in the pulse. During this time the diode current was well behaved and agreed fairly well with the expected bipolar current for a proton-emitting anode. Then, depending on the gap, the diode would eventually transition to an anomalous mode where the current would run away, the impedance would collapse, and the dose production would dramatically decrease. The validity of this physical picture where the diode behaved classically early in the pulse must be reconsidered in light of the results presented in Figs. G1 and G2. Most of the data obtained on Hermes III was collected with a 1-mm cathode with mostly stainless steel anodes. In a similar fashion to RITS-3, the current rose very quickly for small cathodes. In Fig. G2, taking into account only the data for the RT Ta and SS anodes, it is plausible to draw the conclusion that protons might be responsible for the early time impedance behavior for the 2-mm cathode results presented. However, this same conclusion cannot be reached in light of the Xe coated experiments where the high-energy proton content of the beam was substantially reduced and yet no difference is observed in the diode current.

Hermes III experiments did not benefit from a large number of experiments with larger cathodes. Although a few experiments were attempted with larger cathodes, the diode current to was not controllable to the extent that was observed on RITS-3. Significant portions of Hermes III data are lost, thus it is difficult to make comparisons like those shown in Fig. G1. Why the experimental current rise is better matched by the C+ model than the H+ model is not understood. One would think that because of the abundance of protons as evidenced by the activation for shot 763 (6.5e7 dpm/100 $cm^2$) that there would be plenty of protons to satisfy the proton current required for bipolar flow. This implies that either LSP does not adequately model the turn-on and emission of protons or that similarly to the 2-mm cathode results, it may imply that the anode constituents do not play a significant role in determining the behavior of the diode even for larger cathodes.

## Dose production

The ability to model and match the observed dose production is important for a several reasons:

- It independently helps to confirm the validity of the voltage and current measurements.
- It is a metric by which the relative performance of the diode can be compared for different experiments as well as other diodes.
- It can be used for scaling the dose production to future accelerators with higher voltages.
- It can provide insight into possible mechanisms that cause differences in diode behavior.

The ability to model the dose production of the immersed-$B_z$ diode has been previously documented for a single experiment on SABRE.[vii] Figs G3 a and b, compare the measured dose rate to empirically derived dose rates using the same scaling with current and dose as , $IV^{2.3}$ for two 4.76-mm cathode experiments, one at 4 MV (Fig. G3a) and one 5 MV (Fig. G3b). It should be noted that the relative agreement shown in Fig. G3 was only possible on RITS-3 for large cathodes (typically greater than 4.76 mm) that exhibited good impedance behavior throughout the pulse. It was not observed under any other conditions.

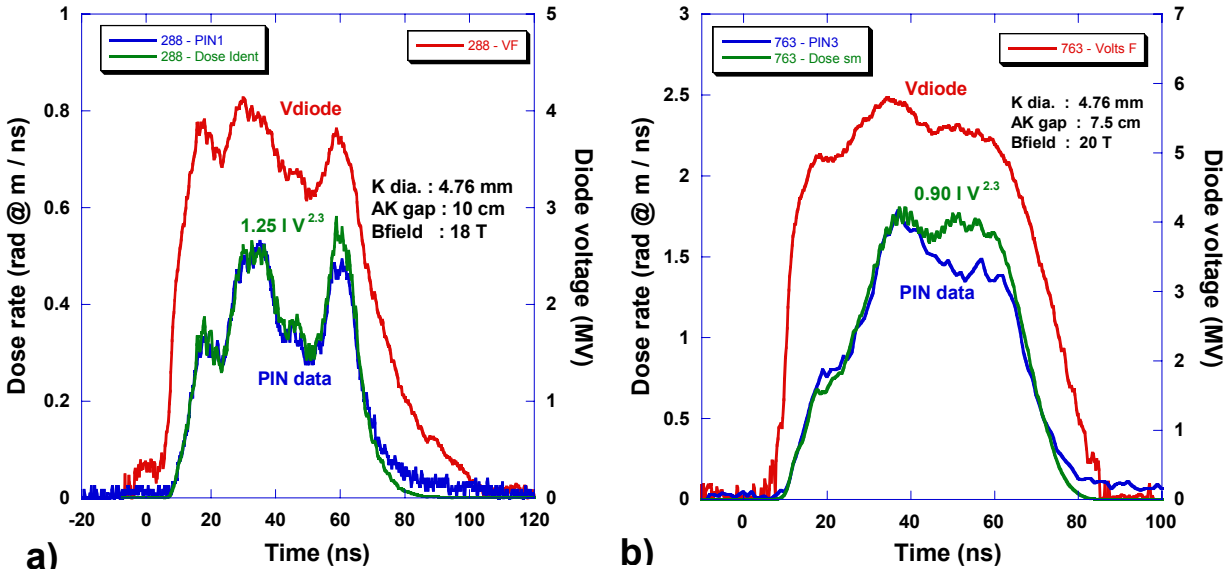


**Figure G3.** Comparison of experimental dose rates (PIN data) to empirically derived dose rate equations for 4.76 mm cathode at a) 4 MV and b) 5 MV.

It should be noted that the constant in front of the IV scaling relationship are considerably lower than that suggest by Ref. [vii], 1.25 and 0.9 vs 2.0. The source for this difference is not understood at this time. Some of the slight difference between the constant for 4MV and 5 MV may be due to the slightly thicker stainless steel beam stops/debris shields and vacuum wall used on the 5 MV diode configuration (.45" vs .26").

## Spot size

Figure G4 shows a comparison of representative analytical (dashed and dotted lines), numerical (open symbols) and experimental spot size results (solid symbols and lines). The equation used for calculating the analytical spot sizes shown in Fig. G4 is an empirical form of adding the cathode radius ($r_K$) and offset ($\varepsilon$) (Eq. 2) due to hose in quadrature and then multiplying by two to get the spot size,

$$Spot\ size = 2 * \sqrt{(C1 * \varepsilon)^2 + (C2 * r_K)^2} \quad (mm) \qquad (G1)$$

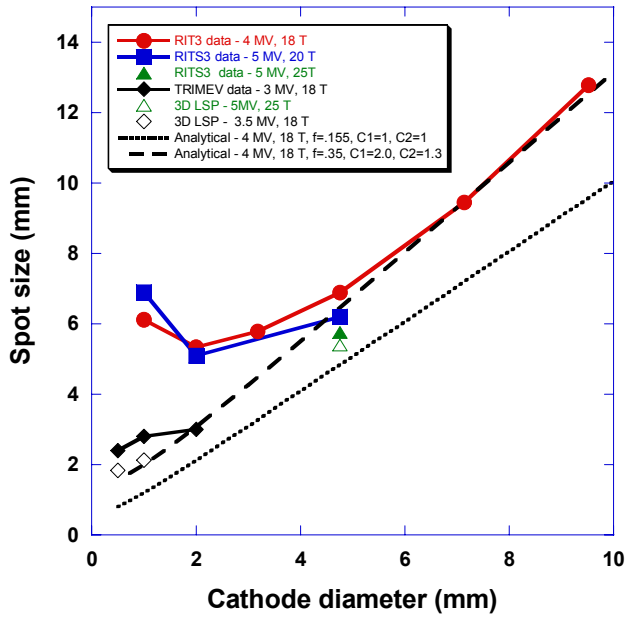


**Figure G4.** Spot size vs. cathode diameter for experimental, analytical, and numerical results.

The dotted line shown in Fig. G4 represents an ideal or pure form of the analytical spot size for operation at 4 MV and 18 T, where f =.155 (Sec. I), and the constants C1 and C2 are set equal to 1. This represents the original ideal scaling for immersed-$B_z$ diode where the spot size was thought to scale directly with the cathode diameter except for very small diameters, where some correction was required to account for the offset due to the ion hose instability.

The dashed line, also assuming operation at 4 MV and 18 T, represents an empirical fit or improvement over the ideal analytical spot size with several adjustments of the free parameters and constants to better match simulated and experimental behavior. The constants f (f = .35) and C2 (C2 = 2.0) have been adjusted to better match the current and size of offset calculated using LSP simulations with more complete models of the anode physics including backscattering of electrons and thermal emission models for ions. The constant C1 has been adjusted to fit the large cathode data from RITS-3 at 4 MV and 18T (red solid line and circle symbols.)

Figure G4 also shows two direct comparisons of LSP calculated spot sizes to experimental spot sizes for both RITS-3 (open vs solid triangles) and TriMeV experiments (open vs. solid diamonds), Both sets of LSP simulations used full 3D simulations with realistic but idealized pulse shapes and full experimental diode geometries including the exact magnetic field shape and upstream transition region. The TriMeV LSP models (3.5 MV, 18T) assumed ideal bipolar operation with protons emitted from the cathode, while the RITS-3 model shown for shot 592 (5 MV, 25 T) used the carbon stripping model.[viii, ix] The other experimental data that is included for comparison is the RITS-3 3 data at 5 MV and 20 T (blue solid line and square symbols).

Figure G5 shows how well the LSF from the LSP simulations at t=40 ns compares to the experimental LSF for shot 592 (5 MV, 25 T). The LSF for shot 763 with the same cathode diameter but slightly slower field of 20 T as 592 is included as another reference point to show how similar shots compared. It should also be noted that another difference was that shot 592 used a RT SS while shot 763 used a RT Ta anode.

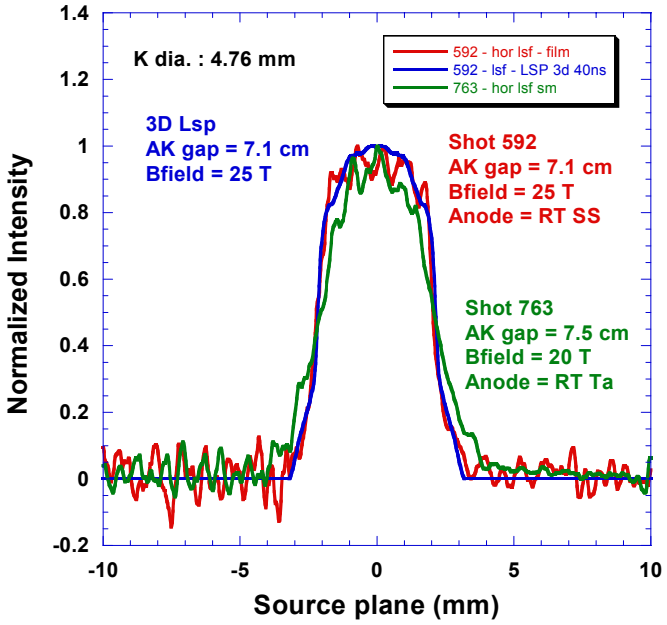


**Figure G5.** Comparison of experimental line spread functions (LSF) to those obtained from a 3D LSP simulation.

There are several observations to be made concerning the comparisons and results presented in Figs. G4 and G5. Good agreement with analytical spot size scaling and simulations are observed for large cathodes $\geq$ 4.76 mm. This coincides with cathode diameters that are nominally well behaved electrically. There is fairly good agreement with analytical spot size scaling and simulations for small cathodes (0.5 – 2 mm) for the TriMeV data. There is fairly poor agreement for small cathodes ($\leq$ 3.18 mm) for the RITS-3 data at 4 and 5 MV. It is believed that the primary reason that TriMeV small cathode data shows better agreement with LSP and analytical scaling than RITS-3 is due to the much shorter pulse width (20 ns compared to 70 ns). Time-resolved spot data from TriMeV showed that the spot grew very quickly to 3.5 to 4 mm.[x] Had the pulse been longer it is believed that the spot size would have grown to at least that level. Another factor may be that power on target was much lower for TriMeV than RITS-3. Peak voltages on TriMeV were around 3 MV with peak diode currents between 15-20 kA. This may also have affected the spot size growth rate.

## Appendix H: Cryogenic coating apparatus and process description

As discussed in section V, the original objective of pursuing *in situ* coatings was the desire to coat thick layers of frozen hydrogen – either $H_2$ or $D_2$ – on the anode. The rational was to eliminate the non-protonic contaminants that exist on untreated electrode surfaces[xi, xii] and thereby eliminate one possible source of charge creation in the gap, namely stripping of ions by ion-ion collision. Because of the severe environment and direct bombardment of the anode by the electron beam, it was felt that layers much thicker than used by Hanson (a few monolayers) for his ion diode experiments[xiii] would require a coating scheme more similar to those used by muon fusion beam experimentalists where coatings 100 of microns of hydrogen are frozen onto thin gold and silver foils. Although our coating system was inspired by those used in muon fusion research[xiv, xv] there was a major difference because of physical access constraints. In muon fusion experiments a coating diffuser is typically inserted radially into the beam line in very close proximity to the foil target during the coating process and then removed prior to the beam experiments. In our case, where the target is surrounded by the magnet and radial access is virtually impossible, it was necessary to mount the coating diffuser directly on to the target or anode as shown in Fig H1a. The configuration shown in Fig. H1a was the original design intended to be used for all of the cryogenic coating experiments. Unfortunately, early in the development the cryogenic coating system, it was realized that the temperature of the LHe-cooled stainless anode was limited to temperatures between 10 and 15K which was not adequate to effectively freeze either $H_2$ or $D_2$ onto the anode surface (for a vacuum pressure of 10-6, the equilibrium temperatures for $H_2$ and $D_2$ are 4.2 and 5.8 deg. K respectively).[xvi]

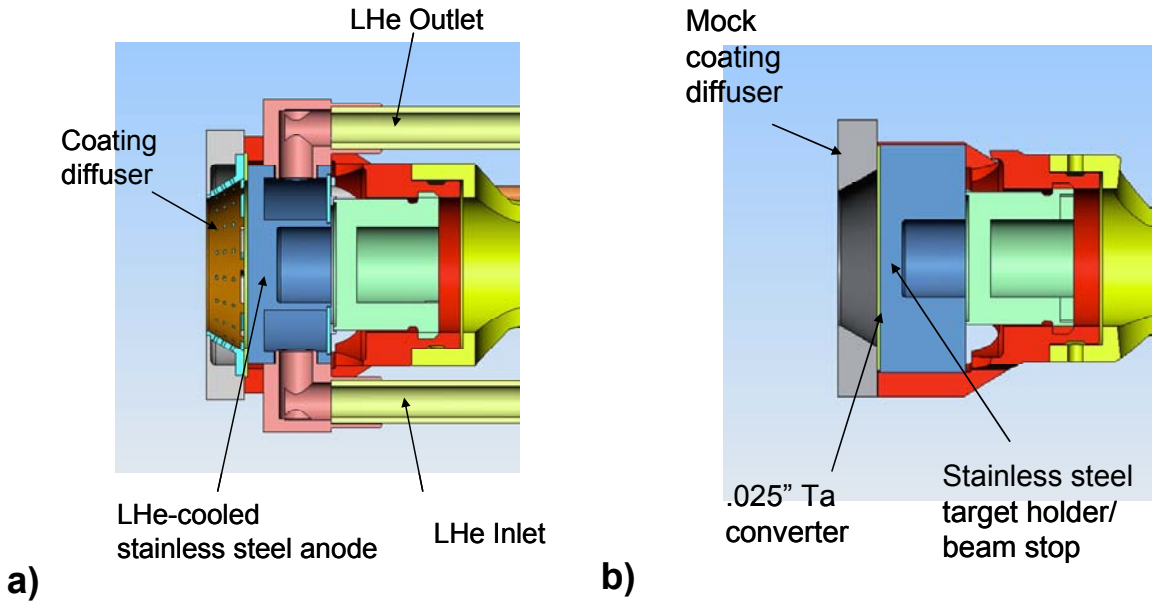


**Figure H1.** a) LHe-cooled stainless steel anode used for Xe coating experiments (767-771) b) room temperature configuration with .025" Ta converter (763-766, 773, 777).

One of the other concerns about the LHe-cooled stainless steel anode was that even if it had been able to achieve the necessary temperatures, there were concerns about the eddy current heating during the magnet pulse. To eliminate these concerns as well as achieve lower temperatures, the stainless steel face of the anode was replaced with a sapphire anode as shown in Fig. H2a. Sapphire was chosen because not only is it an electrical insulator, but also because of its crystal structure it has very good thermal conduction at low temperatures.[xvii] Although it is very brittle, it is also very hard and with the proper techniques it can be readily machined and polished into fairly elaborate topologies, (e.g. the reentrant target design shown in Fig. H2b). The use of a sapphire as an anode material required the use an indium gasket or o-ring to act as a vacuum seal. Typically, pure indium is used to make these types of seals and was also used here during the development of the LHe-cooled sapphire anode. However, because very pure metals have such good electrical conductivity at LHe temperatures, an indium-tin alloy of 95% In and 5% Sn (.020" diameter wire) was custom made by the Indium Corporation. The reasoning was that the electrical conductivity of pure metals is quickly spoiled by introducing impurities. The thinking was that this higher electrical resistivity would allow the pulsed magnetic field to diffuse more easily through the gasket material and also reduce any eddy current heating. Although extensive efforts were made to thermally isolate the sapphire anode from the surrounding metal by using nylon insulators as shown in Fig. H2, it was deemed impractical to try to use a non-metal gasket to make a LHe-vacuum seal. To make the seal, two separate pieces of .020" wire were formed into o-rings and then the location where the ends of the wire overlapped were placed 180 degrees apart.

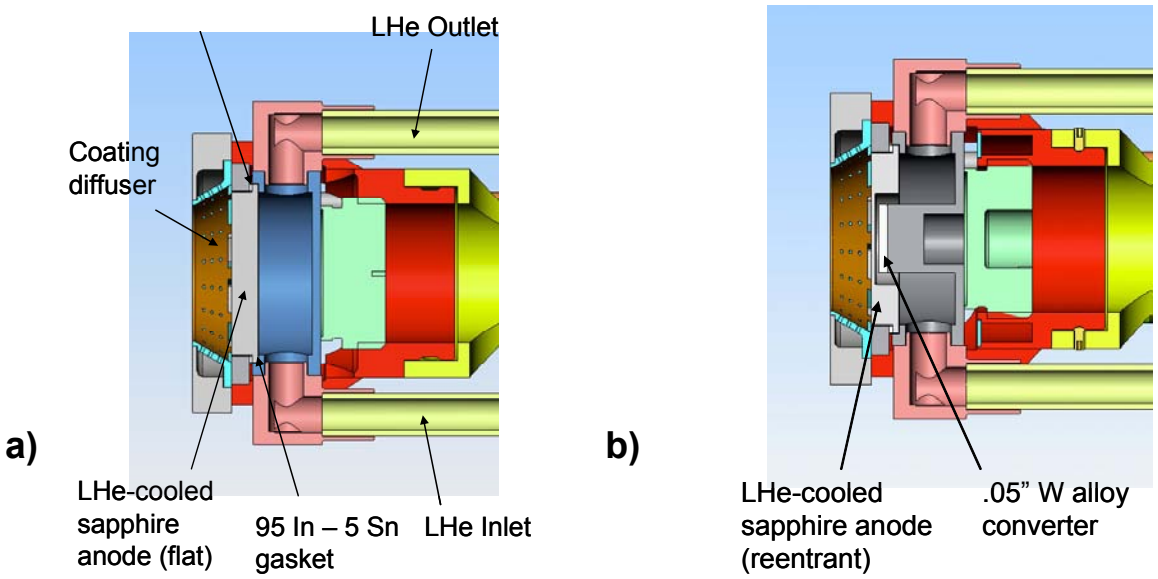


**Figure H2.** a) LHe-cooled anode with flat sapphire anode for frozen H2 and D2 development and initial RITS-3 diode experiments (772-776) b) LHe-cooled sapphire anode with reentrant target designed for radiation production at 10 MV; used on experiments 778 – 784.

Figures H3, H4 and H5 document the capability to coat LHe-cooled sapphire anodes with relatively thick layers of both $H_2$ and $D_2$. These coating and cooling tests were performed on a small vacuum chamber in the light lab with optical access to the front of the anode. Figure H3a shows the time history for of the vacuum pressure and sapphire anode temperature during one of the $D_2$ coating development experiments. In addition to the anode temperature and pressure history, the temperature of the coating diffuser is also recorded in Fig. H3a. Earlier tests had shown that it was necessary to precool the entire anode assembly and coating diffuser to ~ 100 K with LN to achieve the uniformity of the frozen $D_2$ on the sapphire as shown in Fig. H3c. This was achieved by flowing LN through the same lines and plumbing as was used for the LHe cooling. This precooling process was inefficient because of the poor thermal conductivity of stainless steel and poor thermal contact between the stainless body of the anode and the stainless steel diffuser. (In fact, to improve thermal contact conductivity two ribbons of indium wire were squeezed between the anode and the diffuser.) Figure H3b shows how the anode looked prior to coating. The sapphire anode is polished and clear just like a window. The dark-ribbon structure at the bottom of Fig. H3b is actually part of the pure indium gasket material that had squeezed out. Fortunately, the gasket still formed a good tight vacuum seal.

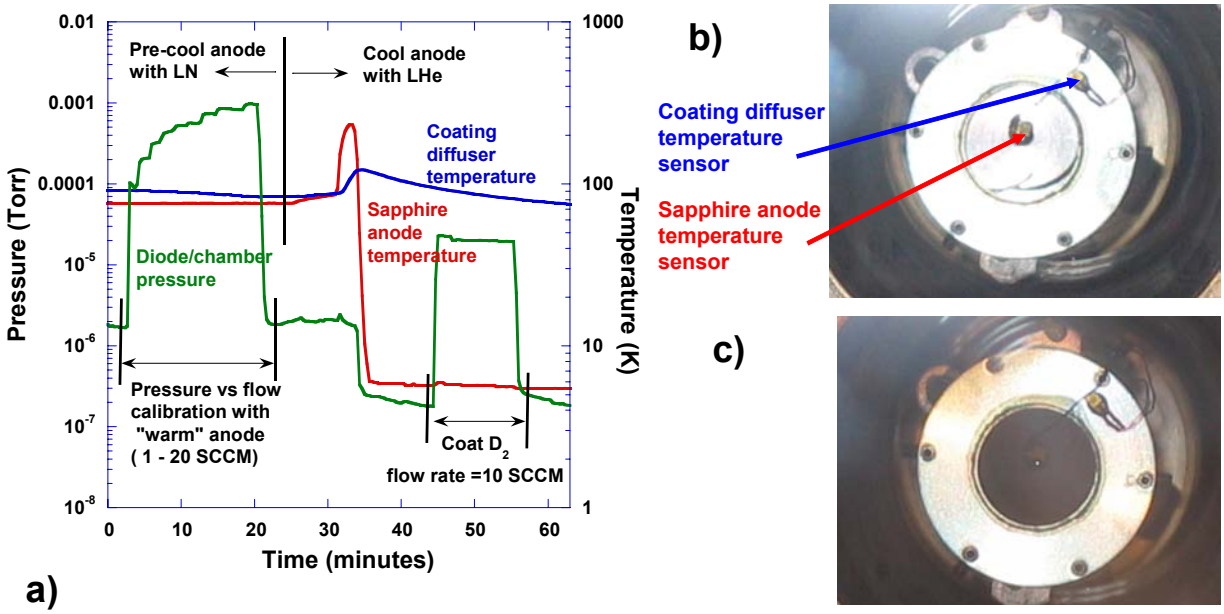


**Figure H3.** a) Temperature and pressure history for $D_2$ coating test on diode test stand 12_22_04. Picture of b) uncoated anode c) anode coated with frozen $D_2$.

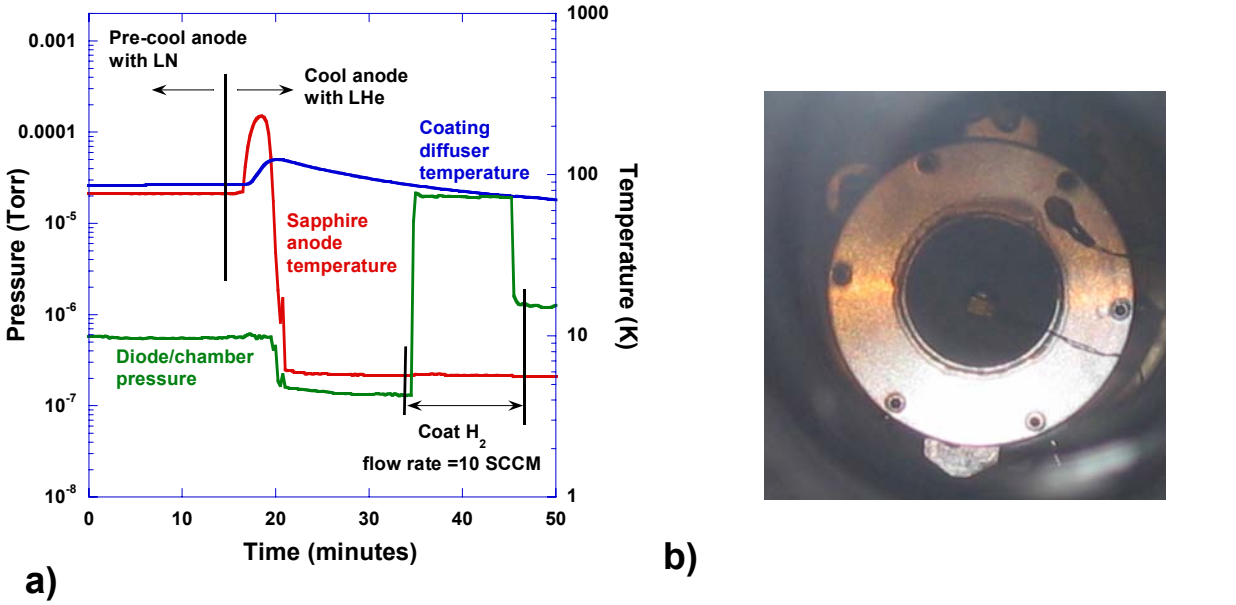


**Figure H4.** a) Temperature and pressure history for $H_2$ coating test on diode test stand 2_16_05. b) Picture of anode coated with frozen $H_2$.

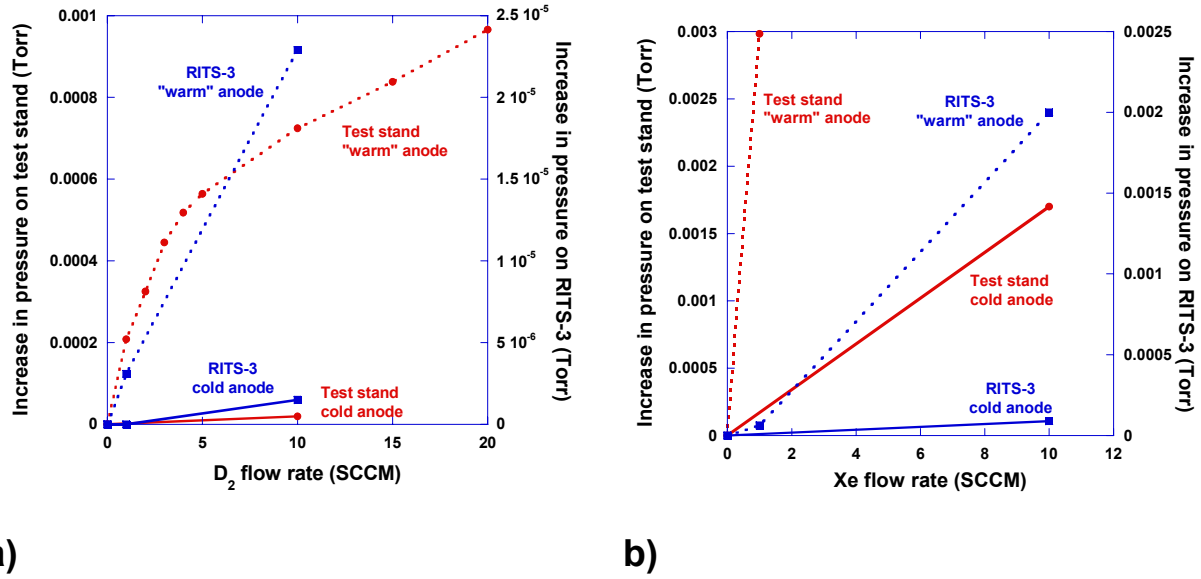


**Figure H5.** Pressure increase vs. flow rate for "warm" and cold operation on the diode test stand and on RITS-3 for a) $D_2$ coating and b) Xe coating.

Besides the very obvious change in appearance after the frozen $D_2$ was applied, the other indicator that $D_2$ was being cryopumped by the LHe-cooled sapphire anode was the difference in vacuum pressures with and without LHe cooling. Figure H3a shows the pressure increases recorded during a "warm" anode calibration flow test during the LN precool and prior to the LHe cooling. During the flow test the flow was varied from 1-20

SCCM and the data for this curve is the dashed red curve shown in Fig. H5a, where the pressure increase is plotted as a function of flow rate. After the warm flow test was conducted the LN was turned off and the cooling was changed over to LHe. There is actually an initial increase in both the temperature of the anode and coating diffuser as the warm air is force out of the cryogenic vacuum lines connecting the 250-liter LHe bottle to the bayonet cryogenic feedthru at the back of the cryogenic anode assembly. However, the sapphire anode temperature only takes a few minutes to cool down to a temperature cold enough to allow coating of the $D_2$, namely 5.5° K. For this test $D_2$ coating was applied by flowing $D_2$ at a rate of 10 SCCM for approximately 10 minutes. Although Fig. H3a shows that there was an appreciable increase in pressure during the coating, it was substantially lower than during the calibration flow test. This dramatic difference is more readily seen in Fig. H5a, where the increase in pressure for the calibration flow test (red dashed line) is compared to the increase in pressure during the $D_2$ coating (solid red line). It is believed that this difference is a true indication that the $D_2$ is being frozen onto the LHe-cooled sapphire anode. It is also believed that the difference between the two can be used to estimate the amount or fraction of the gas that is sticking or freezing to the anode. If one assumes that the pressure increase during coating is caused by gas that does not stick to the anode, then that amount of gas can be estimated by finding the equivalent pressure increase from the calibration flow test. For instance, the equivalent warm amount of flow required to raise the vacuum pressure to the same amount observed during coating would be only .095 SCCM. This would indicate that nearly 99% of the $D_2$ being directed onto the anode through the holes in the diffuser (54 .020" dia. holes) is sticking to the anode. Although this does seem high, this technique was repeated with the diode mounted on the RITS-3 accelerator with a slightly different geometry and different vacuum pumps. The blue dashed line in Fig. H5a corresponds to pressure increase for the warm calibration test (conducted during the LN precool) and the solid line corresponds to the pressure increase recorded during the actual coating. Again, there is a dramatic difference in pressures. However, the equivalent sticking or pumping efficiency in this case is not quite as high but still quite good, 95%.

One interesting difference that is worth noting between the $D_2$ coating tests results shown in Fig. H3 and the $H_2$ results shown in Fig. H4 is the pressure after the gas supply is turned off. Figure H3a shows that the pressure after coating returns to baseline pressure prior to coating. This is an indication that there the $D_2$ is not sublimating. This is not the case for the $H_2$ coating where the pressure after coating is substantially higher than prior to the coating, probably indicating that $H_2$ was sublimating off the anode. Therefore, a relevant question is why the $H_2$ sticks at all to a surface at 5.5° K. The best probable explanation is the effective pressure during coating is much higher than the equilibrium vapor pressure at that temperature.

Similar measurements as discussed above were used to estimate the sticking efficiency for the Xe coating experiments, shown in Fig.H5b for both the test-stand (red lines) and the RITS-3 accelerator (blue lines). The corresponding sticking or coating efficiencies for Xe are calculated to be 94% for the test stand and 89% on RITS-3. The fact that the Xe coating efficiency appears to be slightly less than the $D_2$ is somewhat surprising, given the temperatures of the LHe-cooled stainless anode (10-15 K) are so far below the equilibrium

temperature of 57.7 K at 1 e-6 Torr. However, it should be noted that no pre-cooling of the coating diffuser was performed during the Xe coating tests and so the coating diffuser was effectively at room temperature. Whether or not this could account for difference is unknown. It may be that the technique described here is somewhat limited as an absolute measure of the coating efficiency, but in any case it is believed adequate for the purposes required here and that is to estimate the inventory of gas frozen to the anode for the different experiments.

Figure H6 shows representative cooling and coating timelines with temperature and pressure histories for $D_2$ coated anodes (Fig. H6a.) and Xe coated anodes (Fig. H6b.). Because placing temperature sensors directly on the anode for the beam experiments would have compromised the experiments, the best alternative and relevant location was chosen for both. In the case of the $D_2$ coated anodes, this was the coating diffuser temperature and for the Xe coated anodes, a sensor was placed on the LHe-outlet elbow (Fig. H1a). Note that previous testing done in the light lab showed that for the LHe-cooled stainless anodes the temperature on the elbow was within a few degrees of the temperature on the anode face. For $D_2$ coated anodes the LHe-cooling process started about 40 minutes prior to the shot. The coating of the anode with $D_2$ would begin when the diffuser temperature returned to 100K to ensure uniform coating. In the case of the Xe coated experiments the LHe cooling process usually began 20-25 minutes prior to the shot and the coating process would start as soon as the temperature of the elbow had reached steady state. Once the coating process started the coating process was basically the same for both $D_2$ and or Xe. Initially the flow rate for both gases was set to 10 SCCM to try to coat out substantial quantities/thicknesses of frozen gas. Prior to exiting the test cell, the flow rate was reduced to 1 SCCM. The rationale behind this was to reduce the amount of overall pressure in the diode as well as shorten the amount of time that it took to pump out inventory of the gas in the supply lines prior to the shot. Note that shut-off valve was located as close to the vacuum wall at the back of diode as reasonably achievable (within a few inches). The goal was to limit the time between gas flow shut off and the actual experiment (referred to as the pumpout delay time, $t_d$) to reduce the amount of recontamination of the anode by background contaminants in the vacuum. Note that the temperature and pressure histories shown in Fig. H6 do not extend up to shot time or even up to the time that the gas flow was turned off, because the system was turned-off at the beginning of the Marx generator charge.

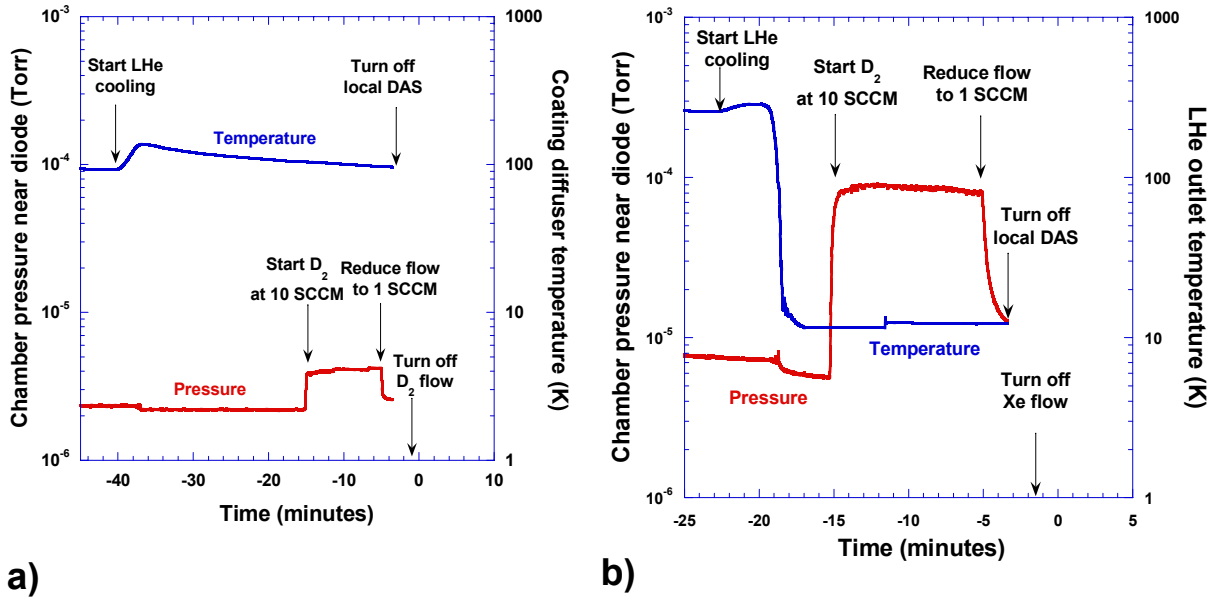


**Figure H6.** Representative cooling and coating timeline on RITS-3 for a) $D_2$ coating and b) Xe coating.

Using the estimated coating efficiency of 0.9 based on techniques discussed above and knowing the approximate surface area of coating area (dia = 2.34 cm.) along with measured flow rates and coating times it is relatively easy to estimate the areal density of the coatings. The areal density for the $D_2$ coating process shown in Fig. H6a is estimated to be 3.92 e-2 g/cm$^2$ assuming 10 SCCM for 10 minutes plus 1 SCCM for 4.5 minutes. Correspondingly, the areal density for the Xe coating process shown in Fig. H6b is estimated to be 1.26 e-1 g/cm$^2$.

It is difficult to estimate the thickness of these coatings because the density is unknown. However, it is possible to estimate the minimum thickness that is represented by assuming that the maximum feasible density, which is equal to crystalline density for each frozen gas. Assuming the density of crystalline $D_2$ is .202 g/cm$^3$ and crystalline Xe is 3.78 g/cm$^3$, the associated thicknesses for Fig. H6 are 194 microns of $D_2$ and 335 microns of Xe. These are fairly representative thicknesses for the all the $D_2$ coated and Xe coated experiments. As is discussed below, because of problems encountered with the frozen $H_2$ and $D_2$ experiments, thinner coatings (~ 20 microns) were tried to see if the problem was related to the coating process and thickness. As is discussed below the only parameter that seemed to affect the anomalous shorting was the strength of the applied B field.

# Appendix I: Frozen Hydrogen and Related Cryogenic Anode Results

As has been discussed previously most of the frozen $H_2$ and $D_2$ experiments exhibited an anomalous shorting of the diode characterized by a rapid rise in diode current and a long current tail where the diode current stayed at very high value long after the pulse was over. Because these results were so anomalous with little or no radiation produced, there is perhaps little value in discussing them in much detail, but it seems worthwhile to at least show their charateristic diode current. Also, because a couple of the $D_2$ experiments at 4 T had quasi-normal behavior, it is worthwhile to put all of this in context and compare the different results. Coincidentally, during these experiments Mark Johnston was just starting to get some interesting spectroscopic results and therefore it is necessary to discuss their electrical results before discussing the associated spectroscopic results in Appendix J.

Figure I1a shows the diode currents of a $H_2$ and $D_2$ experiment that exhibited this anomalous shorting compared to the current for a similar RT Ta experiment. All of these experiments used a 2-mm diameter cathode with a B field of 20T. Figure I1b compares the diode currents for several different frozen hydrogen experiments at different B fields, including the two anomalous 20T shots from Fig. I1a. Attempts were made to try to achieve the highest field possible that might still allow a valid test of the original purpose of eliminating the non-protonic contaminants from the anode. Figure I1b shows that the one experiment at 6T, (black solid line), shows similar anomalous behavior as the 20T experiments. Figure I1b also shows the quasi-normal behavior of the only two frozen $D_2$ experiments (B field = 4 T) that produced a measurable amount of dose and enough dose for the time integrated spot size diagnostics to yield a spot size. Although, the diode currents for these frozen $D_2$ experiments look fairly normal, their behavior are still somewhat suspect when compared to similar experiments conducted with the same parameters but with different cryogenic anode treatment. Figures I2 and I3 compare the electrical and radiographic dose and spot results of the two quasi-normal $D_2$ experiments with a null experiment (LHe-cooled sapphire anode with no coating) and a frozen Ne experiment. These figures show that the two frozen $D_2$ experiments gave very similar results when compared to themselves but noticably different results from the LHe-cooled and frozen Ne experiment which also had similar results.

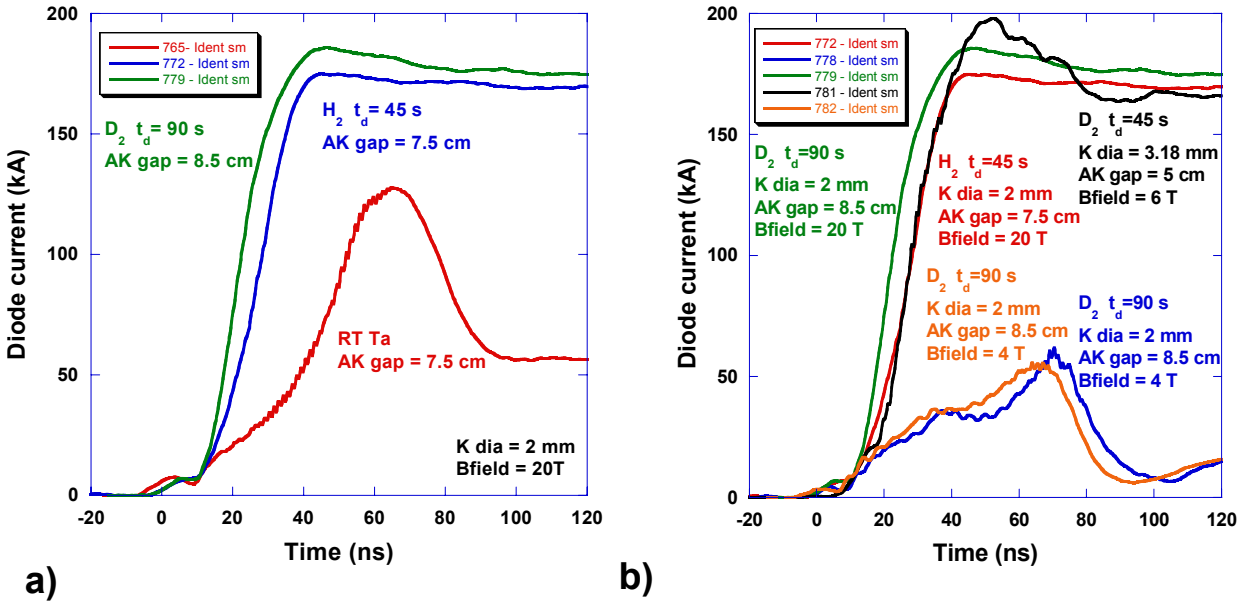


**Figure I1.** a) Comparison of anomalous diode currents from frozen $H_2/D_2$ anodes to RT Ta at 20 T and b) comparison of anomalous diode currents from frozen $H_2/D_2$ at 6 and 20 T with quasi-normal diode currents at 4 T.

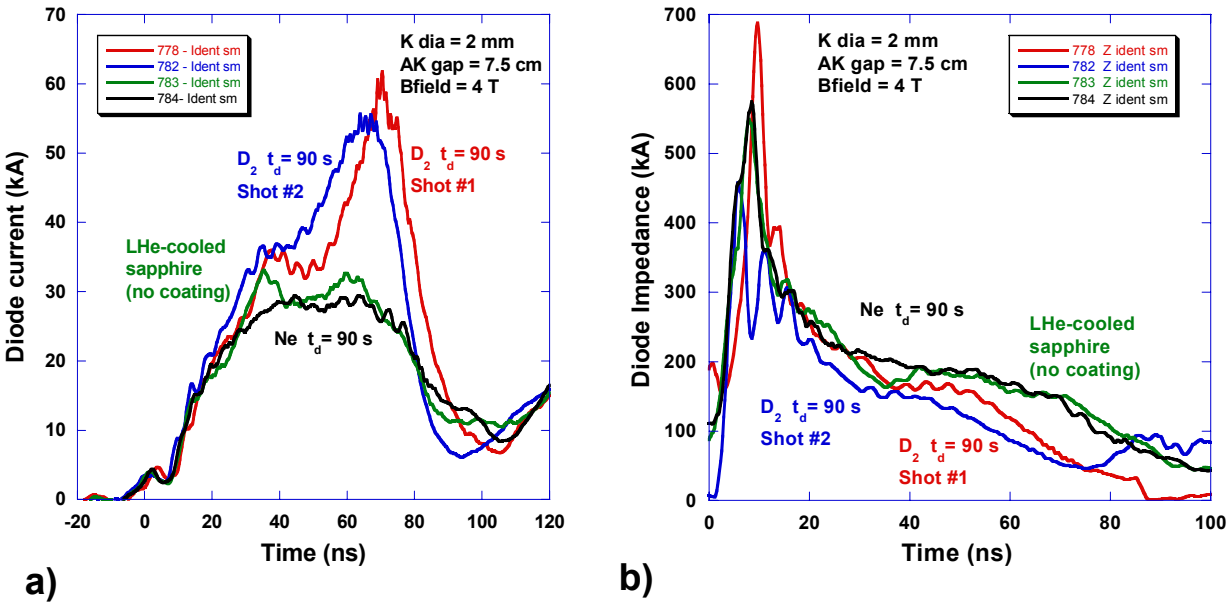


**Figure I2.** a) Diode currents and b) impedance for cryogenic coating variations at 4 T and 5 MV.

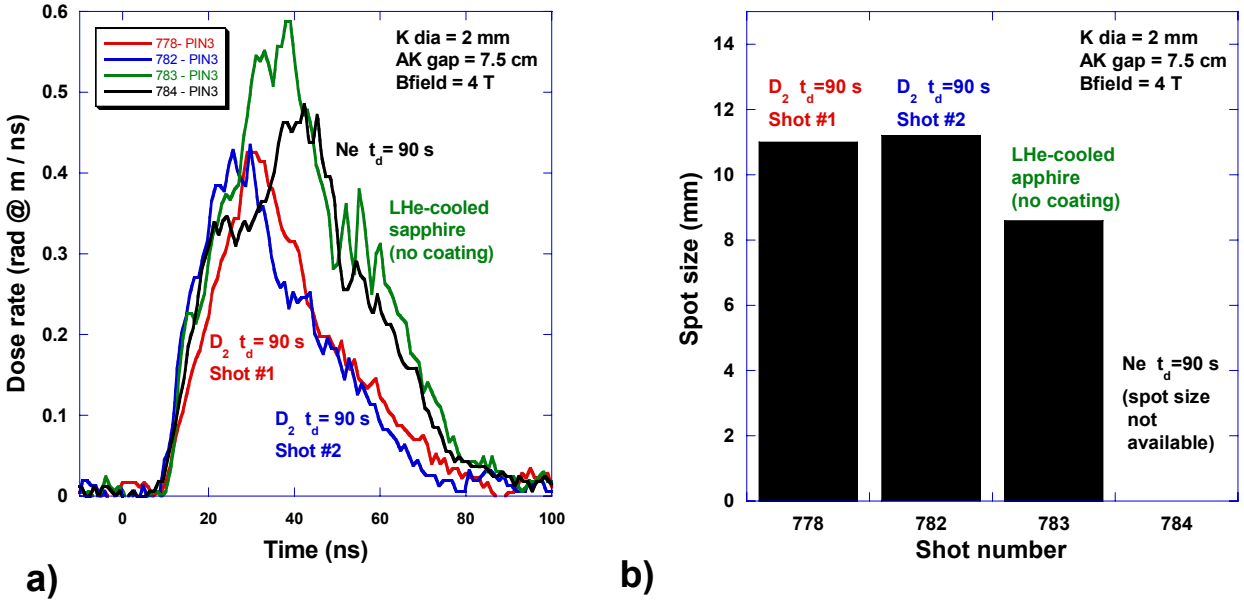


**Figure I3.** a) Dose rate and b) spot size for cryogenic coating variations at 4 T and 5 MV.

At first these results may not seem significant or of much import, however, they are noteworthy for several reasons.

- All the results for the 4-T experiments were obtained using the LHe-cooled sapphire anode with the reentrant target configuration shown in Fig. H2b.
- The fact that quasi-normal behavior was observed with frozen $D_2$ at very low fields indicates that the anomalous behavior of the $D_2$ at higher fields was probably associated with evolution (sublimation) of the frozen $D_2$ due to some mechanism associated with the pulsed magnetic field. The fact that the 4-T $D_2$ results were still different from the null and Ne results, may indicate that these experiments were still near the edge of being anomalous. Because of the extensive measures taken to limit problems due to eddy currents, it is difficult to understand the mechanism that could cause the suspected evolution of the frozen hydrogen into the diode during the magnet pulse. The fact that frozen Ne, which only has a slighlty higher vapor pressure than frozen $D_2$, did not exhibit anamolous behavior tends to discount the eddy current heating supposition. If time and resources had permitted it would have been insightful to conduct a frozen Ne experiment at 20 T.
- The impedance behavior of the null experiment and the Ne experiment are notable because they represent some of the better impedance behaviors observed for any diode configuration. Although it might be tempting to associate this good impedance behavior with the anode treatments, because their behaviors are so similar again reinforces the experimental observation that anode material variations have little effect on diode behavior. Instead, it is conjectured that the good behavior had more to due with the low magnetic field. Although the effect of Bz variations on diode behavior discussed in Appendix A were not as dramatic or consistent as other effects, there was some effect. Figure I4 shows a comparison of

the measured diode currents and dose rates for a 20-T LHe-cooled stainless steel experiment to the 4-T LHe cooled sapphire anode experiment. The 4-T experiment behaved somewhat similarly to the 6-T experiment shown in Fig. A1a where the early time diode currents are nearly identical but then falls off rather abrubtly, rising again later in time for the 6-T case but staying fairly constant for the 4-T results shown in Fig. I4a. Because of the differences in anode configurations used for the 20-T LHe-cooled SS (Fig. H1a) and the 4-T LHe-cooled sapphire experiment, comparisons of the relative magnitudes of the measured dose rates are limited in value. However, irrespective of the magnitudes, Fig. I4b shows that the radiation pulse duration was largely unchanged even though the impedance of the 4-T experiment was dramatically improved over the 20-T experiment. As has been noted previously, this behavior differs from the correlation observed for cathode diamers and AK gaps where improved impedance is usually accompanied by longer radiation pulses.

- The differences in the spectroscopic results with variation in anode material for the 4-T experiments, which are described below, are noteworthy.

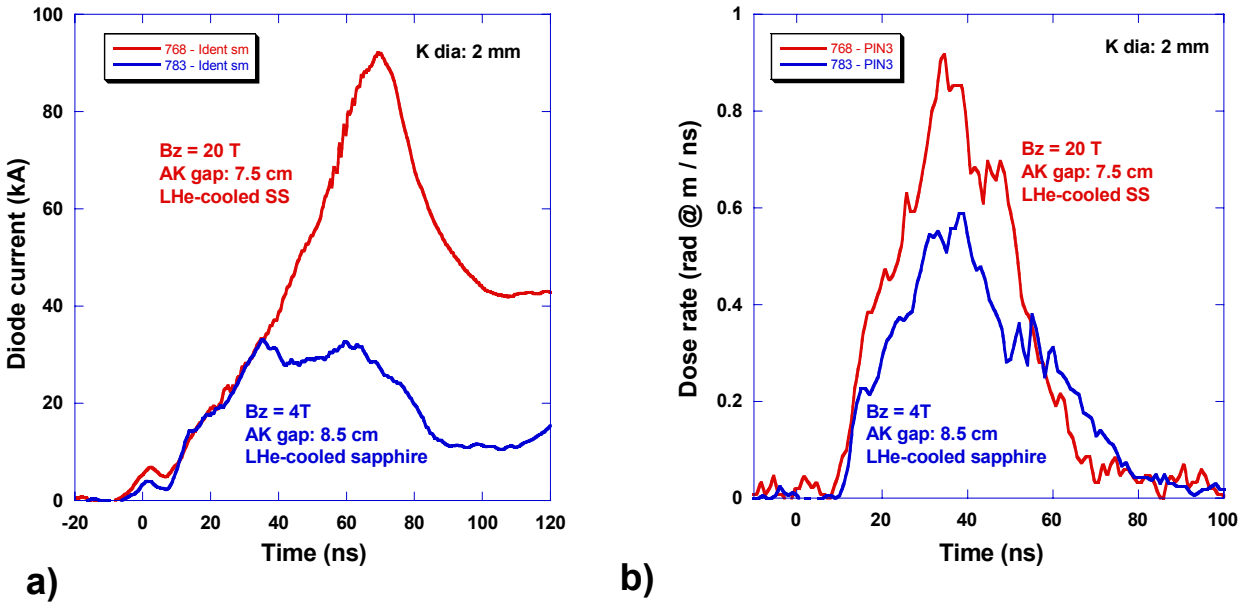


**Figure I4.** a) Diode currents and b) dose rate for 4 and 20 T with 2 mm cathode at 5 MV. Spot size grew from 5.5 mm at 20 T to 8.6 at 4 T.

## Appendix J: Spectroscopy results – plasma velocity implications

Fairly extensive spectroscopic diagnostics were fielded by Mark Johnston during the last immersed-$B_z$ diode shot series on RIT3 (shots763-784).[xviii] The spectroscopic data were recorded using several different techniques including streak cameras, framing cameras and an array of simple PIN diode detectors to measure light intensity. A sample of the emission spectra results obtained by the framing camera was presented in [xviii]. These results showed that early in time there was dense plasma localized at the center of the target

surface as evidenced by very bright continuum. It also showed that lower density plasma was observed at the cathode as evidenced by spectra with fainter continuum and line emission. These results are still being studied and it is anticipated that a report with more complete spectroscopic description of the diagnostic setup and results will be forthcoming.

There are a several reasons for including a separate, preliminary set of spectroscopic results in this report. The data presented here pertains to data obtained with PIN diode arrays that recorded the intensity of light from a couple key lines-of-sight (Fig. J1). As compared to emission spectra data, PIN diode lends itself quite readily to quick analysis and comparison. Another reason to include the results here is to illustrate the potential of these relatively simple spectroscopic diagnostics for providing substantial insight for future experiments. Although preliminary and to some degree unsubstantiated, these results presented below suggest cathode and anode plasma velocities of 10's of cm/μs. If these velocities are real this is a significant finding because they are an order of magnitude higher than thermal plasma velocities typically associated with plasma expansion from electrodes in high-energy pulsed power devices (1-2 cm/μs).[xix]

Figure J1 shows a drawing and schematic of the spectroscopic lines-of-sight (LOS) used to obtain the results presented here. Light from near the cathode tip was collected by a focusing lens unto an array of fibers. The lens and fiber system was located outside the vacuum port along the LOS shown in Fig. J1a. Figure J1b shows a schematic illustrating the exact location of the two lines-of-sight used, one looking directly at the cathode needle, approximately 5 mm from the tip and the other looking out in the AK gap about 5 mm away from the cathode tip.

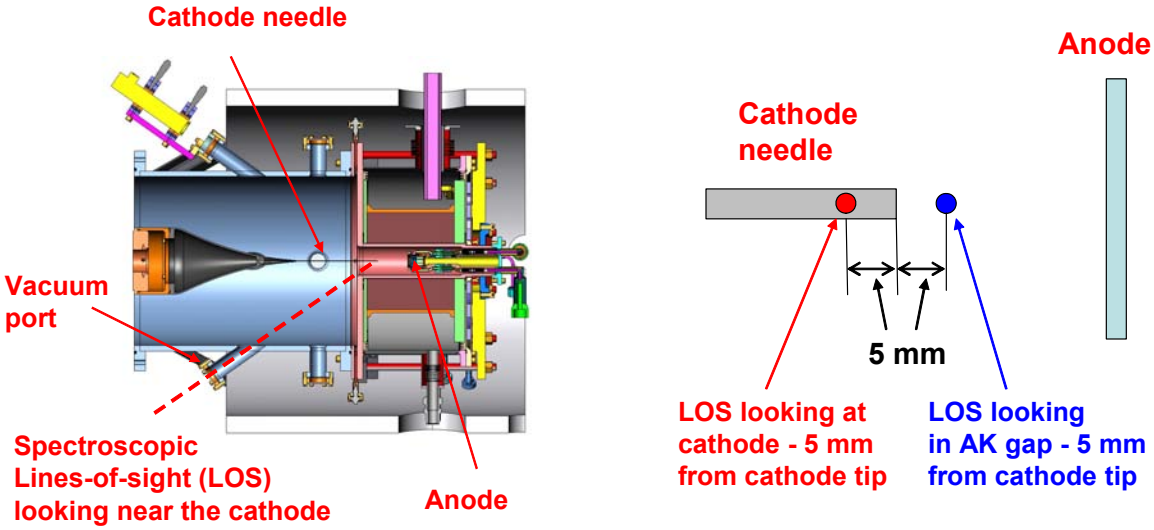


**Figure J1.** a) Drawing of immersed-$B_z$ diode with spectroscopic lines-of-sight near the cathode tip b) schematic showing relative position of lines-of-sight looking at the cathode and in the AK gap.

Figure J2 shows the light intensity measured by the voltage out from a PIN diode as a function of time for three different experiments. The dashed lines are data collected from the LOS looking directly at the cathode and the solid lines are data collected from the LOS looking out into the AK gap. The timing of the signals for the LOS looking at the cathode (dashed lines) have been artificially aligned to the beginning of the diode current for each experiment and the signals for the LOS looking in the gap (solid lines) have been shifted an equal amount (i.e. the relative timing of light from the two different LOS remains unchanged). It should also be noted these data records were recorded on the same scope, so the relative timing is considered absolute and it is the relative timing that we are most interested in here. If one assumes that light is coming from plasma then the relative timing would be a measure of the cathode plasma velocity. For example, using the difference in timing of the dashed and solid lines at a signal level of 1 V, and dividing this by the distance from the tip to the LOS looking in the gap, namely 5 mm, result in calculated velocities of 44, 23 and 20 cm/μs respectively for shots 777, 773 and 776. Shots 773 and 776 used W cathodes, while shot 777 used a Ti alloy cathode. Because of the sparseness of the data, it is difficult to comment on whether or not the difference in velocities observed between the Ti alloy cathode and W cathodes is real or is due to experimental variation. In any case as pointed out in the proceeding paragraphs, the main point to be made from these results are that inferred plasma velocities are very fast.

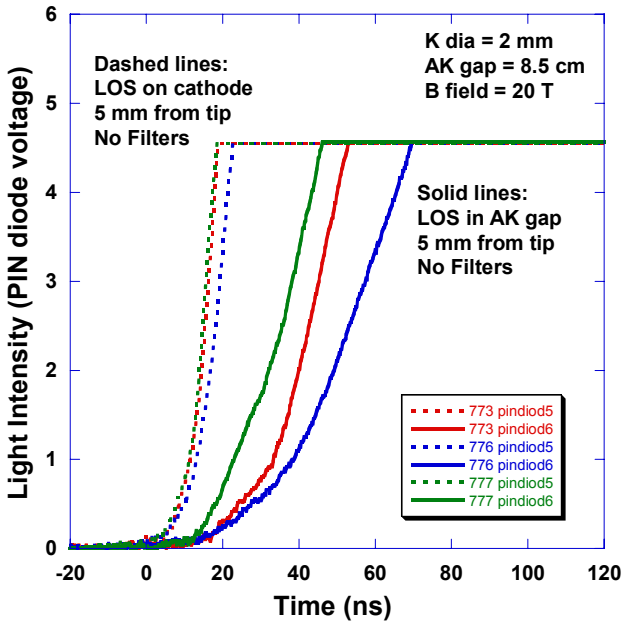


**Figure J2.** Relative timing of light intensity looking at the cathode (dashed lines) and 5 mm into the AK gap (solid lines).

Tantalizing initial results were also obtained with regards to anode plasma velocities. Figure J3 shows the effect of anode material and light filters on the timing and intensity of light collected from the LOS looking at the cathode (Fig. J3a) as well as from the LOS looking 5 mm out in gap (Fig. J3b). These data pertain to the anode material variation

experiments described in Appendix H, namely, the 4-T experiments. In addition, the results from shot 773, a RT Ta shot, have been included as a relative benchmark. Figure J3a shows that there is no effect of anode material on the relative timing of light coming from the cathode. There is however a strong effect with both filters and anode materials on the relative timing and intensity of light coming from the LOS looking out in the gap. The data shown in Fig. J3b can be best digested if it is separated into two groups, those experiments where an H-α filter was not used (orange and black solid lines) and the subset where an H-α filter was used (green, blue and red solid lines). Without an H-α filter there does not appear to be any effect of anode material, RT Ta vs. frozen $D_2$, on the relative timing of light coming from the LOS in the gap (there is an obvious difference in intensity due to the neutral density filter). There is a dramatic effect observed, however, when the H-α filter is added (note the difference in signal for the $D_2$ results with the H-α filter – black solid line – as compared to the $D_2$ results with the H-α filter – the blue solid line. These shots were identical in configuration and had very similar electrical and radiographic results as discussed in Appendix H. With the H-α filter, Fig. J3b shows that there is a large effect of anode material on the relative timing and intensity of the light coming from the LOS in the gap. The logical conclusion is that with the H-α filter in place the resulting signals are from excited hydrogen neutrals that have originated at the anode. It is conjectured that these neutral H-α signatures are remnants of a fast moving anode plasma that is in the process of cooling and recombining. Others have speculated that these H-α signatures result from charge exchange protons that were accelerated to several keV near the anode and then recombined to form fast moving hydrogen neutrals. Without more information it is difficult to know for sure. What is certain is that the speed and relative amount of material coming from the anode is a function of the anode material/treatment. One can estimate the relative velocity of these "anode plasmas" by taking the time at which each signal breaks from the baseline and dividing by distance between the anode and spectroscopic LOS (8 cm). The calculated anode plasma velocities for the LHe-cooled sapphire anode, the frozen $D_2$ anode and the frozen Ne anode are respectively 56, 19 and 15 cm/μs. It is noteworthy that frozen Ne anode had the lowest and slowest H-α signature. This result is consistent with the lower activation results obtained with the frozen Xe experiments discussed above in Sec. V. Similarly to the Xe results, it would appear that dramatic differences observed in anode constituents (as measured here by the H-α signature) does not seem to affect the diode behavior (see corresponding electrical results in Appendix H). Unfortunately, all of the 4-T experiments had reasonable diode behavior (i.e. good impedance), so for these particular experiments, no correlation can be drawn between good or poor diode behavior and the observed H-α signatures. Future work might want to use similar techniques to see if there is a correlation between the anode plasma evolving from the anode and the diode behavior.

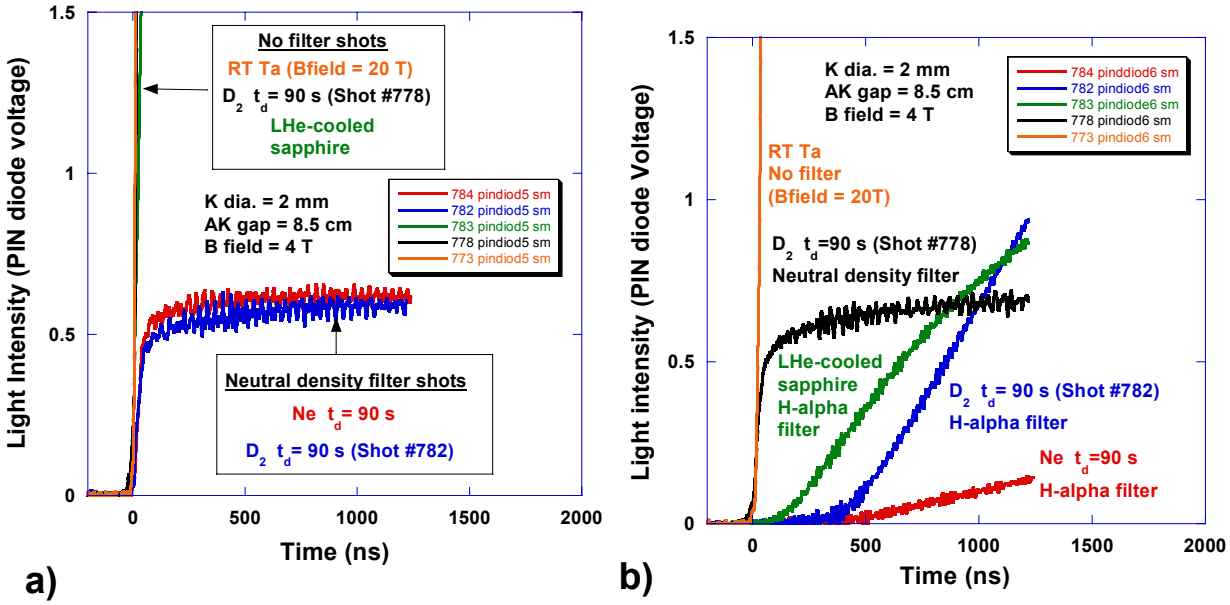


**Figure J3.** a) Effect of anode material and filter variation on spectroscopic diagnostic looking at the cathode (5 mm back from tip) b) effect of anode filter variations on spectroscopic diagnostics looking in the AK gap (5 mm in front of cathode tip).

The other surprising result is that there does not seem to be any indication that large amounts of cathode plasma with an attendant H-α signature are getting out into the gap. Emission spectra reported in [xviii] showed that H-α lines were visible when looking directly at the cathode. So either the fast moving cathode plasmas inferred from the data shown in Fig. J2 are either not very dense or they are highly ionized.

# Appendix K: Experimental Shot Summary

**Table K1 - Summary of RITS-3 shots discussed in the text with characteristic operating voltage (V), physical dimensions (d=cathode diameter, rA=inner radius of diode transport tube, anode-cathode (AK) gap), magnetic field strength (Bz) and anode materials/conditions (RT=room temperature, LHe=liquid helium-cooled, SS=stainless steel, CH is polyethylene, H2=hydrogen, D2= deuterium,Ne=neon,td=pumpout delay time).**

| Shot Number | V (MV) | d (mm) | rA (cm) | AK gap (cm) | Bz (T) | Anode Material | Spot size (mm) | TLD Dose (rad @ m) |
|---|---|---|---|---|---|---|---|---|
| 287 | 4 | 3.18 | 4.45 | 10 | 18 | RT Ta | 5.8 | 20.9 |
| 288 | 4 | 4.76 | 4.45 | 10 | 18 | RT Ta | 6.9 | 23 |
| 291 | 4 | 1 | 4.45 | 10 | 18 | RT Ta | 6.1 | 21.5 |
| 298 | 4 | 1 | 4.45 | 10 | 6 | RT Ta | 8.4 | 21.1 |
| 301 | 4 | 1 | 4.45 | 10 | 12 | RT Ta | 6.4 | 14.5 |
| 303 | 4 | 3.18 | 4.45 | 10 | 12 | RT Ta | 6.4 | 18 |
| 304 | 4 | 1 | 4.45 | 15 | 18 | RT Ta | 7.2 | 24.4 |
| 305 | 4 | 7.14 | 4.45 | 10 | 12 | RT Ta | 10.1 | 20.9 |
| 307 | 4 | 3.18 | 4.45 | 10 | 12 | RT Au | 6.9 | 21.8 |
| 308 | 4 | 7.14 | 4.45 | 5 | 18 | RT Ta | 11 | NA |
| 309 | 4 | 3.18 | 4.45 | 10 | 12 | RT SS | 6.4 | 17.9 |
| 313 | 4 | 3.18 | 4.45 | 10 | 12 | RT C | 5.8 | 13.7 |
| 314 | 4 | 1 | 4.45 | 2 | 18 | RT Ta | 4.8 | 5.7 |
| 315 | 4 | 3.18 | 4.45 | 10 | 12 | RT CH | 8.2 | 24.4 |
| 316 | 4 | 1 | 4.45 | 20 | 18 | RT Ta | 9.2 | 31 |
| 318 | 4 | 1 | 4.45 | 30 | 18 | RT Ta | 11 | 26.4 |
| 320 | 4 | 3.18 | 4.45 | 15 | 12 | RT Ta | 5.9 | 20.1 |
| 321 | 4 | 3.18 | 4.45 | 15 | 12 | RT Ta | 5.2 | 16.8 |
| 324 | 4 | 2 | 4.45 | 15 | 12 | RT Ta | 6.1 | 14.3 |
| 325 | 4 | 3.18 | 4.45 | 15 | 12 | RT Ta | 5.8 | 25.8 |
| 333 | 4 | 2 | 4.45 | 15 | 12 | RT Ta | 13.3 | 38.3 |
| 337 | 4 | 1 | 4.45 | 5 | 18 | RT Ta | 6.1 | 7.3 |
| 339 | 4 | 7.14 | 4.45 | 10 | 18 | RT Ta | 9.4 | 30.9 |
| 341 | 4 | 2 | 4.45 | 10 | 18 | RT Ta | 5.3 | 17.6 |
| 343 | 4 | 3.18 | 4.45 | 10 | 12 | RT CH | 6.2 | 21.5 |
| 345 | 4 | 9.52 | 4.45 | 10 | 18 | RT Ta | 12.8 | 31.6 |
| 592 | 5 | 4.76 | 3.26 | 7.1 | 25 | RT SS | 5.9 | 37.4 |
| 763 | 5 | 4.76 | 3.26 | 7.5 | 20 | RT Ta | 6.2 | 80.7 |
| 765 | 5 | 2 | 3.26 | 7.5 | 20 | RT Ta | 5.1 | 35.2 |
| 766 | 5 | 1 | 3.26 | 7.5 | 20 | RT Ta | 6.9 | 37.4 |
| 767 | 5 | 2 | 3.26 | 7.5 | 20 | RT SS | 5.3 | 34.4 |
| 768 | 5 | 2 | 3.26 | 7.5 | 20 | LHe SS | 5.5 | 31.8 |
| 769 | 5 | 2 | 3.26 | 7.5 | 20 | Xe, td=90 s | 5 | 32.1 |
| 770 | 5 | 2 | 3.26 | 7.5 | 20 | Xe, td=45 s | 4.6 | 34.4 |
| 771 | 5 | 2 | 3.26 | 7.5 | 20 | Xe, td=0 s | 4.5 | 20.3 |
| 772 | 5 | 2 | 3.26 | 7.5 | 20 | H2 td = 90s | 0.7 | NA |
| 773 | 5 | 2 | 3.26 | 8.5 | 20 | RT Ta | 6.9 | 54.5 |
| 776 | 5 | 2 | 3.26 | 8.5 | 20 | Sapphire* | 6.3 | 21.8 |
| 777 | 5 | 2 | 3.26 | 8.5 | 20 | RT Ta | 4.4 | 27.3 |
| 778 | 5 | 2 | 3.26 | 8.5 | 4 | D2 td=90s | 11.1 | 14.5 |
| 779 | 5 | 2 | 3.26 | 8.5 | 20 | D2 td=90s | 0.1 | NA |
| 782 | 5 | 2 | 3.26 | 8.5 | 4 | D2 td=90s | 11.6 | 14.5 |
| 783 | 5 | 2 | 3.26 | 8.5 | 4 | LHe Sapphire | 8.6 | 22.9 |
| 784 | 5 | 2 | 3.26 | 8.5 | 4 | Ne td=90s | NA | 20.1 |

* Temperature unknown; between LHe-cooled and RT

## References for Appendices


[i] D. V. Rose, T. C. Genoni, and D. R. Welch, "Ion-hose instability growth and saturation for counterstreaming electron and ion beams in an applied magnetic field," Phys. Plasmas **11**(11), pp. 4990-4997, (2004).

[ii] J. Maenchen, G. Cooperstein, J. O'Malley, and I. Smith, "Advances in pulsed power-driven radiography systems," Proc. IEEE **92**(7), pp. 1021-1042, (2004).

[iii] I. D. Smith, V. L. Bailey, Jr., J. Fockler, J. S. Gustwiller, D. L. Johnson, and J. E. Maenchen and D. D. Droemer, "Design of a Radiographic Integrated Test Stand (RITS-3) Based on a Voltage Adder to Drive A Diode Immersed in a High Magnetic Field", IEEE Trans. Plasma Sci,, **28**(5), Oct. 2000, pp. 1653-1659.

[iv] T. J. Goldsack, T. F. Bryant, P. F. Beech, S. G. Clough, G. M. Cooper, R. Davitt, R. D. Edwards, N. Kenna, J. McLean, A. G. Pearce, M. J. Phillips, K. P. Pullinger, D. J. Short, M. A. Sinclair, K. J. Thomas, J. R. Threadgold, M. C. Williamson, and K. Krushelnick, "Multimegavolt multiaxis high-resolution flash x-ray source development for a new hydrodynamics research facility at AWE Aldermaston," IEEE Trans. Plasma Sci. **30**(1), pp. 239-253, (2002).

[v] G. Raboisson, P. Eyl, M. Roche, C. Malaval, and A. Johan, "ASTERIX, A High Intensity X-Ray Generator", Proc. 7th IEEE International Conference on Pulsed Power, June 1989, pp. 567-570.

[vi] G. M. Cooper, J. McLean, and R. Davitt, "Recent x-ray diode and magnetically insulated transmission line experiments performed on the 5.5 MV Superswarf machines at AWE Aldermaston," Proc. 13th IEEE International Pulsed Power Conference, June 2001, pp. 393-396

[vii] D. V. Rose, D. R. Welch, B. V. Oliver, R. E. Clark, D. L. Johnson, J. E. Maenchen, P. R. Menge, C. L. Olson, and D. C. Rovang "Coupled particle-in-cell and Monte Carlo transport modeling of intense radiographic sources," J. Appl. Phys., vol. 91, no. 5, pp. 3328-3335, Mar. 2002.

[viii] N. Bruner, B. V. Oliver, D.V. Rose, D. R. Welch, D. C. Rovang and E. Puetz, "The Influence of Anode/Target Ion Species on the Magnetically Immersed Diode", Proc. 15th IEEE International Pulsed Power Conference, June 2005, to be published.

[ix] D. R. Welch, B. V. Oliver, D. V. Rose, N. Bruner, and R. E. Clark, " 2005 Summary Report for the ATK Mission Research Support of the Sandia National Laboratories Radiography Program" , MRC/ABQ-R-2107, August 2005.

[x] P. R. Menge, D. L. Johnson, J. E. Maenchen, C. L. Olson, and D. C. Rovang, D. Droemer, E. Hunt, B. Oliver, D. Rose and D. Welch, "Experimental Comparison of 2-3 MV X-Ray Sources for Flash Radiography", SAND2002-0082, January 2002.

[xi] M. E. Cuneo, P. R. Menge, D. L. Hanson, W. E. Fowler, M. A. Bernard, G. R. Ziska, A. B. Filuk, T. D. Pointon, R. A. Vesey, D. R. Welch, J. E. Bailey, M. P. Desjarlais, T. R. Lockner, T. A. Mehlhorn, S. A. Slutz, and M. A. Stark, "Results of Vacuum Cleaning Techniques on the Performance of LiF Field-Threshold Ion Sources on Extraction Applied-B Ion Diodes at 1-10 TW", IEEE Transactions on Plasma Science, **25**(2), pp. 229-251, April 1997.

[xii] M. E. Cuneo, "The effect of electrode contamination, cleaning, and conditioning on high-energy, pulsed-power device performance," IEEE Trans. Dielect. Elec. Insul., vol. 6, no. 4, pp. 469-485, Aug. 1999.

[xiii] D. L. Hanson, J. L. Porter, and R. R. Williams, "High-purity ion beam production at high current densities with liquid-helium-cooled series-field-coil extraction ion diode", J. Appl. Phys., **70** (6), (September 1991), pp. 2925-2938.

[xiv] P. Strasser, K. Ishida, S. Sakamoto, K. Shimomura, N. Kawamura, E. Torikai, M. Iwasaki, and K. Nagamine, "Muon catalyzed fusion experiments on muonic deuterium atom deceleration in thin solid deuterium films", Physics Letters B, 368 (1996), pp. 32-38.

[xv] P. E. Knowles, G. A. Beer, J. L. Beveridge, J. Douglas, G. M Marshall, F. Mulhauser, M. Maier, M. C. Fujiwara, A. R. Kunselman, and J. Zmeskal, "A windowless frozen hydrogen target system", Nuclear Inst. and Methods in Phys. Res. A, 368 (1996), pp. 604-610.

[xvi] R. A. Haefer, *Cryopumping Theory and Practice*, Clarendon Press-Oxford, 1989.

[xvii] F. Pobell, *Matter and Methods at Low Temperatures*, Springer, 1995.

[xviii] M. D. Johnston, K. Hahn, D. Rovang, S. Portillo, and J. Maenchen, D. Droemer, D. Welch, B. Oliver, D. Rose, E. Schamiloglu, and Y. Maron, "Plasma Spectroscopy Diagnostics in Pulsed-Power X-Ray Radiography Diode Research", Proc. 15th IEEE International Pulsed Power Conference, June 2005, to be published.

[xix] D. Hinshelwood, "Cathode Plasma Formation in Pulsed High Current Vacuum Diodes", IEEE Transactions on Plasma Science, Vol. 11, pp.188-196, 1983.

## Distribution:

10 AWE Aldermaston
Attn: I. Crotch (5)
G. M. Cooper
J. O'Malley
J. McLean
M. A. Sinclair
J. R. Threadgold
Hydrodynamics Department
Building H12
Reading, Berkshire RG7 4PR
UNITED KINGDOM

3 Voss Scientific
Attn: D. R. Welch
D. V. Rose
N. Bruner
418 Washington SE
Albuquerque, NM 87108

3 Los Alamos National Laboratory
Attn: R. D. Fulton (2)
C. A. Swenson, MS E536
P. O. Box 1663
Los Alamos, NM 87545

3 Naval Research Laboratory
Attn: G. Cooperstein (2)
R. Commisso
Code 6770
4555 Overlook Ave. SW
Washington, DC 20375-5346

2 L-3 Pulse Sciences
Attn: I. D. Smith
V. L. Bailey
2700 Merced Street
San Leandro, CA 94577

1 Dept. of Electrical & Computer Engineering
Attn: Edl Schamiloglu
MSC01 1100
1 University of New Mexico
Albuquerque, NM 87131-001

| | | |
|---|---|---|
| 10 | MS 1193 | D. C. Rovang |
| 5 | MS 1193 | B. V. Oliver |
| 1 | MS 1193 | J. E. Maenchen |
| 1 | MS 1193 | M. D. Johnston |
| 1 | MS 1193 | S. Portillo |
| 1 | MS 1193 | E. A. Puetz |
| 1 | MS 1193 | S. R. Cordova |
| 1 | MS 1193 | I. Molina |
| 1 | MS 1193 | K. D. Hahn |
| 1 | MS 1193 | D. L. Johnson |
| 1 | MS 1193 | J. J. Leckbee |
| 1 | MS 1193 | D. W. Droemer |
| 1 | MS 1193 | M. E. Cuneo |
| 1 | MS 1193 | D. L. Hanson |
| 1 | MS 1193 | J. R. Woodworth |
| 1 | MS 1193 | J. M. Lehr |
| | | |
| 1 | MS 1178 | M. E. Sceiford |
| 1 | MS 1178 | D. M. Van De Valde |
| 1 | MS 1181 | T. A. Mehlhorn |
| 1 | MS 1182 | T. J. Renk |
| 1 | MS 1190 | C. L. Olson |
| 1 | MS 1194 | D. E. Bliss |
| 1 | MS 1194 | M. G. Mazarakis |
| 1 | MS 1194 | M. E. Savage |
| 1 | MS 1196 | W. A. Stygar |
| 1 | MS 1423 | P. A. Miller |
| | | |
| 2 | MS 9018 | Central Technical Files, 8944 |
| 2 | MS 0899 | Technical Library, 4536 |